



**Mauritius Research and Innovation Council**  
**INNOVATION FOR TECHNOLOGY**

**MAURITIUS WAVE ENERGY  
RESOURCE MANAGEMENT**

**By**

**The University of Western Australia**

**Report**

*July 2017*

**Mauritius Research and Innovation Council**

*Address:*  
Level 6, Ebene Heights  
34, Cybercity  
Ebene

Telephone: (230) 465 1235  
Fax: (230) 465 1239  
e-mail: [contact@mrhc.mu](mailto:contact@mrhc.mu)  
Website: [www.mrhc.mu](http://www.mrhc.mu)

**This report is based on work supported by the Mauritius Research and Innovation Council. Any opinions, findings, recommendations and conclusions expressed herein are the author's and do not necessarily reflect those of the Council.**

# **Mauritius Wave Energy Resource Assessment**

**Date: 26-07-2017**

**Client:** Carnegie Clean Energy



**UWA Contract Number:** 63005006

**Project Manager:** Andrew W.M. Pomeroy

**Document History:**

REVISION	DATE	NOTES	AUTHOR	REVIEWED
A	31/01/2017	Draft issue for discussion only	AWP	RJL
B	01/05/2017	Draft issue for client review only	AWP, HW	RJL, SD
0	26/07/2017	Issued to client	AWP, HW	RJL, SD

Approved for release:

<b>Dr Andrew W. M. Pomeroy</b> MIEAust CPEng NER	 ENGINEERS AUSTRALIA	<b>National Engineering Register</b>
Signature  Date <u>26/07/17</u>		
Registered on the NER in the area(s) of practice of Civil		

**Disclaimer**

This report has been prepared on behalf of and for Carnegie Clean Energy Limited, and is subject to and issued in accordance with the agree terms and scope between Carnegie Clean Energy Limited and The University of Western Australia. The University of Western Australia accepts no liability or responsibility for it in respect of any use of or reliance upon this report by any third party.



## Contents

1	Executive Summary .....	5
2	Introduction.....	6
2.1	Scope of Work .....	6
2.2	Deliverables .....	6
2.3	Key parameters .....	7
3	Summary of available measurements .....	9
3.1	Overview of available data.....	9
3.2	North East corner of Mauritius .....	10
3.3	Blue Bay .....	15
3.4	Souillac .....	19
3.5	Suitability of buoy measurements.....	23
4	Wave Climate Assessment Methodology .....	24
4.1	General methodology .....	24
4.2	Model discretization .....	24
4.3	Bathymetry.....	25
4.4	Model boundary conditions and physics.....	25
4.5	Model performance .....	27
4.5.1	General performance .....	27
4.5.2	North-East buoy .....	27
4.5.3	Blue Bay buoy .....	29
4.5.4	Souillac buoy.....	30
5	Western Indian Ocean wave climate .....	33
6	Mauritius wave climate .....	37
7	Local south-east Mauritius wave climate.....	40
7.1	Extreme value analysis.....	45
8	Suitability for wave energy device trials .....	47
8.1	Power Generation.....	47
8.2	Extreme Conditions .....	47
8.3	Maintenance and short term trials .....	47
9	Recommendations .....	49
	References.....	50
	Appendix A North-East Buoy Data .....	52
A.1	Original data.....	52
	Appendix B Additional Buoy Data.....	55
B.1	North-East Buoy.....	55
B.2	Souillac Buoy Data .....	58

Appendix C	Performance Results .....	59
C.1	Mauritius Domain: North-East Buoy .....	59
C.2	South-East Domain: Blue Bay Buoy .....	62
Appendix D	South-East coast seasonal wave climate .....	69
Appendix E	Monthly joint occurrence tables.....	71

# 1 Executive Summary

The study was commissioned to determine the wave resource around the island of Mauritius in order to identify priority sites for commercial wave energy device trials.

To quantify the wave resource, a 10-year wave hindcast was conducted. The regional hindcast models were driven by output from The Centre for Australian Weather and Climate Research's global WAVEWATCH III™ re-analysis, which outputs hourly gridded global wind and wave conditions. Three nested model domains were used to model the wave climate from Indian Ocean basin: (1) Mascarene domain, (2) Mauritius Island domain and (3) South East Coast domain - a high resolution domain that extended from Blue Bay to Souillac. The analysis was conducted using the numerical model Simulating WAVes Nearshore (SWAN).

The model predictions were compared to available wave buoy measurements, which were provided in a post-processes form, from three locations along the eastern coastline of Mauritius (North-East, Blue Bay and Souillac). The North-East wave buoy data contained some long period wave data that was questionable (appearing un-physical and differing from other wave buoys in the region), which when removed resulted in a dataset that was more consistent with the measurements at other locations. Data from the Blue Bay buoy covered a long period of time (2009-2015) and exhibited directional variability that was higher than expected. This variability may result from the post-processing as well as technical faults that appeared to occur. The Souillac buoy data was relatively short. Despite the data limitations associated with each wave buoy, the data was acceptable to test the performance of the model.

The model performance was generally good and similar to the performance of other models driven by global wave and wind datasets, especially in tropical wave climates. There were some differences between the model results and the wave buoy data but these differences were generally acceptable in the context of the available bathymetry, forcing conditions and validation information. The model results are considered acceptable for the purpose of a wave resource assessment.

This study concludes that the wave resource on the south-east coastline of Mauritius was greatest and thus the most appropriate location for wave energy device trials. This section of coastline is consistently subjected to incident waves that originate from the Indian Ocean basin with little modification caused by diffraction and refraction.

The recommendations discussed include:

- the need for higher resolution bathymetry along the coastline for any subsequent modelling efforts.
- the need for additional simulations once high resolution bathymetry O(10 m) is available to determine the precise location for deployment.

## 2 Introduction

The University of Western Australia (UWA) has been collaborating with Carnegie Clean Energy (CCE) on the development of offshore wave energy devices. In this project, UWA conducted a 10-year wave climate and resource assessment for the island of Mauritius in order to identify priority sites for commercial wave energy device trials.

In section 3, the wave measurements along the eastern coastline of Mauritius that were made available to this project are analysed and provide direct (*in-situ*) measures of the historical wave conditions at these sites. The numerical modelling methodology is then described in section 4 along with the underlying sources of bathymetric data, forcing conditions, as well as the model physics and configuration. Statistical measures that were used to evaluate the performance of the model are also presented in section 4, along with key hindcast model validation results using the data from section 3. The wave climate is analysed first at the Indian Ocean and Mascarene scale (section 5) and then around the island of Mauritius (section 6). The wave climate along the south-east coastline of Mauritius is then considered in detail in section 7 and accompanied by an analysis of the extreme wave climate. In section 8 the suitability of wave climate for wave energy device trials is discussed with key recommendations in relation to this project presented in section 9.

### 2.1 Scope of Work

The specific scope of work that UWA was engaged to undertake was to:

1. Summarise the data required to complete sub-task 2 (a wave resource assessment for the Island of Mauritius) and to communicate these requirements to CCE who located this data, conduct quality control and provided it to UWA (where available);
2. Develop and run a nested numerical hindcast spectral wave model for the island of Mauritius with a resolution suitable to identify priority sites for the deployment of (a) wave energy generation device(s) and conduct a 10 year wave climate analysis to assess wave energy availability and variability along the coast of Mauritius;
3. Summarise, based on available data and preliminary numerical modelling, priority locations for the deployment of a wave-monitoring device and related model output;
4. Refine the numerical model based upon data collected in situ by CCE (which was collected over a six-month period in 2016); and
5. Review priority sites and prepare a report that outlines the numerical modelling approach, assumptions, key results relevant to the identification of suitable wave energy device deployment locations and any recommendations related to the work undertaken.

### 2.2 Deliverables

There were three deliverables included in this project:

1. A Letter (Ref: 201600602-CWE-D1-R1) that summarises priority locations for the deployment of a wave-monitoring device and related model output.
2. **A report that outlines the numerical modelling approach, assumptions, key results relevant to the identification of suitable wave energy generation device deployment locations and any recommendations related to the work undertaken (THIS REPORT).**
3. A package of data, which consists of: bathymetry files, wave climate files, and model output files that were generated in relation to Deliverable 2.

## 2.3 Key parameters

Table 2-1 Key wave parameters referred to in this report. The shaded cells that contain an 'X' indicates available data at different buoy locations.

Symbol	Interpretation	Unit	Buoy where data is available		
			North -East	Blue Bay	Souillac
$H_{m0} \equiv H_s$	Zeroth moment wave height (approximately equivalent to the significant wave height). Throughout this report we refer to the wave height as the significant wave height irrespective of how the wave height was derived.	m	X	X	X
$T_{m01}$	Mean wave period defined as $2\pi \left( \frac{\iint \omega E(\omega, \theta) d\omega d\theta}{\iint E(\omega, \theta) d\omega d\theta} \right)^{-1}$	s	X		
$T_{m02}$	Mean wave period defined as $2\pi \left( \frac{\iint \omega^2 E(\omega, \theta) d\omega d\theta}{\iint E(\omega, \theta) d\omega d\theta} \right)^{-1}$	s	X		
$T_{m-10} = T_e$	Wave energy period defined as $2\pi \left( \frac{\iint \omega^{-1} E(\omega, \theta) d\omega d\theta}{\iint E(\omega, \theta) d\omega d\theta} \right)$	s			
$\theta_m$	Mean wave direction	°	X	X	
$H_{max}$	Maximum wave height	m	X	X	X
$T_p$	Peak wave period. The wave period associated with the peak frequency of the wave spectrum	s	X	X	X
$\theta_p$	Peak wave direction. The wave direction associated with the peak frequency of the wave spectrum	°	X		
$H_{m0a}$	Wave height associated with the swell partition of the wave spectrum	m	X		
$T_{m02a}$	Mean wave period associated with the swell partition of the wave spectrum	s	X		
$\theta_{ma}$	Mean wave direction associated with the swell partition of the wave spectrum	°	X		
$H_{m0b}$	Wave height associated with the sea partition of the wave spectrum	m	X		
$T_{m02b}$	Mean wave height associated with the sea partition of the wave spectrum	s	X		
$\theta_{mb}$	Mean wave height associated with the sea partition of the wave spectrum	°	X		
Spr	The one-sided directional width of the spectrum	°	X		X
$H_{av}$	Average wave height	m			X

$T_{av}$	Average wave period	s			X
$T_{1/3}$	Mean wave period of the highest 1/3 of the waves in the record	s			X
$\theta_{hf}$	Wave direction associated with high frequency waves	°	X		
F	Wave energy flux (wave power)	kW m <sup>-1</sup>			

*Table 2-2 Nomenclature*

Symbol	Definition	Unit
$f$	Discrete wave frequency	Hz
$\omega$	Discrete angular frequency $2\pi f$	rad s <sup>-1</sup>
$\theta$	Discrete wave direction	°
$E(f, \theta)$	Wave energy directional spectrum	m <sup>2</sup> Hz <sup>-1</sup>

### 3 Summary of available measurements

#### 3.1 Overview of available data

Validation of the nearshore wave climate simulated by the model was undertaken using *in-situ* buoy measurements that were made available for three locations (Figure 3-1). These measurements were not continuous, covering various periods between 2005-2016 (Table 3-1). The data were presented as pre-processed (by others) data files that consisted of bulk parameters only (Table 2-1) and were accompanied with limited metadata. The full 2D directional spectrum of data was not available, which may have provided insight into some data irregularities that were observed (i.e., multiple sources of wave energy coming from different directions and/or have different periods). In this section, data from each buoy are summarized and presented as wave roses and joint probability (percentage) occurrence tables. The bulk parameters presented are the significant wave height  $H_s$ , Peak Wave Period  $T_p$  and Mean Wave Direction  $\theta_m$ , which were available at all three locations.

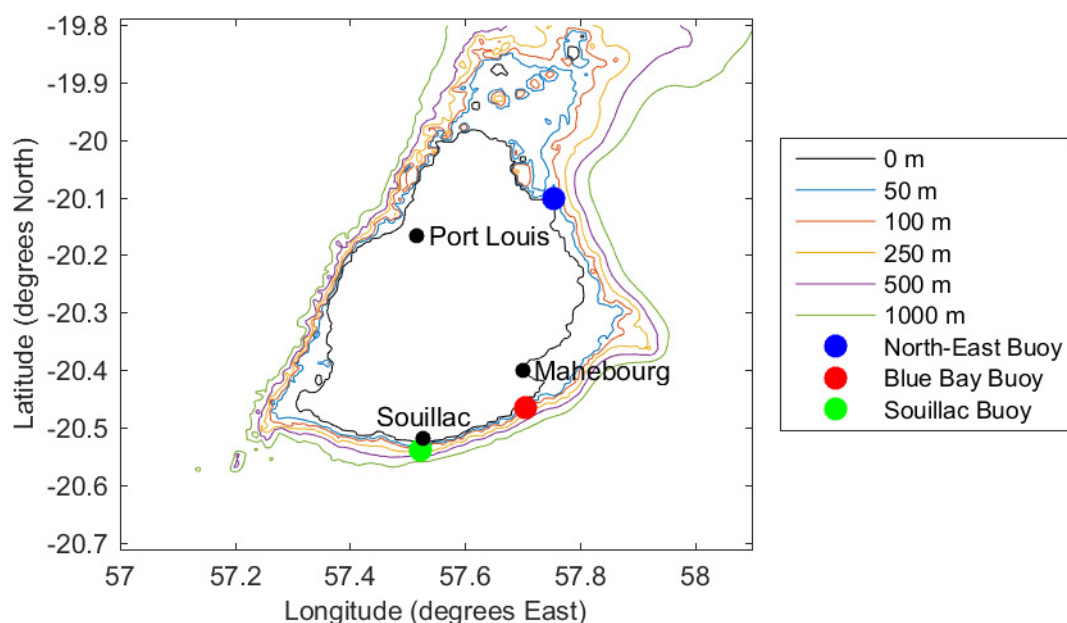


Figure 3-1 Location of North-East, Blue Bay and Souillac measurement buoys around Mauritius. Key contours are also indicated.

Table 3-1 Wave buoy data provided for this study. The shaded periods indicate available data.

	2009	2010	2011	2012	2013	2014	2015	2016	2017
North-East									
Blue Bay									
Souillac									

### 3.2 North East corner of Mauritius

(20° 6'7.72"S, 57°45'17.21"E).

Data from the North-East buoy deployed ~1 km offshore were provided on a 30 minute interval. The exact water depth at the buoy location is not known; however from the interpolated bathymetry used in this model study the water depth appears to be ~50 m. The buoy deployment site had unobstructed exposure to incident waves that originated from ~330-175° (green segment, Figure 3-2). Locally generated wind waves that originate over the segment 260-330° from the lagoon to the north (yellow segment, Figure 3-2) may also be recorded; however the shallow lagoon depth and the presence of a reef is expected to limit the propagation of these waves to the buoy. The site is shadowed from ~SSE-W.



Figure 3-2 Location of North-East measurement buoy and its exposure to incident waves. The coloured segments indicate the incident waves that could be measured by this buoy. The green arc indicates the wind and swell wave exposure sector and the yellow sector indicates wind waves locally generated in the nearby lagoon.

The processed wave data for this buoy consist of a timeseries of wave measurements that have periods of ~5-15 s but also many data points that are distinctly separated in the timeseries with a period of ~17-25 s (Figure 3-3). Throughout the year, the incident waves consistently approached in a narrow directional segment from ESE (Figure A-1). During the warm season (November – April), a small proportion of the waves had a  $H_s$  that was larger than 3 m while the remainder of the measured wave heights were equally distributed within the wave height bins of 1-2 m and 2-3 m (Figure A-2a). A very small fraction of waves approaching from the east exceeded 5 m, probably due to the passage of tropical storms and cyclones. The portion of waves in the 2-3 m height bin was greater in the cool season (May – October, Figure A-2c) and the occurrence of larger waves (3-4 m) did not differ substantially from those measured in the warm season. The joint probability occurrence tables for this data (Table A-1 and Table A-2) suggests the incident waves exhibited a bi-modal distribution that clustered the waves into periods of 5-15 s and 20-25 s. The high proportion (~20%) of waves with very long waves period  $T_p > 20$  s appears to be questionable as waves with these statistical



characteristics were not present in the data available at the other two locations and generally appear as spikes in the data.

When the wave periods for the North-East buoy and the Blue Bay buoy are presented together for waves that originate from 60-175° (the sector where incident waves were measured by both buoys) and for an overlapping period, no long period waves are contained within the Blue Bay timeseries (Figure 3-3). While it is possible that the incident waves measured at the North-East buoy are more bimodal than those recorded at the Blue Bay buoy, we believe that these longer period data points are unlikely to be 'real'. Without the original spectral data from this buoy, this cannot be verified.

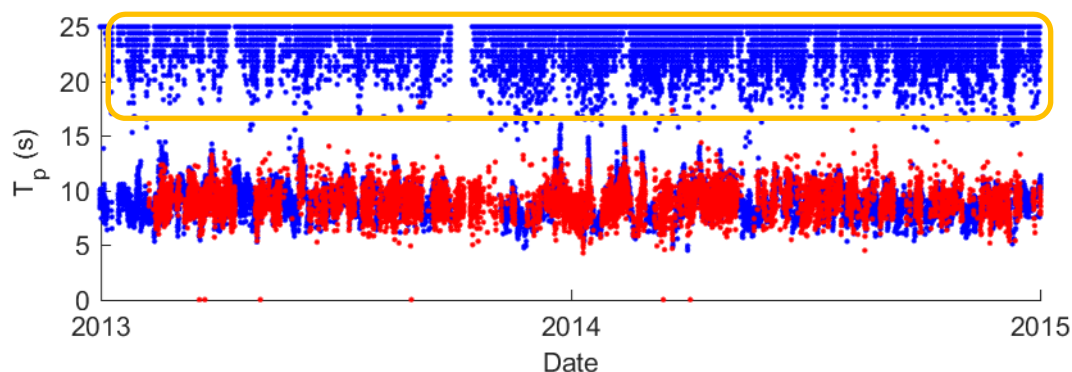


Figure 3-3 Two year timeseries of the peak wave period ( $T_p$ ) recorded by the (blue) North-East buoy and (red) Blue Bay buoy for waves that originate from 60-175°. The data points within the yellow box is questionable as this type of data is not present at the other measurement sites.

**NOTE:** In this study, we have removed the data points where  $T_p > 17$  s from our analysis. We recommend that this analysis be treated with caution.

Re-analysis of the North-East buoy data with the longer period waves ( $>17$  s) excluded resulted in similar trends in the wave heights and directions when compared to original dataset, except that the wave period was smaller:

- the incident waves consistently approached in a narrow directional segment from ESE throughout the year (Figure 3-4).
- a small proportion of the waves had a  $H_s$  that was larger than 3 m during the warm season (November – April), while the remainder of the measured  $H_s$  were equally distributed within the wave height bins of 1-2 m and 2-3 m (Figure 3-5a).
- a very small fraction of waves approaching from the east exceeded 5 m.
- the portion of waves in the 2-3 m height bin was greater in the cool season (May – October, Figure 3-5c). The occurrence of larger waves (3-4 m) did not differ substantially from those measured in the warm season.

The Joint probability occurrence tables (Table 3-2 and Table 3-3) for this reanalyzed data were more consistent with those for Blue Bay and Souillac (see sections 3.3 and 3.4).

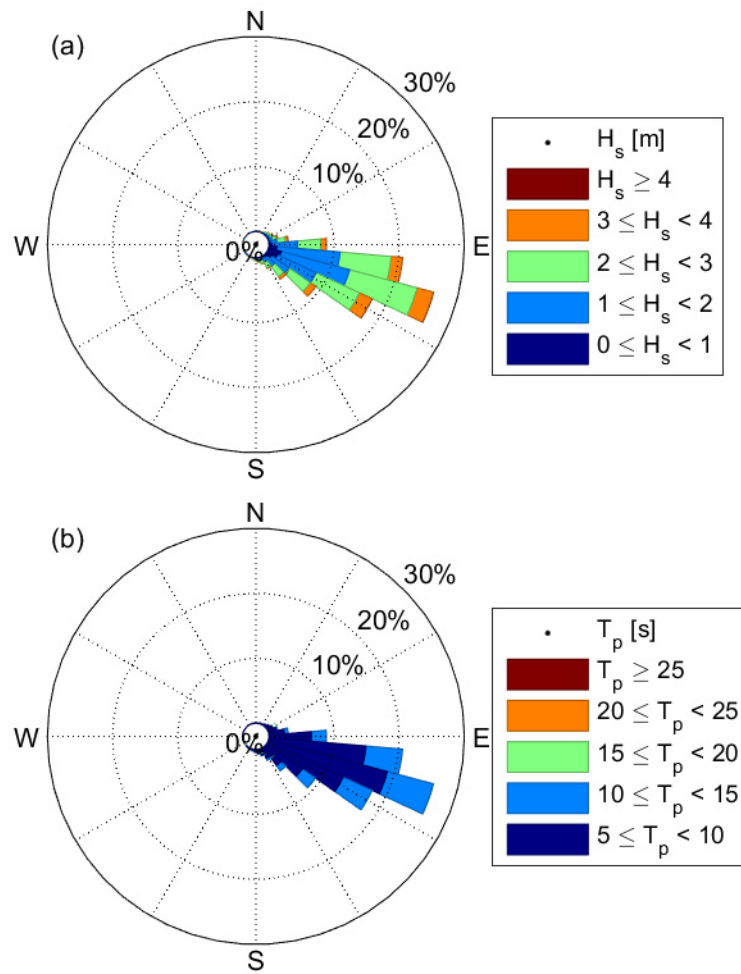


Figure 3-4 Wave roses of the incident waves measured at the North-East buoy during the period 09/02/2012 – 14/01/2015 ( $N=39054$ ). (a) The significant wave height ( $H_s$ ) and (b) peak wave period ( $T_p$ ). Note that data points with  $T_p > 17$  s have been removed (refer to Figure 3-3).

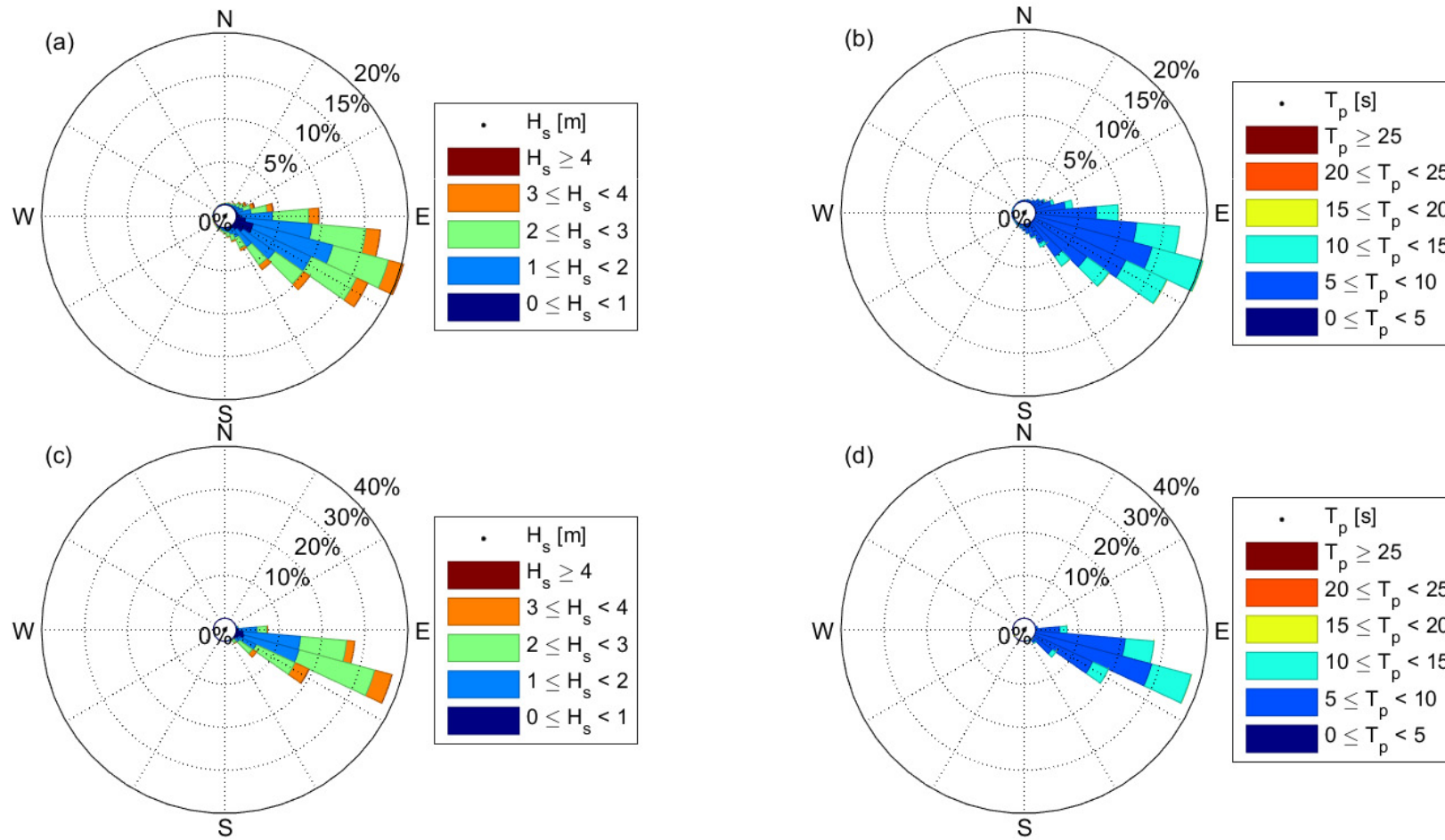


Figure 3-5 Wave roses of the incident waves measured at the North-East buoy during the period 09/02/2012 – 14/01/2015. (a) The significant wave height ( $H_s$ ) and (b) peak wave period ( $T_p$ ) during the warm season (November – April,  $N=25509$ ). (c)  $H_s$  and (d)  $T_p$  during the cool season (May – October,  $N=13545$ ). Note that data points with  $T_p > 17$  s have been removed (refer to Figure 3-3).

Table 3-2 Warm season joint probability occurrence between significant wave height ( $H_s$ ) and peak wave period ( $T_p$ ) (percentage) for measurements at the North-East buoy obtained during the period 09/02/2012 to 14/01/2015 (N=25509). Note: data points with  $T_p > 17$  s have been removed. Refer to Appendix A for joint probability occurrence tables for the full dataset.

		Peak Period ( $T_p$ )																			
		5	6	7	8	9	10	11	12	13	14	15	16	17	18	19	20	21	22	23	>24
Significant wave height ( $H_s$ )	0	0	0	0	0.1	0	0	0	0	0	0	0	0	0	0	0	0	0	0	0	0
	0.5	0.1	0.6	2.3	3.2	1.7	0.3	0.1	0	0	0	0	0	0	0	0	0	0	0	0	0
	1	0.2	1	2.9	7.1	7.1	2.3	0.7	0.2	0.1	0	0.1	0.1	0	0	0	0	0	0	0	0
	1.5	0.1	0.9	2.4	5.4	7	4.1	0.9	0.3	0.1	0.1	0	0	0	0	0	0	0	0	0	0
	2	0	0.5	2.2	5.2	6.5	4.5	1.2	0.6	0.2	0	0	0	0	0	0	0	0	0	0	0
	2.5	0	0.1	1.2	4.2	5.6	3.8	1.6	0.3	0.1	0.1	0	0	0	0	0	0	0	0	0	0
	3	0	0	0.2	1.3	3.2	2.3	0.8	0.1	0	0	0	0	0	0	0	0	0	0	0	0
	3.5	0	0	0	0.2	0.8	0.8	0.1	0	0	0	0	0	0	0	0	0	0	0	0	0
	4	0	0	0	0	0.1	0.1	0.1	0	0	0	0	0	0	0	0	0	0	0	0	0
	4.5	0	0	0	0	0	0.1	0	0	0	0	0	0	0	0	0	0	0	0	0	0
	>5	0	0	0	0	0	0	0	0	0	0	0	0	0	0	0	0	0	0	0	0

Table 3-3 Cool season joint probability occurrence between significant wave height ( $H_s$ ) and peak wave period ( $T_p$ ) (percentage) for measurements at the North-East buoy obtained during the period 09/02/2012 to 14/01/2015 (N=13545). Note: data points with  $T_p > 17$  s have been removed. Refer to Appendix A for joint probability occurrence tables for the full dataset.

		Peak Period ( $T_p$ )																			
		5	6	7	8	9	10	11	12	13	14	15	16	17	18	19	20	21	22	23	>24
Significant wave height ( $H_s$ )	0	0	0	0	0	0	0	0	0	0	0	0	0	0	0	0	0	0	0	0	0
	0.5	0	0.3	1.5	2.2	0.8	0.1	0	0	0	0	0	0	0	0	0	0	0	0	0	0
	1	0.1	0.5	2.2	5.1	5.5	1.5	0.7	0.1	0	0	0	0.1	0	0	0	0	0	0	0	0
	1.5	0.2	0.8	2.3	6.2	7.3	4	0.6	0.1	0	0	0	0	0	0	0	0	0	0	0	0
	2	0	0.7	2.9	6.6	7.8	4.6	1	0.4	0.1	0	0	0	0	0	0	0	0	0	0	0
	2.5	0	0.2	1.8	6.1	7.9	4.4	1.6	0.1	0	0	0	0	0	0	0	0	0	0	0	0
	3	0	0	0.2	1.8	4.1	2.3	0.8	0	0	0	0	0	0	0	0	0	0	0	0	0
	3.5	0	0	0	0.1	0.8	0.9	0.1	0	0	0	0	0	0	0	0	0	0	0	0	0
	4	0	0	0	0	0.1	0.1	0.1	0	0	0	0	0	0	0	0	0	0	0	0	0
	4.5	0	0	0	0	0	0	0	0	0	0	0	0	0	0	0	0	0	0	0	0
	>5	0	0	0	0	0	0	0	0	0	0	0	0	0	0	0	0	0	0	0	0

### 3.3 Blue Bay

(20°27.932'S 57°42.331'E).

The Blue Bay buoy was located approximately 1 km offshore at the center of a large bay, and bulk parameters (Table 2-1) were provided at an hourly interval. The water depth at the buoy location is not known; however from the interpolated bathymetry used in this model study the water depth appears to be ~17 m. Consequently, it is possible that the waves measured were influenced by the bottom (i.e. via refraction). North-East of the measurement location is Blue Bay Marine Park, which consists of a large lagoon fronted by a fringing reef. The buoy deployment site had unobstructed exposure to incident waves that originated from ~60-240° (green segment, Figure 3-6). Locally generated wind waves that originate in the Blue Bay Marine Park lagoon over the segment ~35-60° to the north (yellow segment, Figure 3-6) may also be recorded; however the shallow depth of the lagoon and the presence of a reef is expected to limit the propagation of these waves to the measurement location. The site is shadowed from SW-NNE.



*Figure 3-6 Location of the Blue Bay measurement buoy and its exposure to incident waves. The coloured segments indicate the incident waves that could be measured by this buoy. The green arc indicates the wind and swell wave exposure sector and the yellow sector indicates locally generated wind waves generated in the nearby lagoon.*

The incident waves measured at Blue Bay (Figure 3-7) can be separated into two distinct groups. The first group of waves approached from the SE, while the second group of waves approached from SSW. The same separation in the incident conditions was also observed during the warm season (Figure 3-8a,b) and the cool season (Figure 3-8c,d). A similar directional range of incident waves were also observed at the Souillac buoy although the relative directional weighting was different, which is probably due to the shorter monitoring period. The absence of incident waves from the SSW at the North-East buoy measurements is due to the shadowing of this buoy from waves that propagate from that direction. No separation was observed in the joint probability occurrence tables for either season (Table 3-5 and Table 3-4) and thus does not appear to be associated with differing wind and swell wave directions.



Most of the waves were contained within the 1-3 m wave bins; the remainder of the waves occurring in the 3-4 m wave bin. The waves originating from the SE were generally of 6-12 s, while the waves the originated from SSW were typically longer (9-15 s). During the warm season, the waves were generally larger with a small proportion of substantially larger waves (>4 m) also measured (Figure 3-8).

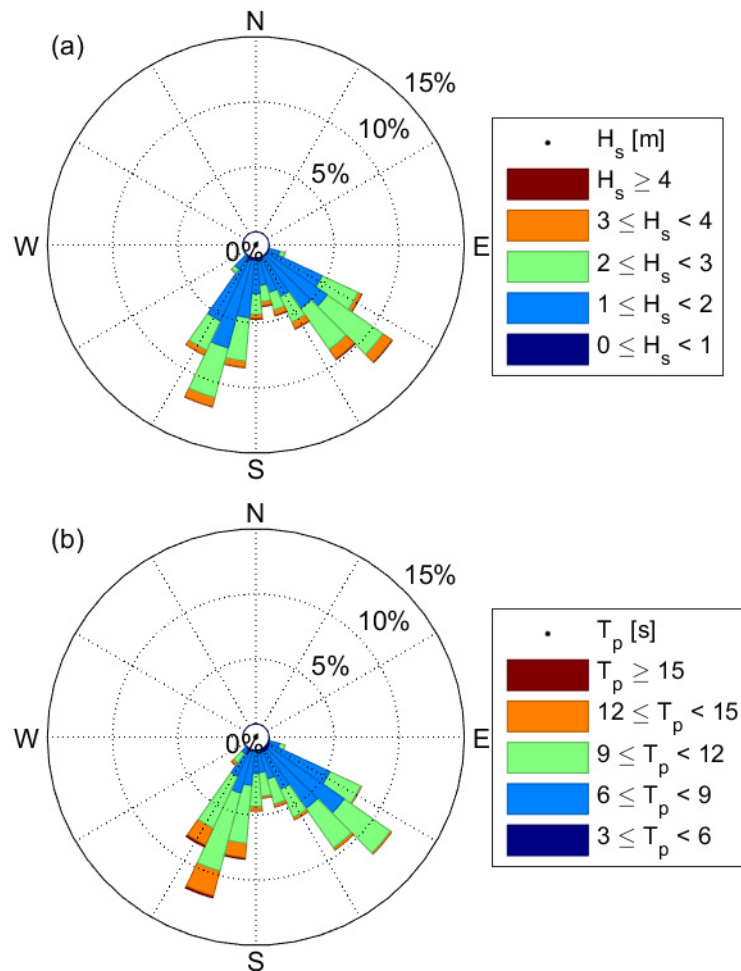


Figure 3-7 Wave roses of the incident waves measured at the Blue Bay buoy during the period 01/08/2009 – 31/12/2015 ( $N=339361$ ). (a) The significant wave height ( $H_s$ ) and (b) the peak wave period ( $T_p$ ).

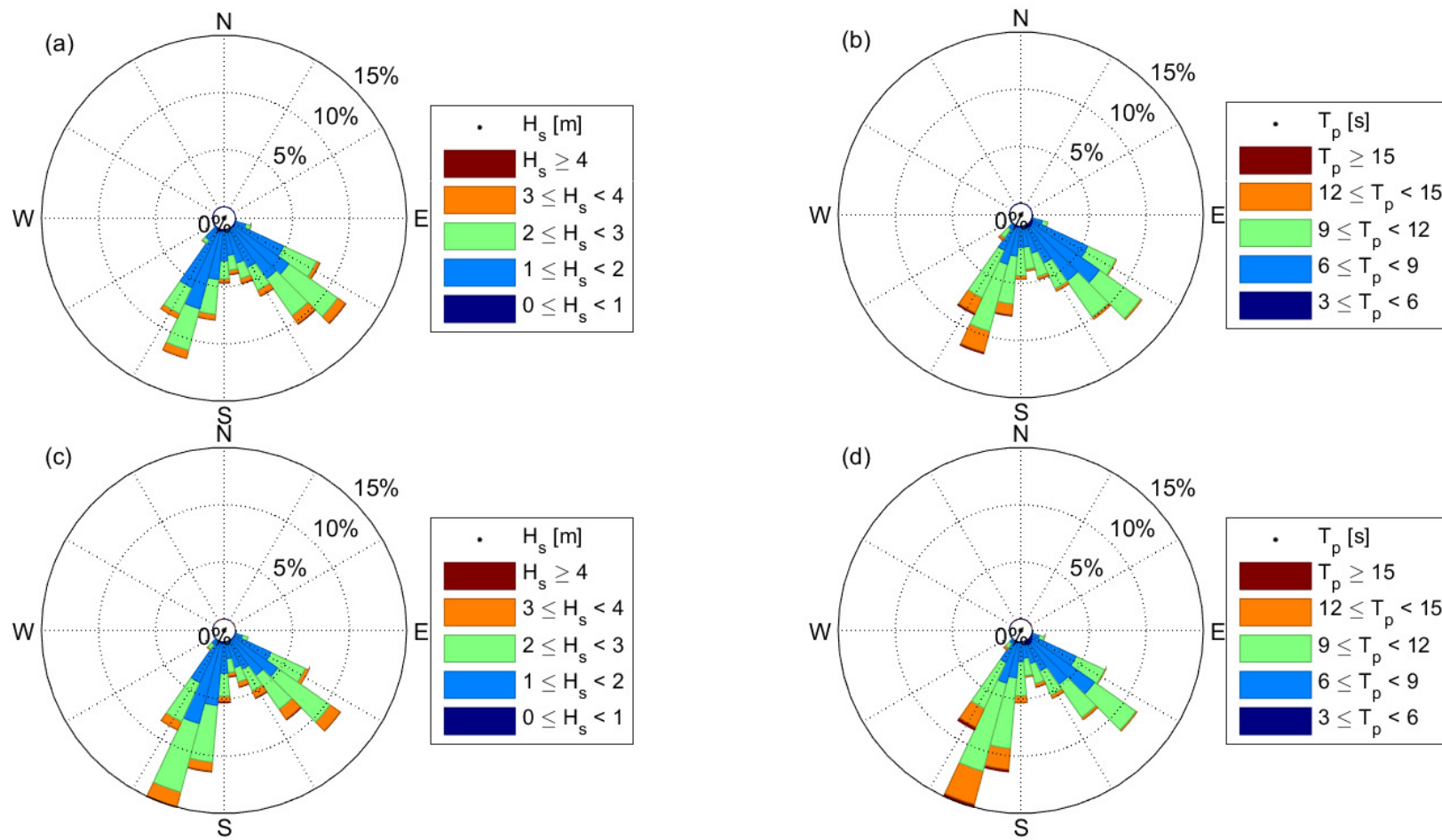


Figure 3-8 Wave roses of the incident waves measured at the Blue Bay buoy during the period 09/02/2012 – 14/01/2015. (a) The significant wave height ( $H_s$ ) and (b) peak wave period ( $T_p$ ) during the warm season (November – April,  $N=83042$ ). (c)  $H_s$  and (d)  $T_p$  during the cool season (May – October,  $N=256319$ ).

Table 3-4 Warm season joint probability occurrence between significant wave height ( $H_s$ ) and peak wave period ( $T_p$ ) (percentage) for measurements at the Blue Bay buoy obtained during the over period 01/08/2009 to 31/12/2015 (N=83042).

		Peak Period ( $T_p$ )																			
		5	6	7	8	9	10	11	12	13	14	15	16	17	18	19	20	21	22	23	>24
Significant wave height ( $H_s$ )	0	0	0	0	0	0	0	0	0	0	0	0	0	0	0	0	0	0	0	0	0
	0.5	0	0	0.1	0.3	0.3	0.2	0.1	0	0	0	0	0	0	0	0	0	0	0	0	0
	1	0.4	1.4	3.3	5.8	5.2	3.1	1.5	0.8	0.3	0.1	0.1	0	0	0	0	0	0	0	0	0
	1.5	0.7	2.6	5.6	8.2	7.6	5	2.5	1.4	0.6	0.3	0.1	0.1	0	0	0	0	0	0	0	0
	2	0.1	1.3	3.7	5.4	5.1	3.3	1.9	1	0.6	0.3	0.1	0	0	0	0	0	0	0	0	0
	2.5	0	0.5	1.9	3.3	2.8	1.7	1	0.6	0.3	0.2	0.1	0	0	0	0	0	0	0	0	0
	3	0	0.1	0.6	1.3	1.2	0.7	0.4	0.3	0.2	0.1	0	0	0	0	0	0	0	0	0	0
	3.5	0	0	0.1	0.3	0.4	0.2	0.2	0.2	0.1	0	0	0	0	0	0	0	0	0	0	0
	4	0	0	0	0.1	0.2	0.1	0.1	0.1	0	0	0	0	0	0	0	0	0	0	0	0
	4.5	0	0	0	0	0	0	0	0	0	0	0	0	0	0	0	0	0	0	0	0
	>5	0	0	0	0	0	0	0	0	0	0	0	0	0	0	0	0	0	0	0	0

Table 3-5 Cool season joint probability occurrence between significant wave height ( $H_s$ ) and peak wave period ( $T_p$ ) (percentage) for measurements at the Blue Bay buoy obtained during the over period 01/08/2009 to 31/12/2015 (N=256319).

		Peak Period ( $T_p$ )																			
		5	6	7	8	9	10	11	12	13	14	15	16	17	18	19	20	21	22	23	>24
Significant wave height ( $H_s$ )	0	0	0	0	0	0	0	0	0	0	0	0	0	0	0	0	0	0	0	0	0
	0.5	0	0	0	0.1	0.2	0.2	0	0	0	0	0	0	0	0	0	0	0	0	0	0
	1	0.3	0.6	1.3	2.6	3.1	1.9	1.2	0.6	0.3	0.1	0	0	0	0	0	0	0	0	0	0
	1.5	0.7	2	4.1	7.1	7.6	6	3.6	2	0.9	0.4	0.2	0.1	0	0	0	0	0	0	0	0
	2	0.2	1.4	3.6	5.3	5.3	4.2	2.6	1.7	1	0.5	0.2	0.1	0	0	0	0	0	0	0	0
	2.5	0	0.7	2.6	4.4	3.7	2.2	1.4	0.9	0.5	0.3	0.1	0.1	0	0	0	0	0	0	0	0
	3	0	0.2	0.9	1.8	1.7	0.9	0.5	0.4	0.3	0.1	0	0	0	0	0	0	0	0	0	0
	3.5	0	0	0.1	0.5	0.5	0.3	0.2	0.2	0.1	0.1	0	0	0	0	0	0	0	0	0	0
	4	0	0	0	0.2	0.2	0.1	0.1	0	0	0	0	0	0	0	0	0	0	0	0	0
	4.5	0	0	0	0	0	0	0	0	0	0	0	0	0	0	0	0	0	0	0	0
	>5	0	0	0	0	0	0	0	0	0	0	0	0	0	0	0	0	0	0	0	0



### 3.4 Souillac

(20°32.28'S 57°31.332'E).

The Souillac buoy was deployed ~1.5-2 km offshore in ~40-50 m water depth, depending on the prevailing current direction. The buoy deployment site had unobstructed exposure to incident waves that originated from ~70-280° (green segment, Figure 3-9). While the incident waves measured at this site originated over a wide directional segment (SSW to SE), most of the waves were contained within the ~S-SSE segment (Figure 3-10). During the cool season (Figure 3-11a), waves were generally 2-3 m with a smaller proportion of waves also recorded in the ranges of 1-2 m and 3-4 m. Waves >4 m were also recorded from all directions but only accounted for ~1% of the records and typically originated from the SSW. A similar range of wave heights were also recorded in the warm season (Figure 3-11c), although there was a noticeably larger proportion of waves in the range 1-2 m occurring from the SE during this season. Long period waves (12-20 s) originated from the SSW-S throughout the year, however the more easterly the wave origin, the greater proportion of shorter 9-12 s waves. In the warm season (Figure 3-11b), the waves were slightly longer than in the cool season (Figure 3-11d, see also Table 3-7 and Table 3-6).



Figure 3-9 Location of the Souillac measurement buoy and its exposure to incident waves. The coloured segments indicate the incident waves that could be measured by this buoy. The green arc indicates the wind and swell wave exposure sector.

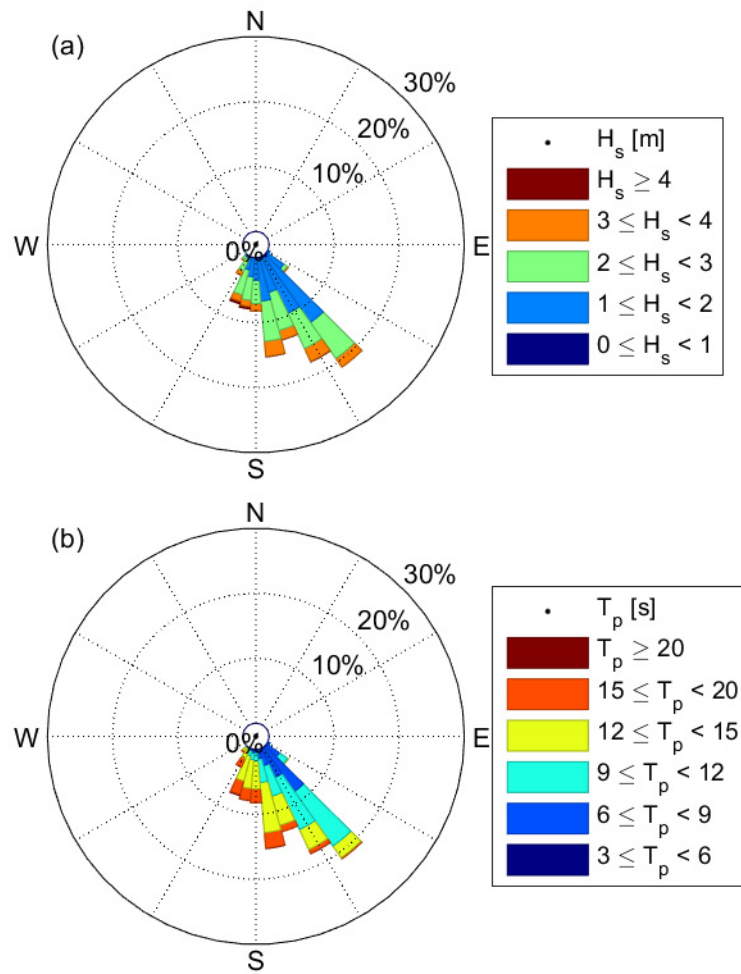


Figure 3-10 Wave roses of the incident waves measured at the Souillac buoy during the period 30/06/2016 – 25/01/2017. (a) The significant wave height ( $H_s$ ) and (b) the peak wave period ( $T_p$ ).

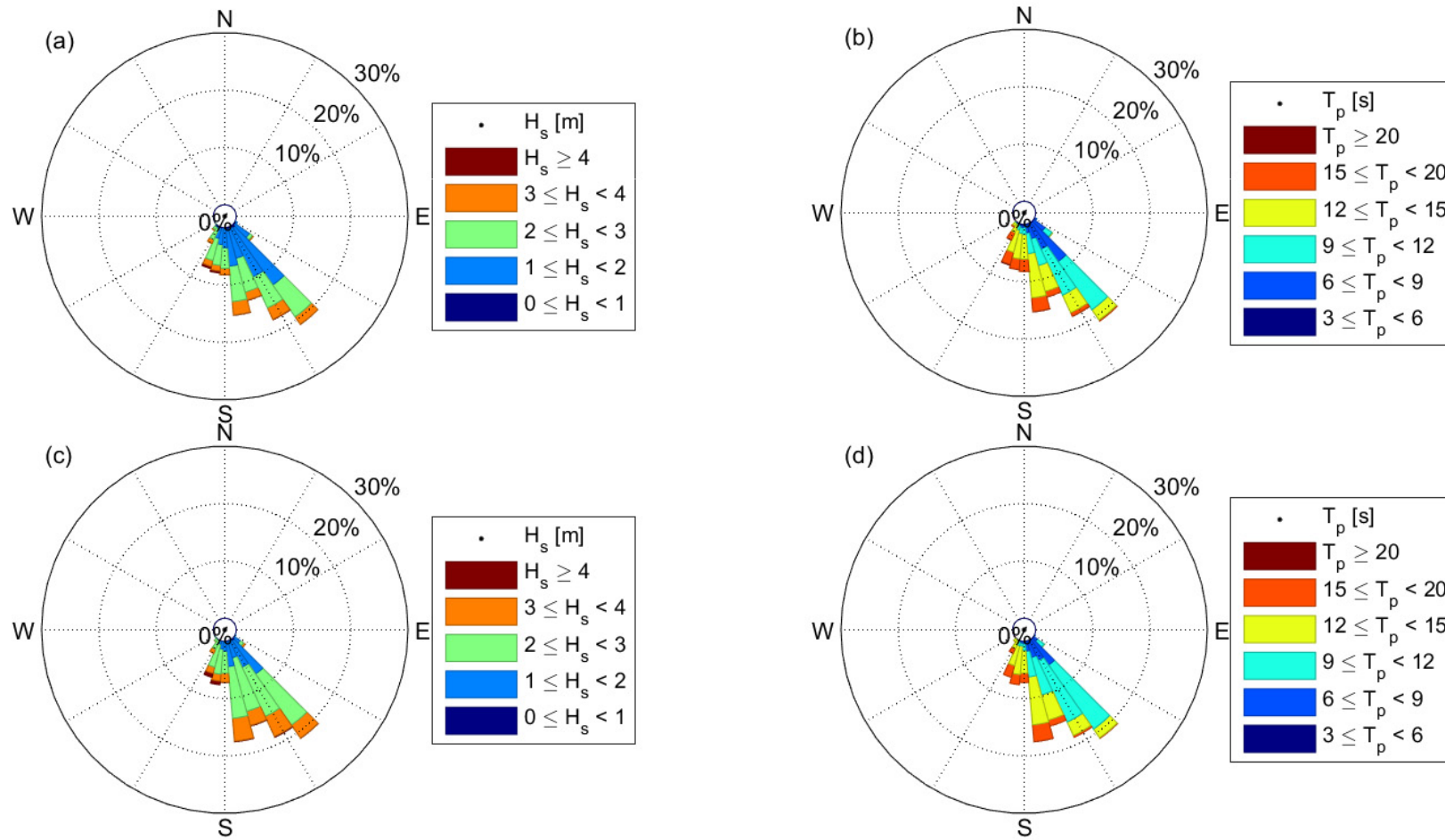


Figure 3-11 Wave roses of the incident waves measured at the Souillac buoy during the period 30/06/2016 – 25/01/2017. (a) The significant wave height ( $H_s$ ) and (b) peak wave period ( $T_p$ ) during the warm season (November – April,  $N=4703$ ). (c)  $H_s$  and (d)  $T_p$  during the cool season (May – October,  $N=2693$ ).

Table 3-6 Warm season joint probability occurrence between significant wave height ( $H_s$ ) and peak wave period ( $T_p$ ) (percentage) for measurements at the Souillac buoy obtained during the period 30/06/2016 to 25/01/2017 (N=4703).

		Peak Period ( $T_p$ )																			
		5	6	7	8	9	10	11	12	13	14	15	16	17	18	19	20	21	22	23	>24
Significant wave height ( $H_s$ )	0	0	0	0	0	0	0	0	0	0	0	0	0	0	0	0	0	0	0	0	0
	0.5	0	0	0.1	0.7	0.2	0.1	0.1	0.2	0	0	0	0	0	0	0	0	0	0	0	0
	1	0.2	0.5	2.6	6.2	4.1	1.9	1.3	3.6	1.7	1.3	0.7	0.3	0	0.1	0	0.1	0	0.1	0	0
	1.5	0.1	0.3	0.8	3.3	4.3	1.7	0.8	2.7	2.3	2.4	1.4	0.8	0	0.3	0	0.1	0	0	0	0
	2	0	0.4	0.9	2	3.9	4.1	1.1	2.7	3.7	4.1	2.9	1	0	0.2	0	0.1	0	0	0	0
	2.5	0	0.1	0.3	1.2	1.5	1.9	0.7	1.4	1.5	2.1	1.3	0.5	0	0.1	0	0	0	0	0	0
	3	0	0	0.3	1.3	2.3	1.4	0.4	0.5	1.1	1.3	1.3	0.6	0	0	0	0	0	0	0	0
	3.5	0	0	0	0.3	0.4	0.1	0	0	0.2	0.1	0.1	0	0	0	0	0	0	0	0	0
	4	0	0	0	0.1	0.2	0	0	0	0	0.2	0.2	0.1	0	0	0	0	0	0	0	0
	4.5	0	0	0	0	0	0	0	0	0	0	0.1	0	0	0	0	0	0	0	0	0
	>5	0	0	0	0	0	0	0	0	0	0	0	0	0	0	0	0	0	0	0	0

Table 3-7 Cool season joint probability occurrence between significant wave height ( $H_s$ ) and peak wave period ( $T_p$ ) (percentage) for measurements at the Souillac buoy obtained during the period 30/06/2016 to 25/01/2017 (N=2693).

		Peak Period ( $T_p$ )																			
		5	6	7	8	9	10	11	12	13	14	15	16	17	18	19	20	21	22	23	>24
Significant wave height ( $H_s$ )	0	0	0	0	0	0	0	0	0	0	0	0	0	0	0	0	0	0	0	0	0
	0.5	0	0	0	0.1	0.1	0	0	0	0	0	0	0	0	0	0	0	0	0	0	0
	1	0	0	0.4	1.7	1.9	0.7	0.5	1.4	0.6	0.4	0.2	0	0	0.1	0	0	0	0	0	0
	1.5	0.1	0.3	0.3	2.2	4.5	1.8	0.5	1.8	1.6	1.7	1.5	0.4	0	0.1	0	0	0	0	0	0
	2	0	0.7	1.2	2.7	6.5	7.1	1.8	4	4.3	4.5	2.9	0.6	0	0.3	0	0	0	0	0	0
	2.5	0	0.1	0.4	2.1	2.7	3.3	1.2	2.1	2.2	2.8	1.1	0.3	0	0	0	0	0	0	0	0
	3	0	0	0.5	2.2	4.1	2.5	0.7	0.8	1.4	1.9	1.7	0.7	0	0	0	0	0	0	0	0
	3.5	0	0	0	0.4	0.8	0.1	0	0	0.1	0.2	0.3	0	0	0	0	0	0	0	0	0
	4	0	0	0	0.2	0.3	0	0	0	0	0.3	0.4	0.1	0	0	0	0	0	0	0	0
	4.5	0	0	0	0	0.1	0	0	0	0	0.1	0.2	0	0	0	0	0	0	0	0	0
	>5	0	0	0	0	0	0	0	0	0	0	0.1	0	0	0	0	0	0	0	0	0

### 3.5 Suitability of buoy measurements

The location of the three wave buoys along the eastern coastline of Mauritius was sufficient to evaluate the performance of the model.

There is some uncertainty with the peak wave period from the North-East buoy. It is highly likely that the longer period waves ( $T_p > 17$  s) within this data are not physically 'real' but the source of these data points is unclear. When these data points are omitted, the results are similar conditions to the Blue Bay buoy for an overlapping period where incident waves were measured at both locations. Despite these limitations, the measurements at the North-East buoy were considered suitable for model evaluation.

The Blue Bay buoy data had a noticeable absence of waves from the SSE and the waves were instead grouped into two distinct groups (SE and SSW) while the incident waves at the Souillac buoy (which was also a shorted monitoring period) were more directionally distributed. There is some uncertainty about the depth of the Blue Bay wave buoy, which is compounded by the coarse bathymetry data that was available for the shallow coastal areas of Mauritius (see Section 4.3). The dominance to the two incident wave directions may be real or a consequence of some local bathymetry near the deployment location influencing wave refraction patterns. This cannot be determined from the coarse bathymetry. There were times when the buoy data was very different to the wave model results and appeared physically not possible; this suggests that there may have been a fault with the instrument during those periods (discussed further below). Despite these observations, the Blue Bay buoy data (in particular the wave height and period) was suitable for comparison with the model.

The data collected by the Souillac buoy was relatively short (compared to the other measurement stations) but provided important information on the incident waves in the south-east corner of the island. This data was suitable for the model-data comparison.

## 4 Wave Climate Assessment Methodology

### 4.1 General methodology

To assess the wave climate around the island of Mauritius and identify suitable locations for wave energy device trials, a 10-year hindcast wave model analysis was conducted. The hindcast model predictions spanned from Indian Ocean basin scale to a high-resolution island model around Mauritius, then down to a finer coastal scale at key areas of interest. The hindcast performance was measured by comparing the modelled wave conditions with measurements obtained at three locations along the coastline. These measurements spanned different periods of time over an ~6 year period (section 3), which provided a good basis to assess the model performance over the hindcast period. The data produced by the model was then analyzed to obtain an understanding of the monthly, seasonal and annual wave conditions around the island.

### 4.2 Model discretization

The model employed in this study was the Simulating Waves Nearshore (SWAN) wave model Cycle III Version 41.10. SWAN is an energy transformation model that has been specifically developed to simulate the redistribution of wave energy in the nearshore. The model considers a number of important depth-dependent processes as well as wind-wave and wave-wave interactions. The model solves the spectral action balance equation, which determines the evolution of the wave action density spectrum in both frequency and direction. The model is described in detail in the Scientific and Technical Documentation for the model [SWAN Team, 2016]. The model was driven by output from The Centre for Australian Weather and Climate Research's WAVEWATCH III™ re-analysis (CAWCR), which outputs hourly gridded global wind and wave conditions at  $0.4^\circ \times 0.4^\circ$  resolution. This model was validated using remotely sensed satellite altimeter observations (eight instruments from 1985-1989 and then continuously from 1993-2010) and *in-situ* buoy measurements that were predominantly located in the Pacific as well as along the Pacific coastline of the United States of America [Durrant *et al.*, 2014]. For the year 2016, which is outside the CAWCR reanalysis period, the model was driven by output from the NOAA WAVEWATCH III™ operation hindcast model with NCEP winds. We compare the results obtained by the two different forcing conditions for an overlapping period in section 4.5.

Grids of different resolution were nested within the global model to increase the model analysis resolution around Mauritius (Table 4-1). The regional Mascarene grid included the islands of Reunion, Mauritius and Rodrigues, which are poorly resolved in the global wave model. The Mauritius grid focused on the entire island of Mauritius, which enabled coarse changes in bathymetry, and its impact on wave transformations to be evaluated. Finally, the SE Coast grid spanned the coastline of Mauritius from Souillac to Blue Bay in high resolution. This grid was implemented in the model because this section of coastline was considered to be the most viable for wave resource development and thus wave energy device trials.

Table 4-1 - Model grids

Model	Region	Longitude	Latitude	$n_x$	$n_y$	Resolution
WW3	Indian Ocean	22.0 to 89.5 E	50.0 to 5.0 S	270	180	$0.4^\circ$ (~40 km)
SWAN	Mascarene	54.0 to 65.2 E	23.2 to 18.0 S	140	65	$0.08^\circ$ (~8 km)
SWAN	Mauritius	56.56 to 58.56 E	21.28 to 19.28 S	100	100	$0.02^\circ$ (~2 km)
SWAN	SE Coast*	57.3 to 58.09 E	20.7 to 20.51 S	210	50	$0.004^\circ$ (~400 m)

$n_x$  and  $n_y$  are the number of grid cells in the longitudinal and latitudinal directions.

\* SE Coast model was rotated by  $20^\circ$ .

### 4.3 Bathymetry

The large-scale model bathymetry data was sourced from the General Bathymetric Chart of the Oceans (GEBCO, [www.gebco.net](http://www.gebco.net)), which was available on a 0.5° grid. Closer to the island of Mauritius, the GEBCO bathymetry data was supplemented by CMAP data obtained from DHI. Some isolated survey data was also available for specific locations around Mauritius and has been used to enhance the model at those locations. The bathymetric data (Table 4-2) were triangulated and then interpolated onto the grids used in the model (Figure 4-1). The shoreline was defined using data obtained from the National Geophysical Data Center NOAA coastal database [Wessel and Smith, 1996]. We note that additional high-resolution bathymetry datasets are available within the Republic of Mauritius; these datasets were not made available for this study.

Table 4-2 – Bathymetry data used in the model

Data Source	Region Covered	Resolution	Notes
GEBCO	Global coverage	0.5° X 0.5°	-
CMAP (via DHI)	Mauritius Economic Zone	Varies	-
Unknown (via CCE)	Isolated locations around Mauritius	Varies	Depth survey points

### 4.4 Model boundary conditions and physics

The coarse resolution SWAN model (Mascarene) was forced with wave parameters from the global CAWCR and NOAA WWIII models. Bulk parameters from these models were used to define Pierson–Moskowitz (PM) spectra along the nested model boundaries, which were discretised over 38 frequencies that were exponentially spaced from 0.03 Hz to 1 Hz in 180 directions (2° directional resolution). The higher resolution models (Mauritius and SE Coast) were then forced by output from the Mascarene and the Mauritius model, respectively. All models were forced along the boundary at 0.4° resolution, as well as by surface winds (10 m winds:  $U_{10}$  and  $V_{10}$ ) applied spatially over the entire domain.

A spectral numerical model such as SWAN is based on the surface elevation variance (a spectral density function), which is a function of both wave number  $k$  and direction  $\theta$ . This spectral density function  $F(k, \theta)$  is developed in both space and time by various sources and sinks of energy:

$$\frac{DF}{Dt} = S_{source} - S_{sink}$$

There are a number of different physics options that can be selected in both WWIII and SWAN and the choice of physics employed in this study were based upon the project objectives and comparison of the model data with measurements obtained at three locations along the Mauritius coastline (section 5):

1. 3<sup>rd</sup> Generation Model Physics for wind input, quadruplet interactions and white capping. We used the nonlinear saturation-based white capping combined with the wind input of [Yan, 1987].
2. Depth-induced breaking with a constant dissipation proportionality coefficient of 1.0 and a breaker index (ratio of maximum individual wave height over depth) of 0.73.
3. JONSWAP bottom friction [Hasselmann *et al.*, 1973] with a constant coefficient of 0.038.
4. Wave boundary conditions were modelled as a Pierson–Moskowitz (PM) spectrum from bulk parameters obtained from the global wave model at hourly time steps.



5. The Discrete Integration Approximation is used to compute non-linear wave-wave interactions.
6. Empirical diffraction was turned off in the Mascarene domain but was included in the Mauritius and South-East Coast domains.
7. A first order upwind scheme (backward in space, backward in time) was employed in the model with a 15-minute time-step.

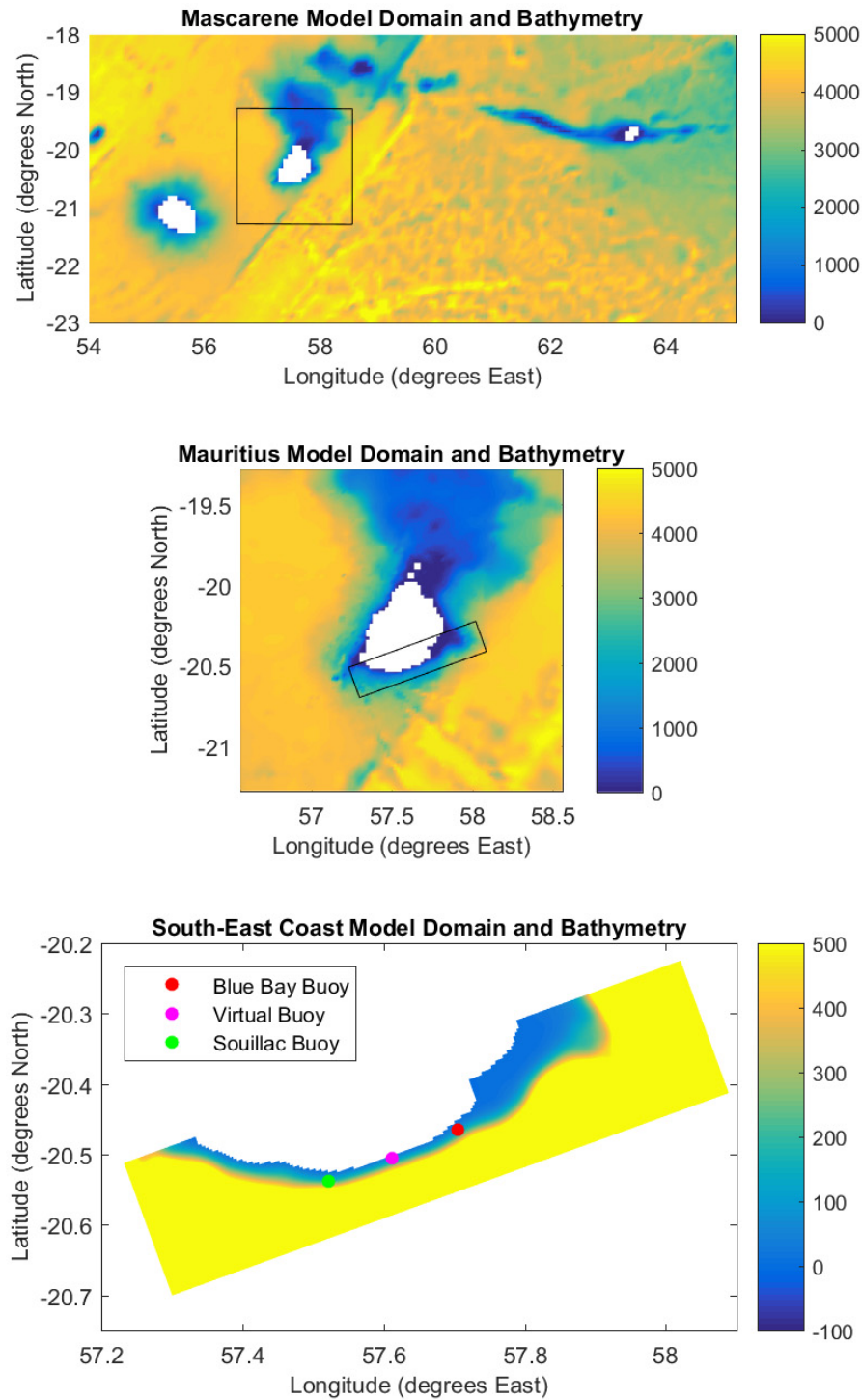


Figure 4-1 (top) Model domain extent and bathymetry for the (top) Mascarene model, (middle) Mauritius model and (bottom) South-East Coast model. The black boxes indicate the nested Mauritius and South-East Coast model domains and the colourbar indicates the depth (in meters).



## 4.5 Model performance

The performance of the model was evaluated by statistically comparing the data obtained from *in-situ* buoy measurements (section 3) to the results obtained at the same coordinates in the numerical model. Three statistical parameters were used: 1) the root-mean-square-error (RMSE) that quantifies the error in the model results when compared to the measured data (equation 1), 2) the constant bias in model results when compared to the measured data (equation 2), and the scatter index (SI), which is the RMSE normalized by the mean measured value (equation 3):

$$\text{RMSE} = \sqrt{\frac{1}{N} \sum_{i=1}^N (M_i - O_i)^2} \quad (1)$$

$$\text{Bias} = \frac{1}{N} \sum_{i=1}^N (M_i - O_i) \quad (2)$$

$$\text{SI} = \frac{\sqrt{\frac{1}{N} \sum_{i=1}^N (M_i - O_i)^2}}{\frac{1}{N} \sum_{i=1}^N O_i} \quad (3)$$

where  $M_i$  is the model value,  $O_i$  is the observed value and  $N$  is the number of timestamps.

Model performance results at the three buoy locations are presented for selected years; the performance results for all periods for which buoy data is available are presented in Appendix A. For each comparison case, the observed and measured  $H_s$ ,  $T_p$  and  $\theta_m$  are compared as a scatter density plot. These figures weight the model performance with the number of samples. To evaluate the capacity of the model to reproduce the wave events in a given year, a timeseries of the measurements and the model is presented for each year.

### 4.5.1 General performance

The model predictions generally agreed well with the model predictions within the constraints of the available data. Overall the model tended to have a wave height ( $H_s$ ) absolute RMSE of <0.4 m and a SI of <20%. This RMSE is consistent and in many cases less than that observed for the comparisons between the buoy data and the CAWCR model [Durrant *et al.*, 2014], where the performance of the model is typically reduced close to coastlines. The reduction in performance in that study was attributed to the application of global winds that do not account for the local variability nor the effects of sea-land boundary interactions. The bias varied between  $\pm 0.2$  m and is consistent with the bias observed in global models [Durrant *et al.*, 2014]. In these models, this bias has been attributed to variations in wind forcing measurement approaches. It is expected that variability in these global forcing conditions will also be prevalent in higher resolution models such as the present model that are nested within these global models.

### 4.5.2 North-East buoy

The North-East buoy was located outside the fine model grid and thus the performance results presented here compare the buoy measurements with model results from the Mauritius model domain. The results show good agreement between the observed and measured  $H_s$  through the densest cluster of data. The RMSE was ~0.4 m and the bias between the measured and modelled data as well as the scatter index was small. The timeseries data demonstrate that at this location and for the time period considered, the model could not only reproduce the variability in the wave conditions but also captured the very large events. There was more scatter in the  $T_p$  and  $\theta_m$  in the buoy data, however the statistical performance of the model with respect to these variables was generally good (Table 4-3).

Similar performance was observed for the periods presented in Appendix A except that for these periods the bias increased for later years considered. This was also observed in the timeseries data where the peak events are reproduced but not always of the correct magnitude; the peak events were usually underestimated.

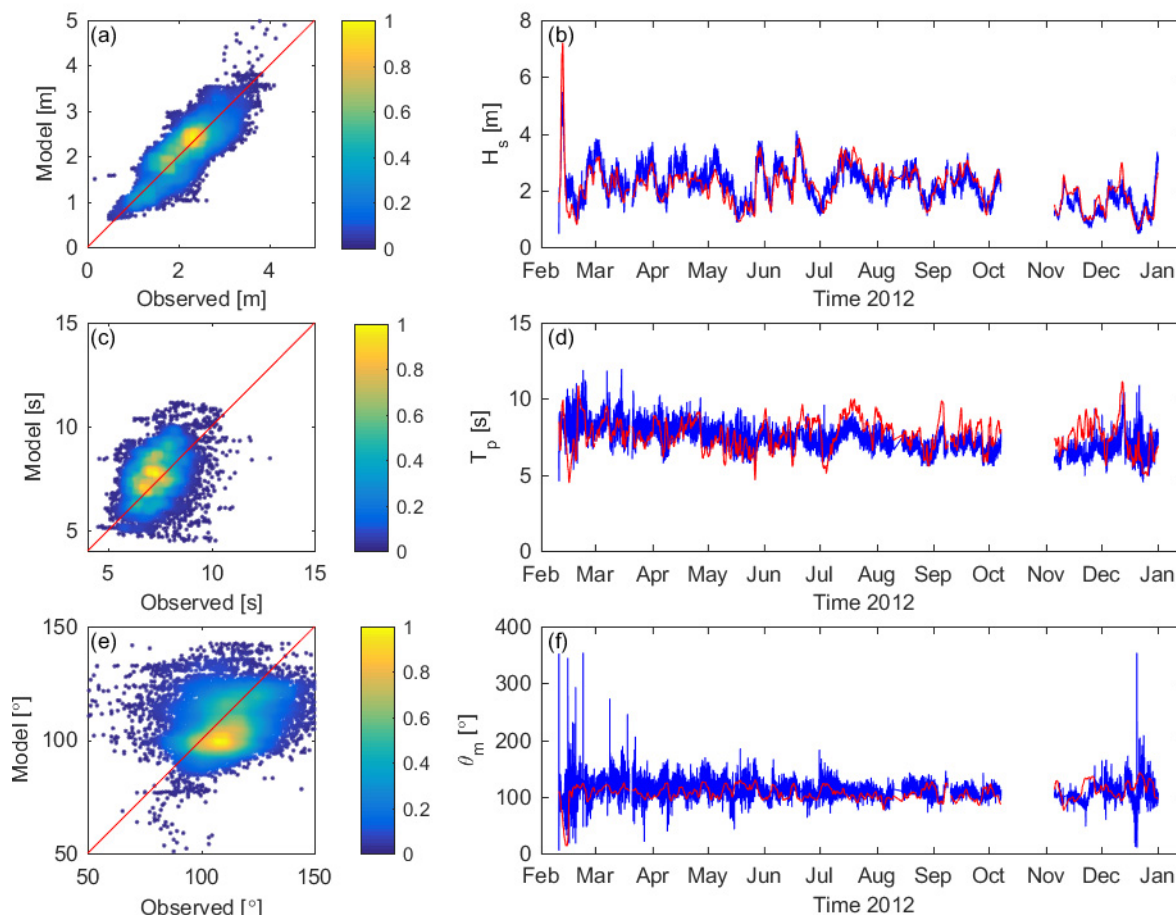


Figure 4-2 Validation of the Mauritius domain with buoy data from the North-East measurement location for 2012. Normalized scatter density plot with the red line indicating 1:1 agreement of (a) significant wave height ( $H_s$ ), (c) Peak Wave Period ( $T_p$ ) and (e) Mean Wave Direction ( $\theta_m$ ). Timeseries from the buoy (blue) and the model (red) of (b)  $H_s$ , (d)  $T_p$  and (f)  $\theta_m$ . The colorbar indicates the normalized density of measurements.

Table 4-3 Statistical measures of the model performance in comparison to the North-East buoy data for 2012 for the significant wave height ( $H_s$ ), Peak Wave Period ( $T_p$ ) and Mean Wave Direction ( $\theta_m$ ). The statistical measures used here were the Root-Mean-Squared Error (RMSE), Bias and the Scatter Index (SI).

Parameter	RMSE	Bias	SI
$H_s$	0.39	0.00	0.18
$T_p$	1.1	0.3	0.15
$\theta_m$	19.3	-4.24	0.17

### 4.5.3 Blue Bay buoy

The Blue Bay buoy was located within all model domains; we consider here the performance within the high-resolution South-East coast domain. The results demonstrated that there was good agreement between the observed and measured  $H_s$  through the densest cluster of data compared in 2014. The bias between the measured and modelled data, SI and RMSE were all similar to those calculated with the North-East buoy (Table 4-4). The model reproduced the variability in the wave heights well. Some peak events were captured well while other events were captured but with slightly lower wave heights than those measured by the buoy. There was more scatter in the  $T_p$ , with the model on average predicting slightly higher peak wave periods. The  $\theta_m$  in the buoy data exhibited substantial directional variability. This variability suggests that the  $\theta_m$  reported in the data may actually be the direction of the peak frequency. This results in much greater variability in the direction due to shifts in the peak frequency of the spectrum as different waves propagate to the measurement location.

The performance results were similar for 2009-2011 except that the bias was larger. The performance was considerably poorer for 2012 (Appendix A) but it should be noted that the 2012 wave buoy data suggests that there may have experienced technical faults with the buoy throughout that year.

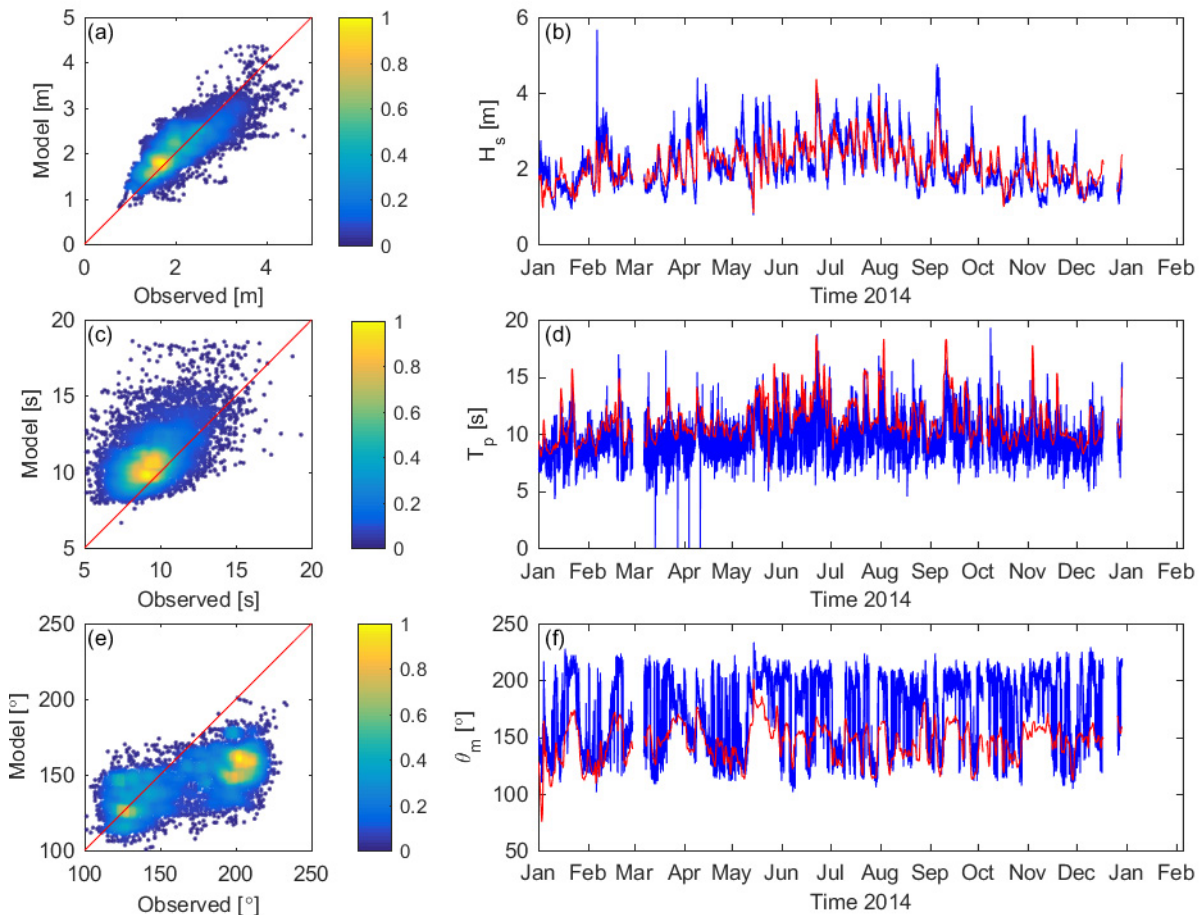


Figure 4-3 Validation of the South-East Coast domain with buoy data from the Blue Bay measurement location for 2014. Normalized scatter density plot red line indicating 1:1 agreement of (a) significant wave height ( $H_s$ ), (c) Peak Wave Period ( $T_p$ ) and (e) Mean Wave Direction ( $\theta_m$ ). Timeseries from the buoy (blue) and the model (red) of (b)  $H_s$ , (d)  $T_p$  and (f)  $\theta_m$ . The colorbar indicates the normalized density of measurements.

Table 4-4 Statistical measures of the model performance in comparison to the Blue Bay buoy data for 2014 for the significant wave height ( $H_s$ ), Peak Wave Period ( $T_p$ ) and Mean Wave Direction ( $\theta_m$ ). The statistical measures used here were the Root-Mean-Squared Error (RMSE), Bias and the Scatter Index (SI).

Parameter	RMSE	Bias	SI
$H_s$	0.38	0.00	0.18
$T_p$	2.2	1.4	0.23
$\theta_m$	35.2	-23.7	0.21

#### 4.5.4 Souillac buoy

The Souillac buoy was located within all model domains; we consider the performance within the high-resolution South-East coast domain. The buoy deployment period was after the most recent global hindcast re-analysis. To evaluate the performance of the hindcast model, the NOAA driven model data was first compared to the CAWCR driven reanalysis model data for an overlapping period (first half of 2016). Here we compare the **mean energy weighted period ( $T_{m01}$ )**, which provides a better representation of the wave climate for wave energy applications. The buoy data was then compared to the model data that was produced with the forcing imposed by the NOAA WaveWatch III (section 4.2).

The  $H_s$  calculated at the Souillac buoy location for both model forcing (NOAA and CAWCR) was similar through the densest cluster of data (Figure 4-4a). The  $T_{m01}$  was observed to be slightly lower in the CAWCR model than in the NOAA WWIII model (Figure 4-4b), but the  $\theta_m$  was similar (Figure 4-4c). The most likely reason for the difference between the two models is the specification of the boundary conditions, which for the CAWCR model was a mean PM spectrum whereas for the NOAA model was a peak PM spectrum; mean parameters are inherently more stable. Overall, the agreement between the two models was similar (Figure 4-4d); thus the use of the NOAA WWIII forcing conditions for comparison with the Souillac seems appropriate over the period when the CAWCR model output was not available.

Assessment of the model performance (Figure 4-5, Table 4-5) indicates that there was good agreement between the observed and modelled  $H_s$  through the densest cluster of data compared in the latter half of 2016. The Bias between the measured and modelled data, SI and RMSE were all similar to those calculated in the North-East buoy comparison. Some peak events were captured well while other events were captured but with slightly lower wave heights than those measured by the buoy. The  $T_p$  was reproduced reasonably well. While a large proportion of the  $\theta_m$  was reproduced in the model, not all directional peaks were reproduced.

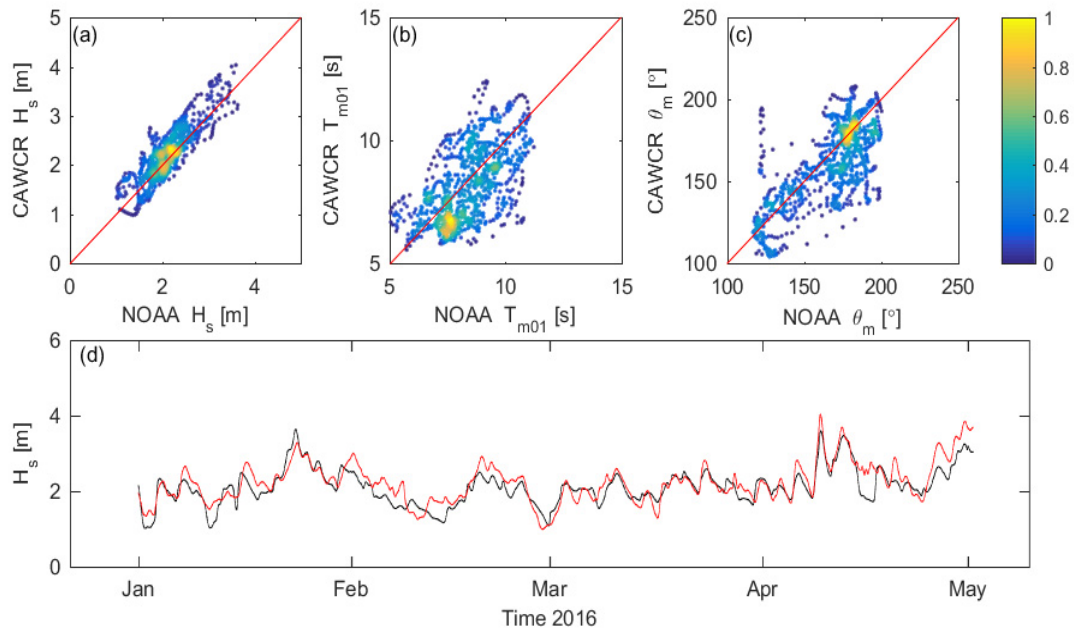


Figure 4-4 Comparison of NOAA and CAWCR driven model for the overlapping period in 2016 at the Souillac measurement location in the South-East Coast domain. Quantity-Quantity plots of (a) significant wave height ( $H_s$ ), (b) Mean Wave Period ( $T_{m01}$ ) and (c) Mean Wave Direction ( $\theta_m$ ). In each plot the red line indicates indicate 1:1 agreement. (d) Timeseries of  $H_s$  from the NOAA driven model (black) and CAWCR driven mode (red). The colorbar indicates the normalized density of measurements.

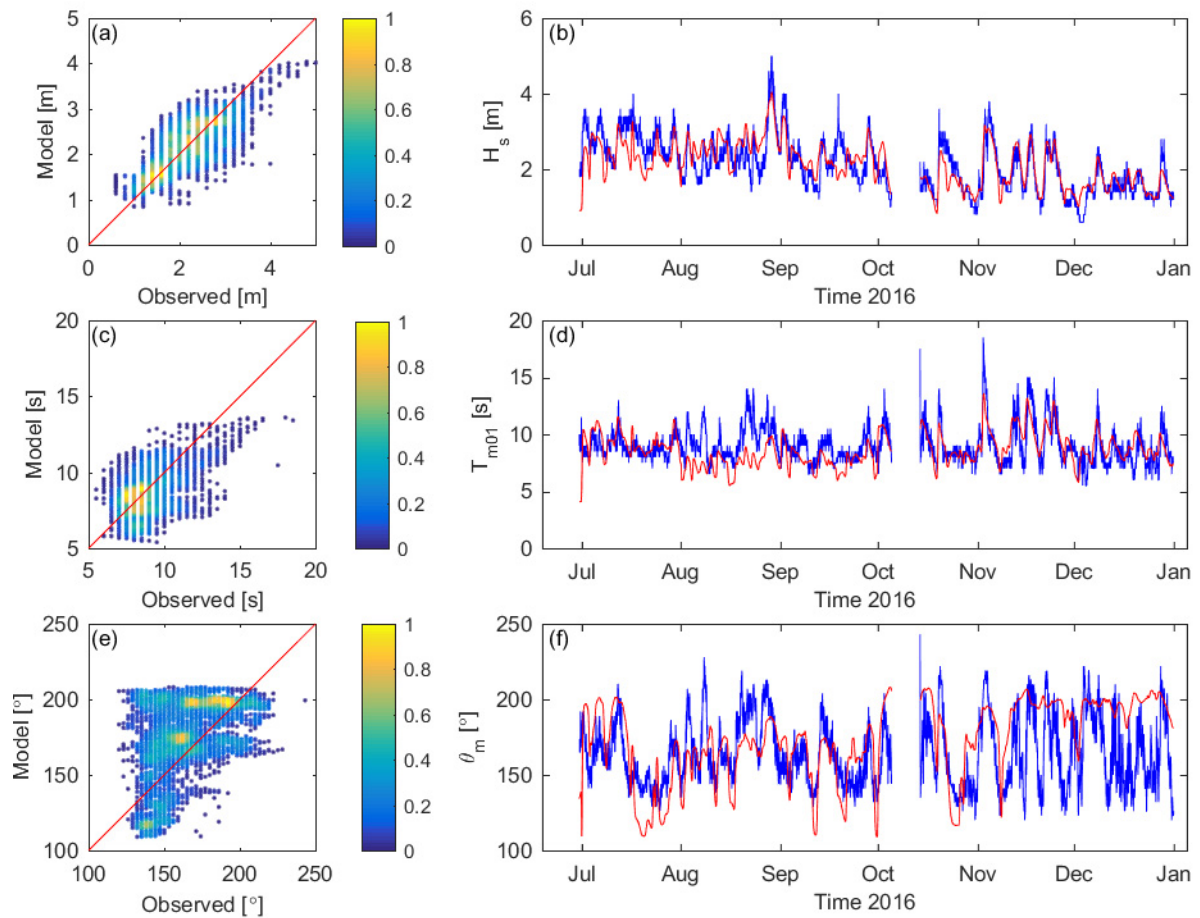


Figure 4-5 Validation of the South-East coast domain with buoy data from the Souillac measurement location for 2016. Normalized scatter density plot red line indicating 1:1 agreement of (a) significant wave height ( $H_s$ ), (c) Peak Wave Period ( $T_p$ ) and (d) Mean Wave Direction ( $\theta_m$ ). Timeseries from the buoy (blue) and the model (red) of (b)  $H_s$ , (d)  $T_p$  and (f)  $\theta_m$ . The colorbar indicates the normalized density of measurements.

Table 4-5 Statistical measures of the model performance in comparison to the Souillac buoy data for 2016 for the significant wave height ( $H_s$ ), Peak Wave Period ( $T_p$ ) and Mean Wave Direction ( $\theta_m$ ). The statistical measures used here were the Root-Mean-Squared Error (RMSE), Bias and the Scatter Index (SI).

Parameter	RMSE	Bias	SI
$H_s$	0.45	-0.00	0.21
$T_{m01}$	1.6	-0.40	0.18
$\theta_m$	27.5	9.0	0.17



## 5 Western Indian Ocean wave climate

It is instructive to start with an analysis of the western Indian Ocean wave climate to establish the source and direction of wave propagation within the basin. Here we consider the significant wave height ( $H_s$ ) and the **Mean Energy Weighted Period** ( $T_{m01}$ ), which provide a better representation of the wave climate than the peak period for wave energy applications.

The 10-year wave climate hindcast for the south-west Indian Ocean indicates that the  $H_s$  is largest in the south-east of the basin and decreases with latitude to the north and with longitude to the west. The mean  $H_s$  averaged over the 10-year period near the island of Mauritius is in the order of ~2.5 m (Figure 5-1a) with a mean  $T_{m01}$  of ~10 s (Figure 5-1b). The 10-year warm season (November – April)  $H_s$  was slightly larger (~2.6 m, Figure 5-2a) while for the cool season (May – October) the average was slightly smaller (~2.2 m, Figure 5-2b).

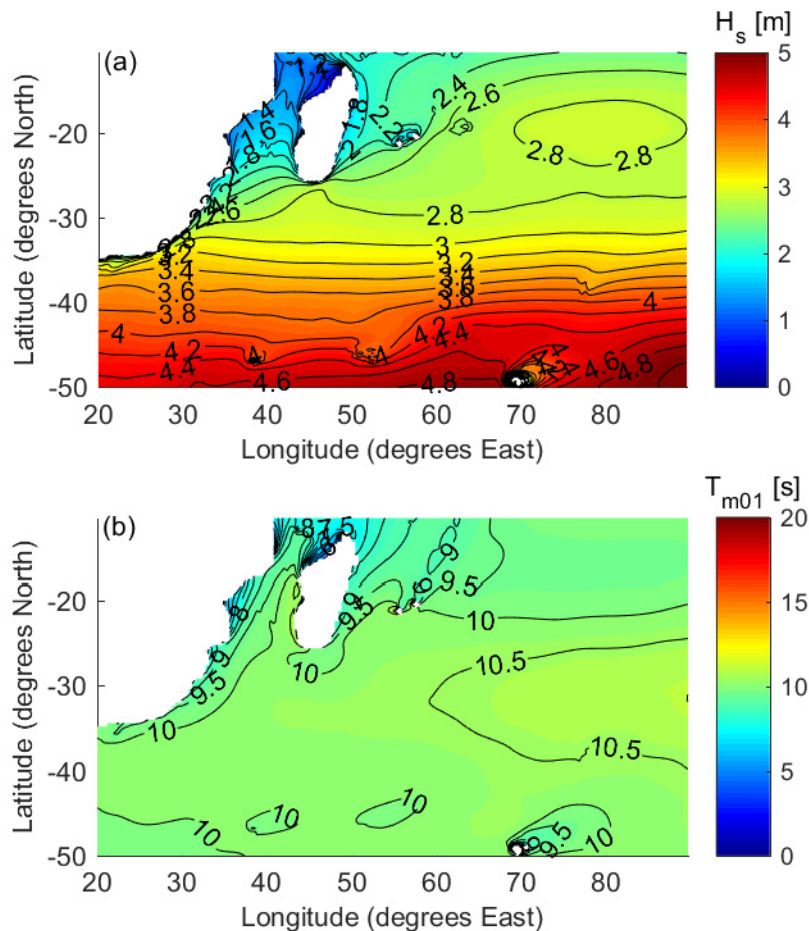


Figure 5-1 The mean (a) significant wave height ( $H_s$ ) and (b) mean energy weighted wave period ( $T_{m01}$ ) for the 10-year hindcast.

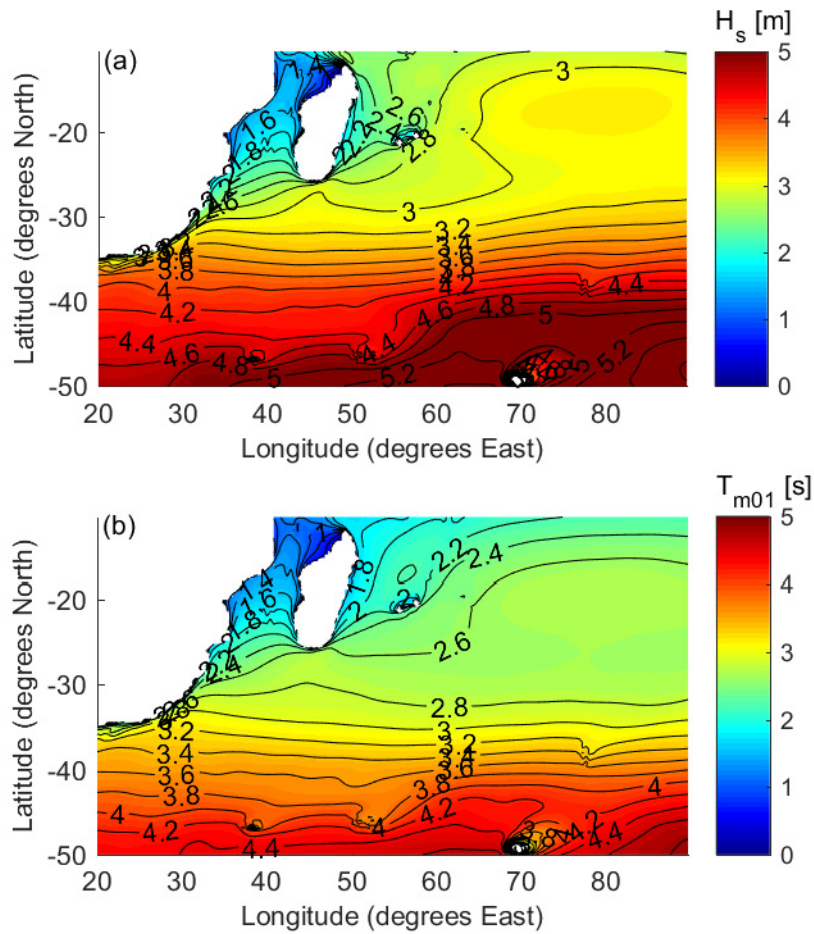


Figure 5-2 Mean significant wave height ( $H_s$ ) for the (a) cool season (May – October) and (b) warm season (November - April) season for the 10-year hindcast.

The maximum  $H_s$  in a given cell over the 10-year wave climate hindcast were much larger, reaching values of ~6-18 m with  $T_{m01}$  in the range 16-18 s (Figure 5-3). While most of these large waves are restricted to the interface between the Indian and the Southern Oceans, bands of larger waves also occurred at lower latitudes towards the equator. These bands of large waves are associated with the propagation of severe tropical storms and cyclones that have traversed through this region during the hindcast period (Figure 5-4). These wave conditions are likely to be beyond the operational conditions of many wave energy devices and thus will serve as an ultimate limit state for the design of the infrastructure.

Closer inspection of the Mascarene region indicates that the  $H_s$  ranges from ~1.8-2.6 m with a  $T_{m01}$  of 6-10 s (Figure 5-5). The maximum  $H_s$  indicated that the wave heights associated with the propagation of cyclones appear to be greatest on the western side of Mauritius (Figure 5-4). However, this is likely due to an individual cyclone passing to the northwest of Mauritius and future cyclones may follow different pathways.



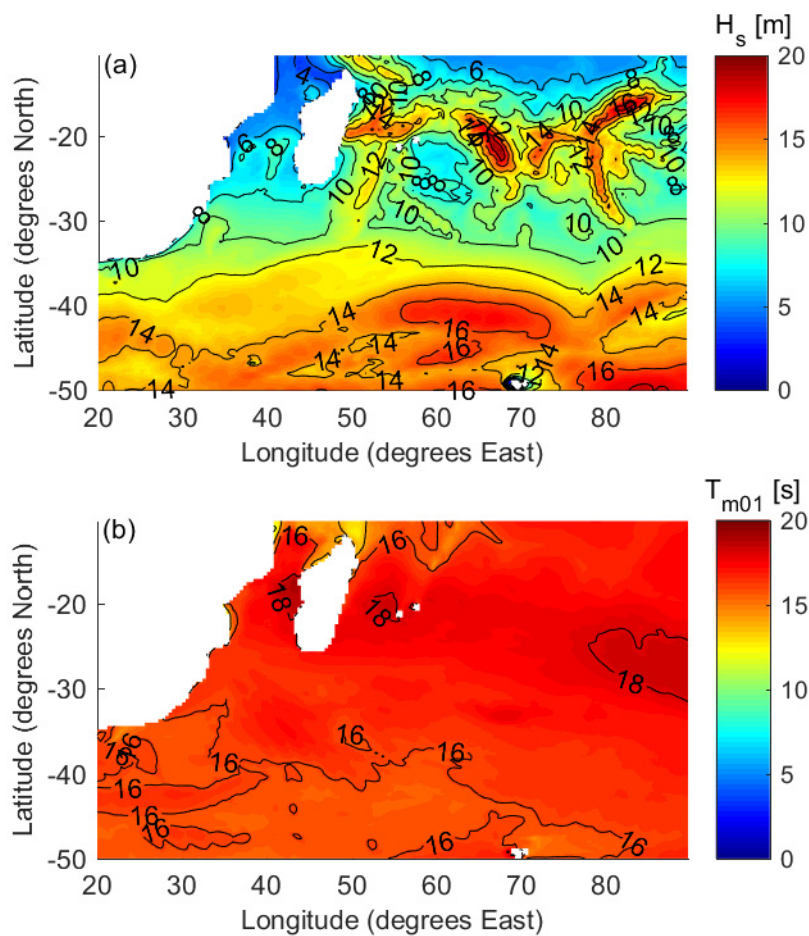


Figure 5-3 The maximum (a) significant wave height ( $H_s$ ) and (b) mean energy weighted wave period ( $T_{m01}$ ) for a given cell over the 10-year wave climate hindcast.

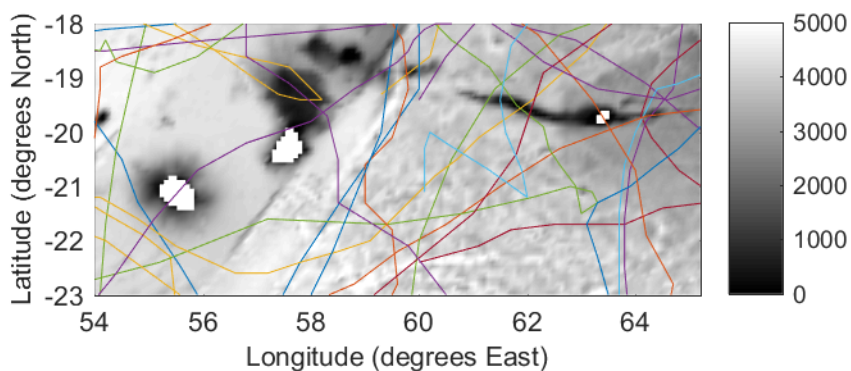


Figure 5-4 Cyclone tracks over the hindcast period [National Oceanic and Atmospheric Administration, 2017]. The coloured lines indicate the different cyclone tracks within the Mascarene region from 2006-2015.

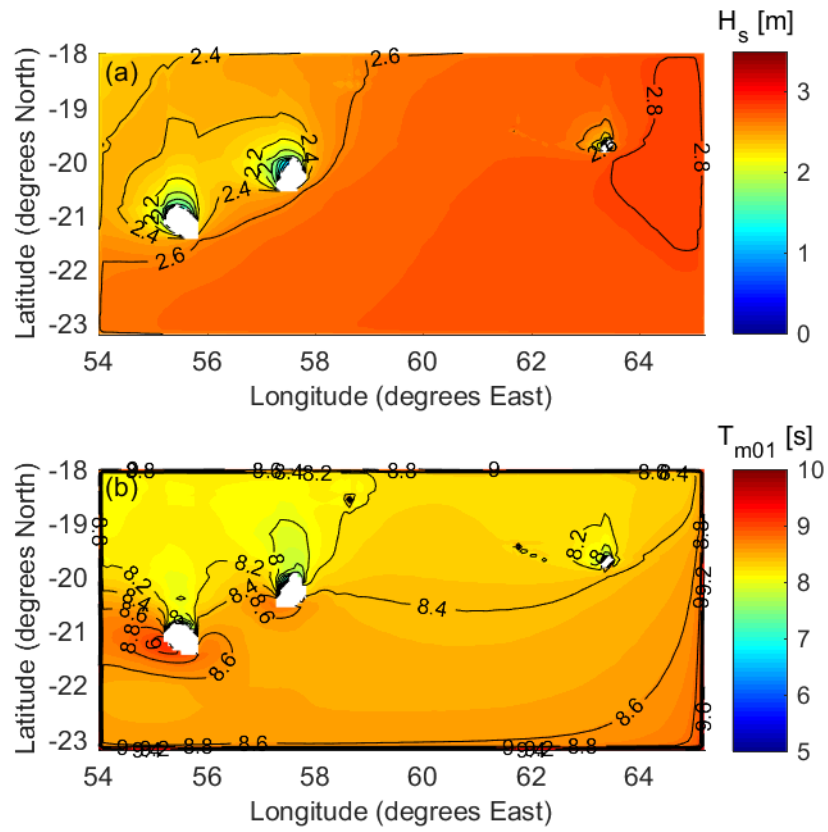


Figure 5-5 Mean wave parameters for the 10-year period from 2006-2015. (a) Significant wave height ( $H_s$ ) and (b) mean energy weighted wave period ( $T_{m01}$ ).

## 6 Mauritius wave climate

Mauritius experiences consistent trade winds from the south-east, which are typically stronger during the cool season. The tide is a very small semi-diurnal tide that ranges from ~0.5 m during neap tide to ~0.6 m during spring tide [Fagoonee, 1990].

The mean  $H_s$  around the island is largest on the southern and south-eastern coastline (Figure 6-1a). Along this section of the coast, large waves that originate from the Indian Ocean propagate to Mauritius and arrive near-normally incident to the coastline. A clear shadow of lower wave heights is observed to the north-east of Mauritius where waves only diffract around the island. The waves here are ~1 m smaller due to the shadowing effect of the island from the dominant wave direction (SSE). In the warm season (Figure 6-2a), the  $H_s$  was ~10% smaller than the annual values while in the cool season (Figure 6-2d) the  $H_s$  was ~10% larger than the  $H_s$  for the hindcast period. These results are similar with the coarse model results obtained near Mauritius from other global wave climate and energy studies [e.g., Cornett, 2008; Arinaga and Cheung, 2012; Reguero et al., 2015]. The  $T_{m01}$  was similar around the island and exhibited little seasonal variability (Figure 6-1b and Figure 6-2b,e).

The wave power (Figure 6-1c) was greatest along the southern and south-eastern coastline, with a 10-year mean value of ~20 kW m<sup>-1</sup>. The wave power was slightly lower (~15 kW m<sup>-1</sup>) during the warm season (Figure 6-2c) but was slightly larger during the cooler season (~25-30 kW m<sup>-1</sup>) (Figure 6-2f). To provide some context to these values, the West Coast of Australia experiences an average wave power of 25-32 kW m<sup>-1</sup> [Hemer et al., 2016], Iberian Peninsula (Spain) experiences 15-50 kW m<sup>-1</sup> [e.g., Iglesias et al., 2009] and the Atlantic coastlines of France, Portugal and the United Kingdom experience 40, 30-40 and 25-40 kW m<sup>-1</sup>, respectively [e.g., Clément et al., 2002].

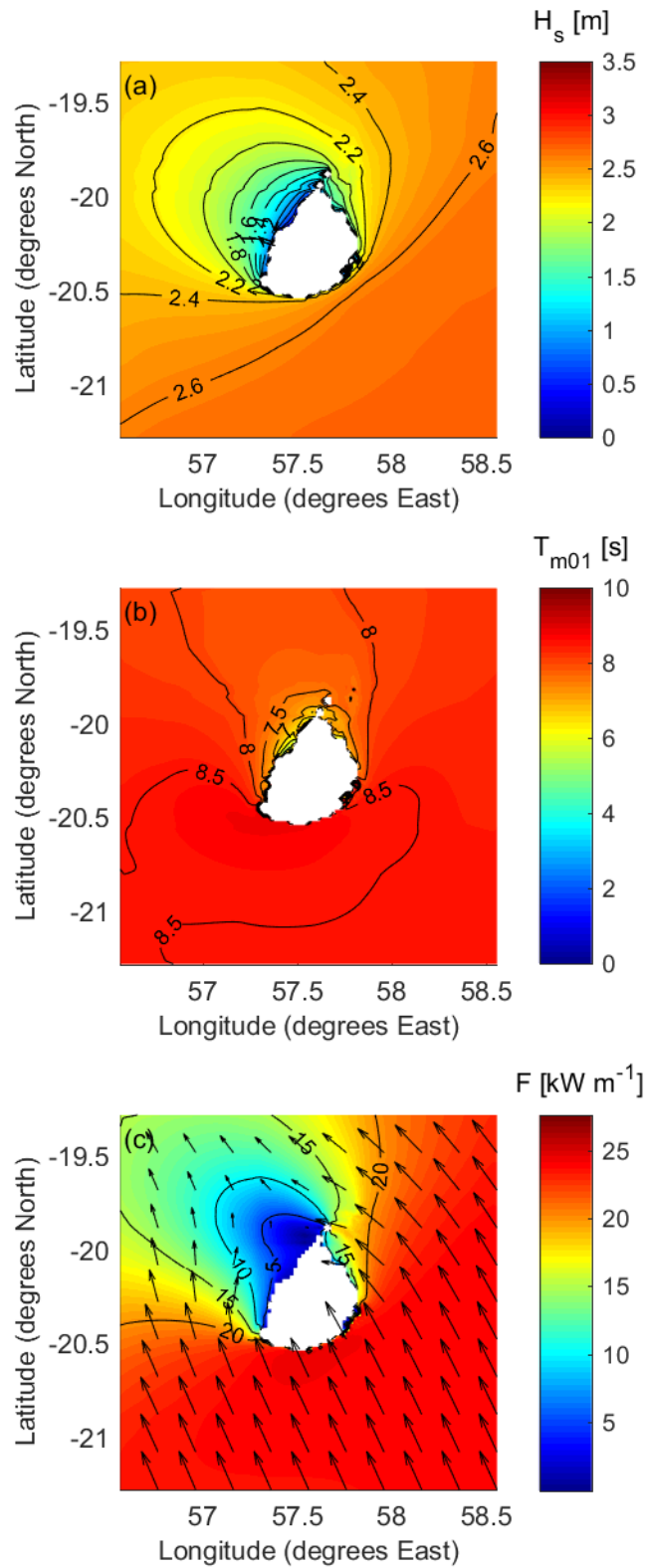


Figure 6-1 Spatial distribution of the (a) significant wave height ( $H_s$ ), (b) mean energy weighted wave period ( $T_{m01}$ ) and (c) wave energy flux ( $F$ ) for the hindcast period 2006-2015.

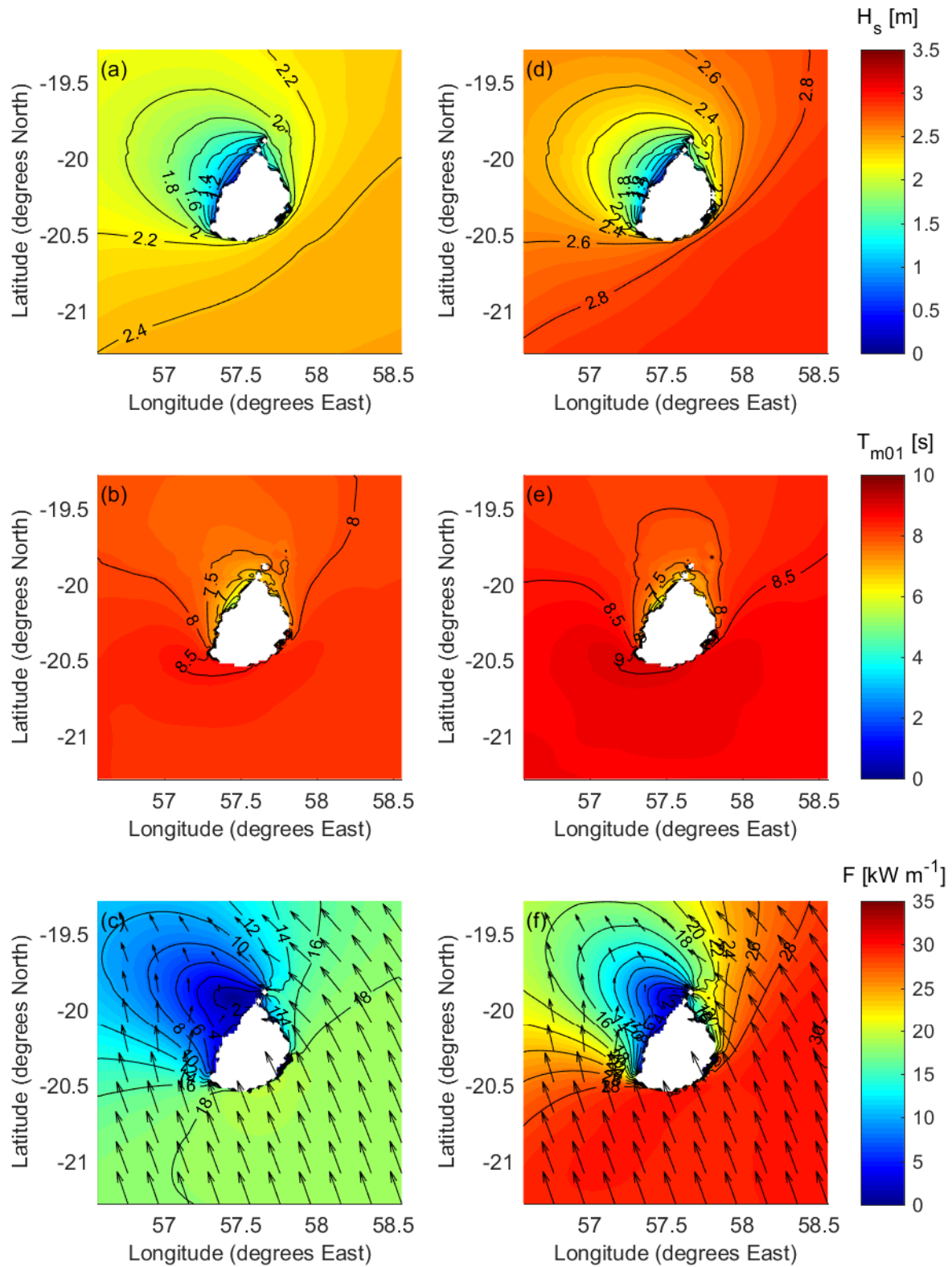


Figure 6-2 Spatial distribution of the (a,d) significant wave height ( $H_s$ ), (b,e) mean energy weighted wave period ( $T_{m01}$ ) and (c,f) wave energy flux ( $F$ ) for the hindcast period 2006-2015 for the (left) warm season (November – April) and (right) cool season (May – October).

## 7 Local south-east Mauritius wave climate

Based upon the results obtained from the wave model of Mauritius, further analysis was conducted to assess the wave climate along the south-east coast of Mauritius. The coastline identified for further investigation was bounded by Souillac in the south and Blue Bay in the north. A wave buoy was deployed by CCE to evaluate the wave conditions near Souillac (section 3), supplementing the Blue Bay wave measurements at the northern end of this section of coast. A higher-resolution numerical model domain (section 3.5) evaluated the wave conditions in water depths that are feasible for the deployment of wave energy devices (<150 m).

Throughout this nearshore model domain, the 10-year average  $H_s$  was largest along the coast between Souillac and Blue Bay (not differing substantially within this region). The  $T_{m01}$  along this section of coastline was between 8 and 9 s. The wave heights decreased north of Blue Bay where the fringing reef and lagoon in the Blue Bay National Park dissipated larger waves as well as to the south of Souillac due to the change in the coastline orientation. Similar spatial observations can be made from the seasonally-averaged figures included in Appendix D.

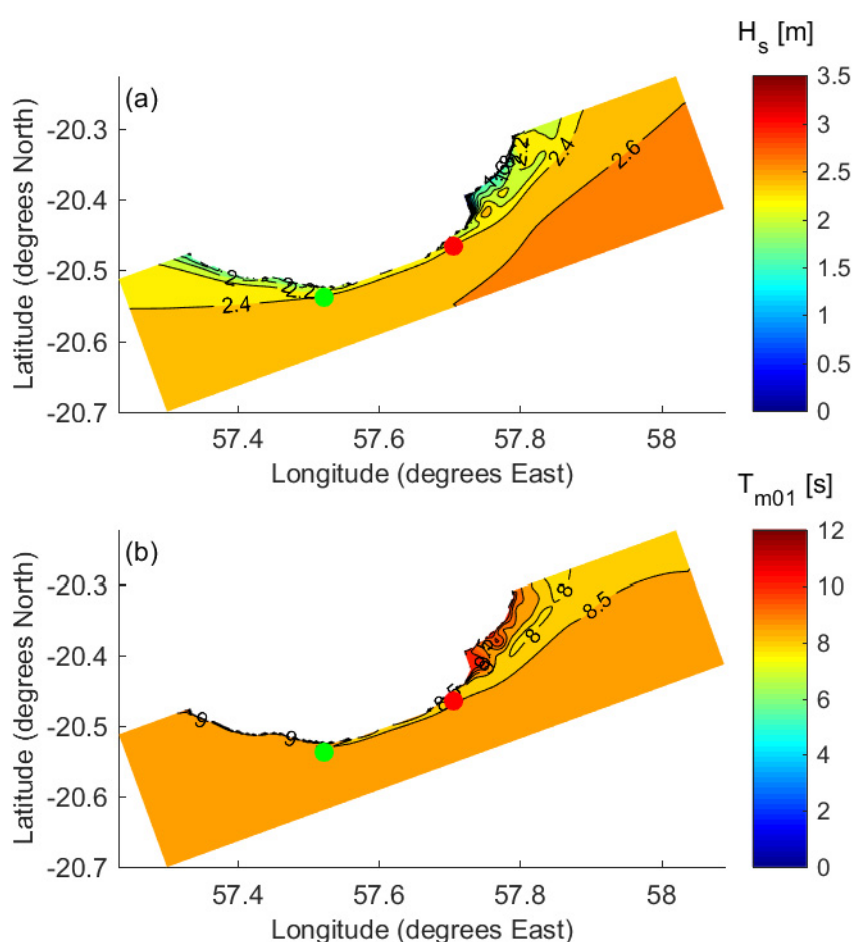


Figure 7-1 Mean wave parameters for the 10-year period from 2006-2015. (a) Significant wave height  $H_s$ . (b) Mean wave period  $T_{m01}$ . The Souillac buoy is located at the green dot and the Blue Bay buoy at the red dot.

The wave climate was characterized in further detail by evaluating the 10-year hindcast data at a virtual buoy located in ~50 m water depth (Figure 4-1c). This depth was selected because it represents the optimum depth that the present generation of wave energy devices are expected to operate in. A transect of the interpolated bathymetry extracted at the location from the coastline of Mauritius into deep water of 500 m demonstrates that the seabed rises rapidly from depth and that the 50 m contour is located only ~600 m from the shoreline at this location. We note here the coarseness of the bathymetry data, particularly in shallow water where the bathymetry is linearly interpolated from only 3 measurement points.

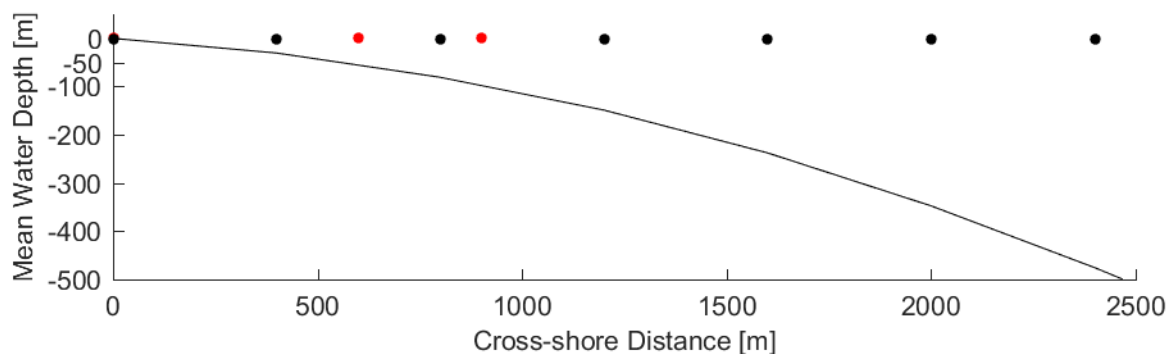


Figure 7-2 Typical cross-shore bathymetry transect at representative buoy location (solid line). The red dots indicate the location where CMAP contours were available and the black dots indicate the locations where GEBCO gridded bathymetry points were approximately located.

This virtual buoy location was selected as it was centered on the highest energy coastal region and located approximately mid-way between the existing buoy data from Souillac and Blue Bay. At this virtual buoy location, there was a clear seasonal variability in the wave conditions (Figure 7-3). A median  $H_s$  of ~2.0 m occurred during the warmer months (November – April), which increased to ~2.5 m during the cooler months (May–October). The upper and lower quartiles were typically 0.4 m on either side of the median value. During the warm season (November–April) the maximum value that was not considered a rare event was ~3.0 m, while during the cool season (May–October) the maximum values was approximately a meter larger (~4.0 m). Here rare events are defined as those waves that are larger than 1.5 times the range of values contained within 25<sup>th</sup> and 75<sup>th</sup> percentiles, but it is noted that these events should be real. While the median periods ( $T_{m01}$  and  $T_e$ ) varied slightly throughout the year, this variation was small ~1 s with the maximum and minimum periods not considered rare events usually within  $\pm 3$  s of the median value. Similarly, there was some variability in the incident wave direction for both the peak and mean wave directions but had a range of ~20°. There is some variability about these values, which can be observed in the joint occurrence tables (Table 7-1 and Appendix E). Thus, the variation in wave height was the predominant factor that determined the seasonal variability in the wave power at this depth, for which the median value ranged from ~17-40 kW m<sup>-1</sup>.

The wave height persistence probabilities for every month (Table 7-3) offer valuable information about the seasons of the year that are most viable for wave energy extraction. During the warm season significant wave heights more often fall below 1.5 m (more than 6% of the time from October to December and more than 10% of the time from January to March) than during the cool season (April to September). In June, July and August the wave heights are consistently high and do not fall below 2 m for more than 10% of the time. The persistence probabilities do not differ noticeably between 3, 6, 12 and 24 hour periods and thus any wave condition tends to be consistent for longer than 24 hours.



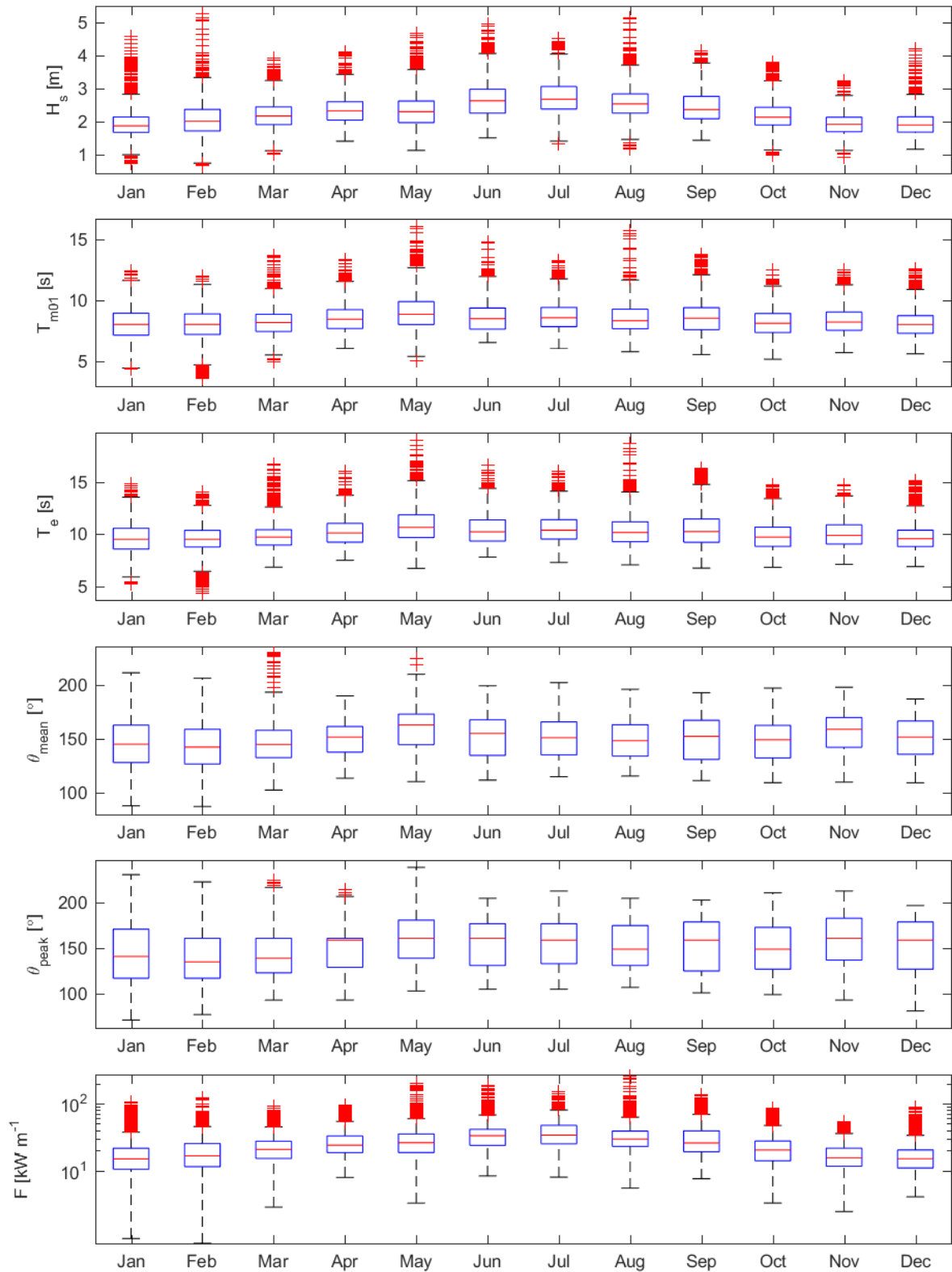


Figure 7-3 Monthly box plots for the hindcast period 2006-2016 of (a) significant wave height ( $H_s$ ), mean wave period ( $T_{m01}$ ), mean wave period ( $T_e$ ), mean wave direction ( $\theta_m$ ), peak wave direction ( $\theta_p$ ) and the wave energy flux ( $F$ ). In each plot, the median value is indicated by the red line, the upper and lower quartiles by the blue box, For each box, the central mark is the median, the edges of the box are the 25th ( $q_1$ ) and 75th ( $q_3$ ) percentiles, the whiskers extend to the most extreme data points not considered rare events. Rare events are plotted individually and were defined as  $q_3 \pm 1.5(q_3 - q_1)$ .



Table 7-1 Joint probability occurrence between significant wave height ( $H_s$ ) and mean energy weighted wave period ( $T_{m01}$ ) (percentage) for model results at the representative buoy located at 50 m depth for the period 2006 – 2015. Monthly tables are presented in Appendix E.

		Mean Period ( $T_{m01}$ )																			
		5	6	7	8	9	10	11	12	13	14	15	16	17	18	19	20	21	22	23	>24
Significant wave height ( $H_s$ )	0	0	0	0	0	0	0	0	0	0	0	0	0	0	0	0	0	0	0	0	0
	0.5	0	0	0	0	0	0	0	0	0	0	0	0	0	0	0	0	0	0	0	0
	1	0.4	1.2	1.2	0.8	0.3	0.1	0	0	0	0	0	0	0	0	0	0	0	0	0	0
	1.5	0.7	4.7	10.2	8.9	3.1	1.1	0.2	0	0	0	0	0	0	0	0	0	0	0	0	0
	2	0.1	3	10.7	12.2	7.3	2.6	0.6	0.1	0	0	0	0	0	0	0	0	0	0	0	0
	2.5	0	1	5.9	6.1	4.8	2.2	0.8	0.1	0.1	0	0	0	0	0	0	0	0	0	0	0
	3	0	0.1	1.3	2.3	1.7	1	0.5	0.2	0.1	0	0	0	0	0	0	0	0	0	0	0
	3.5	0	0.1	0.2	0.5	0.6	0.3	0.1	0.1	0	0	0	0	0	0	0	0	0	0	0	0
	4	0	0	0	0.1	0.1	0.1	0	0	0	0	0	0	0	0	0	0	0	0	0	0
	4.5	0	0	0	0	0	0	0	0	0	0	0	0	0	0	0	0	0	0	0	0
	>5	0	0	0	0	0	0	0	0	0	0	0	0	0	0	0	0	0	0	0	0

Table 7-2 Joint probability occurrence between significant wave height ( $H_s$ ) and mean peak wave period ( $T_p$ ) (percentage) for model results at the representative buoy located at 50 m depth for the period 2006 – 2015. Monthly tables are presented in Appendix E.

		Peak Period ( $T_p$ )																			
		5	6	7	8	9	10	11	12	13	14	15	16	17	18	19	20	21	22	23	>24
Significant Wave Height ( $H_s$ )	0	0	0	0	0	0	0	0	0	0	0	0	0	0	0	0	0	0	0	0	0
	0.5	0	0	0	0	0	0	0	0	0	0	0	0	0	0	0	0	0	0	0	0
	1	0	0.1	0.1	0.5	1	1	0.6	0.5	0.3	0.1	0	0	0	0	0	0	0	0	0	0
	1.5	0	0	0.1	0.8	4.5	7.6	7	4.2	2.3	1.3	0.6	0.2	0.1	0	0	0	0	0	0	0
	2	0	0	0	0.1	1.7	7.6	10.1	8	4	2.2	1.8	0.8	0.2	0.1	0	0	0	0	0	0
	2.5	0	0	0	0.1	0.5	3.2	4.9	4.5	3	2	1.2	0.8	0.4	0.2	0	0	0	0	0	0
	3	0	0	0	0	0.1	0.4	1.2	1.5	1.5	1.1	0.6	0.3	0.3	0.2	0.1	0	0	0	0	0
	3.5	0	0	0	0	0	0.1	0.1	0.2	0.4	0.4	0.2	0	0.1	0.1	0	0	0	0	0	0
	4	0	0	0	0	0	0	0.1	0	0.1	0	0.1	0	0	0	0	0	0	0	0	0
	4.5	0	0	0	0	0	0	0	0	0	0	0	0	0	0	0	0	0	0	0	0
	>5	0	0	0	0	0	0	0	0	0	0	0	0	0	0	0	0	0	0	0	0

Table 7-3 Monthly persistence probability (percentage) table for models results at the virtual buoy located at 50 m depth for the period 2006 – 2015. This table presents the percentage of the time that waves less than a given height typically occur. The shading spans the range 0-99%.

Significant wave height [m]	January				February			
	>6 hrs	>9 hrs	>12 hrs	>24 hrs	>6 hrs	>9 hrs	>12 hrs	>24 hrs
<0.5	0	0	0	0	0	0	0	0
<1.0	0.3	0.2	0.2	0	0.3	0.2	0.2	0
<1.5	12.3	12.2	12.2	10.6	12.3	12.2	12.2	10.6
<2.0	61.4	61	61	58.5	61.4	61	61	58.5
<2.5	89.9	89.9	89.3	89.1	89.9	89.9	89.3	89.1
<3.0	96.8	96.8	96.8	96.8	96.8	96.8	96.8	96.8
<3.5	97.9	97.9	97.9	97.9	97.9	97.9	97.9	97.9
<4.0	99.7	99.7	99.7	99.7	99.7	99.7	99.7	99.7
<4.5	99.9	99.9	99.9	99.9	99.9	99.9	99.9	99.9
<5.0	100	100	100	100	100	100	100	100
<5.5	100	100	100	100	100	100	100	100
	March				April			
	>6 hrs	>9 hrs	>12 hrs	>24 hrs	>6 hrs	>9 hrs	>12 hrs	>24 hrs
<0.5	0	0	0	0	0	0	0	0
<1.0	0.3	0.2	0.2	0	0	0	0	0
<1.5	12.3	12.2	12.2	10.6	0.2	0.2	0.2	0
<2.0	61.4	61	61	58.5	20.9	20.6	20.4	17.9
<2.5	89.9	89.9	89.3	89.1	67.3	67.1	66.9	65.4
<3.0	96.8	96.8	96.8	96.8	92.8	92.8	92.8	91.9
<3.5	97.9	97.9	97.9	97.9	99.1	99.1	99.1	98.9
<4.0	99.7	99.7	99.7	99.7	99.8	99.8	99.8	99.8
<4.5	99.9	99.9	99.9	99.9	100	100	100	100
<5.0	100	100	100	100	100	100	100	100
<5.5	100	100	100	100	100	100	100	100
	May				June			
	>6 hrs	>9 hrs	>12 hrs	>24 hrs	>6 hrs	>9 hrs	>12 hrs	>24 hrs
<0.5	0	0	0	0	0	0	0	0
<1.0	0	0	0	0	0	0	0	0
<1.5	2.4	2.3	2.3	2	0	0	0	0
<2.0	26.6	26.3	26	23.1	9.6	9.4	9.1	7.2
<2.5	66.8	66.4	66.4	65.3	39.7	39.5	39.1	36.3
<3.0	90.6	90.6	90.5	90.2	82.5	82.5	82.2	81.3
<3.5	98.1	98.1	98.1	97.8	95.6	95.6	95.4	95.1
<4.0	99.4	99.4	99.4	99.4	98.3	98.3	98.3	98.3
<4.5	99.9	99.9	99.9	99.9	99.7	99.7	99.7	99.7
<5.0	100	100	100	100	100	100	100	100
<5.5	100	100	100	100	100	100	100	100
	July				August			
	>6 hrs	>9 hrs	>12 hrs	>24 hrs	>6 hrs	>9 hrs	>12 hrs	>24 hrs
<0.5	0	0	0	0	0	0	0	0
<1.0	0	0	0	0	0	0	0	0
<1.5	0.2	0.2	0.2	0	0.2	0.2	0.2	0
<2.0	7	6.7	6.6	4.8	10.1	9.9	9.4	7.9
<2.5	34.8	34.7	34.2	30.2	45.9	45.5	45.4	42.6
<3.0	71	70.7	70.4	69.1	84.4	84.4	84.2	83
<3.5	93.4	93.3	93.3	93.1	96.1	96	95.9	95.9
<4.0	98.6	98.5	98.5	98.5	99.2	99.2	99.2	99.2
<4.5	100	99.9	99.9	99.9	99.8	99.8	99.8	99.8
<5.0	100	100	100	100	99.9	99.9	99.9	99.9
<5.5	100	100	100	100	100	100	100	100

Table continues on next page

Significant wave height [m]	September				October			
	>6 hrs	>9 hrs	>12 hrs	>24 hrs	>6 hrs	>9 hrs	>12 hrs	>24 hrs
<0.5	0	0	0	0	0	0	0	0
<1.0	0	0	0	0	0.1	0	0	0
<1.5	0.2	0.2	0.2	0	4.4	4.4	4.1	3.5
<2.0	16.6	16.5	16.1	12.7	37.2	36.9	36.4	33.5
<2.5	58.5	58.2	57.8	55.2	79.5	79.5	79.1	78.5
<3.0	83.8	83.8	83.8	82.8	94.7	94.7	94.7	94.2
<3.5	96.4	96.4	96.3	95.9	99	99	99	99
<4.0	99.8	99.8	99.8	99.8	100	100	100	100
<4.5	100	100	100	100	100	100	100	100
<5.0	100	100	100	100	100	100	100	100
<5.5	100	100	100	100	100	100	100	100
	November				December			
	>6 hrs	>9 hrs	>12 hrs	>24 hrs	>6 hrs	>9 hrs	>12 hrs	>24 hrs
<0.5	0	0	0	0	0	0	0	0
<1.0	0	0	0	0	0	0	0	0
<1.5	8.1	7.7	7.7	7	6.2	6.2	6.2	4.6
<2.0	60.9	60.6	60.2	56.5	61.9	61.8	61.5	60
<2.5	95.9	95.9	95.9	95.9	94.6	94.6	94.6	94.5
<3.0	99.6	99.6	99.6	99.6	98.7	98.7	98.6	98.6
<3.5	100	100	100	100	99.4	99.4	99.4	99.4
<4.0	100	100	100	100	99.8	99.8	99.8	99.8
<4.5	100	100	100	100	100	100	100	100
<5.0	100	100	100	100	100	100	100	100
<5.5	100	100	100	100	100	100	100	100

## 7.1 Extreme value analysis

The Point-Over-Threshold (POT) method was used to systematically analyze the distribution of the rare events and to estimate the expected wave height for different annual return intervals (ARI) outside the range of observed values. A fundamental assumption that underpins this approach is that the extreme tail of the distribution takes a simple form irrespective of the form of the central parts of the distribution. A fit can then be made to this extreme tail and expected values estimated.

To define the threshold used in the POT analysis, a de-clustering algorithm was used to identify peaks that were sufficiently far apart to be independent from which the largest waves could then be identified. To determine the suitability of the threshold, it was assumed that these peaks occur randomly in time and thus can be considered a Poisson process. Based on this assumption the dispersion index was calculated, which is the ratio between the variance and the expectation of the number of peaks. A threshold that results in a dispersion index close to one was considered acceptable. To estimate the expected values for various ARI (Table 7-4), the Generalized Pareto Distribution was used.

There are a number of importance limitations that must be considered with regards to the extreme value analysis presented here:

- the uncertainty of the analysis increases for return intervals longer than 10 years;
- the results may be biased high, i.e., if an event with a return period larger than 10 years occurred within the hindcast period.
- extreme wave heights related to tropical cyclones are strongly reliant on the pathway of the cyclone, i.e. on which side of the island and at what distance the cyclone passes;
- it is assumed that the wave statistics do not change in the future, however the effect of climate change on the global and regional weather patterns is likely to affect the Indian Ocean wave climate and thus the expected return levels presented here.

Table 7-4 Expected values for various Annual Return Intervals

Annual Return Interval [years]	Significant wave height [m]		
	50% Confidence (Lower Band)	Expected Return Level	50% Confidence (Upper Band)
<b>1</b>	3.9	4.6	6.2
<b>2</b>	4.0	4.9	6.8
<b>5</b>	4.2	5.2	7.4
<b>10</b>	4.3	5.4	7.8
<b>20</b>	4.4	5.7	8.1
<b>50</b>	4.6	5.9	8.5
<b>100</b>	4.7	6.1	8.8

## 8 Suitability for wave energy device trials

In this section the suitability of the South East Coastline of Mauritius for wave energy devices is considered. Specifically, attention is placed on potential power generation and extreme conditions, which represent both opportunities and challenges for wave energy generating devices. The simulated wave climate is also interpreted in regards to the possibility of device maintenance and short term trials.

### 8.1 Power Generation

As noted in section 6, the wave energy flux approaching the South Eastern Coastline of Mauritius is  $\sim 20 \text{ kW m}^{-1}$ , varying between averages of  $\sim 15 \text{ kW m}^{-1}$  in the warm season to  $\sim 25\text{--}35 \text{ kW m}^{-1}$  in the cooler season. These values are lower than that experienced on the West Coast of Australia ( $25\text{--}32 \text{ kW m}^{-1}$ ), the Iberian Peninsula ( $15\text{--}50 \text{ kW m}^{-1}$ ), and the Atlantic coastlines of the UK and France ( $25\text{--}40 \text{ kW m}^{-1}$ ). It should be noted that the peak period predicted by the model is larger than that recorded at the Blue Bay buoy (see Appendix C). This means that the model will tend to over-predict power to some extent, although how much is difficult to determine. Note that the peak period value from the model is not used to calculate power. This uncertainty highlights the importance of comparison with buoy spectral data, which would allow the energy transport (flux) to be compared with the model. In comparison to electricity consumption in Mauritius, which was  $\sim 2500 \text{ GWh year}^{-1}$  (285 MW) in 2012 [Brizmohun *et al.*, 2015], the wave energy flux incident on the South Eastern Coastline is approximately 2-3 times total electricity demand.

As is well-known, intra-annual variability tends to be lower in the southern hemisphere, particularly when compared to the North Atlantic (e.g. a factor of 10 difference between the mean monthly power in mid-winter and mid-summer reported for the Irish west coast in Ramos and Ringwood [2016]).

Table 7-1 indicates the range of wave height and period experienced at a depth of 50 m aggregated between 2006-2015. Most sea-states have a mean period in the range 5-11 seconds, with 7-9 seconds the most frequent. The significant wave height ( $H_s$ ) is normally less than 4 m, with 1.5-2.5 m most common. This range in occurrence is important because the Power Take Off (PTO) for wave energy devices must normally be 'tuned' for different seastates to keep efficiency high. In a similar vein, the spectral bandwidth is important [e.g., Saulnier *et al.*, 2007].

### 8.2 Extreme Conditions

Wave energy device design should take into account extreme loads and the waves that cause them. In this report  $H_s$  are given for various return intervals up to 100 years. For the virtual buoy location on the south coast the mean  $H_s$  is approximately 2-2.5 m and the 100-year  $H_s$  is estimated to be up to 8.8 m. As the mean  $H_s$  approximately corresponds to income, and the max  $H_s$  to cost, the ratio is instructive – and is estimated here to be  $\sim 4$  or less. This compares to values for 12 sites in the North Atlantic and North Sea given in Santo *et al.* [2016] from which the same ratio may be calculated as between 6 and 7.

For nearshore wave energy devices the wave height will eventually be limited by breaking, although not for the depths and wave heights discussed here.

### 8.3 Maintenance and short term trials

For a wave energy device deployment, particularly at trial stage, it is necessary to have adequate weather windows for installation activities to take place. In this respect, the persistence data in Table 7-3 clearly shows that the warm season generally has more favourable weather windows, although there is a slight offset – October-March is favourable from this standpoint rather than November-April as defined above. However, this period is also tropical cyclone season in Mauritius, suggesting that perhaps the end of the period (e.g.

November and March) may be preferable to the middle of the warm season from this perspective.

## 9 Recommendations

The scope of the present study was limited to an assessment of the wave-resources around the island of Mauritius, with the aim to identify suitable site(s) for the deployment of wave energy devices. The aim of this study was not to conduct a detailed specific site assessment. The following recommendations are made based on the results of this study:

- 1. The South-East coastline spanning ~20 km from Souillac to Blue Bay appears to offer the wave conditions well-suited for the current generation of wave energy devices.**

Based on the 10-year period considered in this wave climate assessment, the south-east coastline of Mauritius appears to offer the wave conditions most suitable for the deployment of wave energy devices. This section of coastline is consistently subjected to incident waves that originate from the Indian Ocean basin with little modification caused by diffraction and refraction. The wave energy resource along this section of coastline does not appear to vary significantly.

- 2. Higher resolution bathymetry is required along the coastline for any subsequent modelling efforts.**

The bathymetry that was used in this study was a combination of the General Bathymetry Chart of the Oceans and CMAP data. While this data was suitable to evaluate the propagation of waves through the Indian Ocean basin to Mauritius, the resolution is insufficient to evaluate the local transformation of the waves as they approach the island. The geological form of the island means that the bathymetry rises rapidly from large depths over short horizontal distances that are not well resolved by these global bathymetry datasets and available nautical charts.

- 3. Additional simulations with high resolution bathymetry (order 10 m) are recommended prior to wave energy device trials to determine the precise location for deployment along the section of coastline.**

The model developed and used in the present study assessed the wave propagation from the Indian Ocean basin to, and around, Mauritius. The model did not resolve bathymetric features that may locally affect the wave climate at a scale that would be considered for the deployment of a wave energy device (i.e., scale of a project site). If a wave energy device deployment is considered, additional simulations are recommended with high resolution bathymetry (order 10 m) to ensure there are no unusual topographic features that could locally influence coastal wave fields (e.g., via refraction).

## References

- Arinaga, R. A., and K. F. Cheung (2012), Atlas of global wave energy from 10 years of reanalysis and hindcast data, *Renew. Energy*, 39(1), 49–64, doi:10.1016/j.renene.2011.06.039.
- Brizmohun, R., T. Ramjeawon, and A. Azapagic (2015), Life cycle assessment of electricity generation in Mauritius, *Bridg. More Sustain. Future Join. Environ. Manag. Sustain. Univ. EMSU Eur. Roundtable Sustain. Consum. Prod. ERSCP Conf.*, 106, 565–575, doi:10.1016/j.jclepro.2014.11.033.
- Clément, A. et al. (2002), Wave energy in Europe: current status and perspectives, *Renew. Sustain. Energy Rev.*, 6(5), 405–431, doi:10.1016/S1364-0321(02)00009-6.
- Cornett, A. M. (2008), A Global Wave Energy Resource Assessment, in *ISOPE-I-08-370*, International Society of Offshore and Polar Engineers, ISOPE.
- Durrant, T., D. Greenslade, M. Hemer, and C. Trenham (2014), *A global wave hindcast focussed on the Central and South Pacific*.
- Fagoonee, I. (1990), Coastal marine ecosystems of Mauritius, *Hydrobiologia*, 208(1–2), 55–62, doi:10.1007/BF00008443.
- Hasselmann, K., T. P. Barnett, E. Bouws, H. Carlson, D. E. Cartwright, K. Enke, J. A. Ewing, H. Gienapp, D. E. Hasselmann, and P. Kruseman (1973), *Measurements of wind-wave growth and swell decay during the Joint North Sea Wave Project (JONSWAP)*, Deutsches Hydrographisches Institut.
- Hemer, M. A., S. Zieger, T. Durrant, J. O’Grady, R. K. Hoeke, K. L. McInnes, and U. Rosebrock (2016), A revised assessment of Australia’s national wave energy resource, *Renew. Energy*, doi:10.1016/j.renene.2016.08.039.
- Iglesias, G., M. López, R. Carballo, A. Castro, J. A. Fraguera, and P. Frigaard (2009), Wave energy potential in Galicia (NW Spain), *Renew. Energy*, 34(11), 2323–2333, doi:10.1016/j.renene.2009.03.030.
- National Oceanic and Atmospheric Administration (2017), Joint Typhoon Warning Centre Best Tracks, *Jt. Typhoon Warn. Cent. JTWC*. Available from: [https://metoc.ndbc.noaa.gov/en/web/guest/jtwc/best\\_tracks/](https://metoc.ndbc.noaa.gov/en/web/guest/jtwc/best_tracks/)
- Ramos, V., and J. V. Ringwood (2016), Exploring the utility and effectiveness of the IEC (International Electrotechnical Commission) wave energy resource assessment and characterisation standard: A case study, *Energy*, 107, 668–682, doi:10.1016/j.energy.2016.04.053.
- Reguero, B. G., I. J. Losada, and F. J. Méndez (2015), A global wave power resource and its seasonal, interannual and long-term variability, *Appl. Energy*, 148, 366–380, doi:10.1016/j.apenergy.2015.03.114.
- Santo, H., P. H. Taylor, and R. Gibson (2016), Decadal variability of extreme wave height representing storm severity in the northeast Atlantic and North Sea since the foundation of the Royal Society, *Proc. R. Soc. Math. Phys. Eng. Sci.*, 472(2193), doi:10.1098/rspa.2016.0376.



- Saulnier, J.-B., P. Ricci, M. T. Pontes, and A. de O. Falcão (2007), Spectral bandwidth and WEC performance assessment, in *EWTEC 2007-7th European Wave and Tidal Energy Conference*.
- SWAN Team (2016), *SWAN Scientific and Technical Documentation, SWAN Cycle III version 41.10*, Delft University of Technology.
- Wessel, P., and W. H. F. Smith (1996), A global, self-consistent, hierarchical, high-resolution shoreline database, *J. Geophys. Res. Solid Earth*, 101(B4), 8741–8743, doi:10.1029/96JB00104.
- Yan, L. (1987), *An improved wind input source term for third generation ocean wave modelling*, KNMI.

## Appendix A North-East Buoy Data

### A.1 Original data

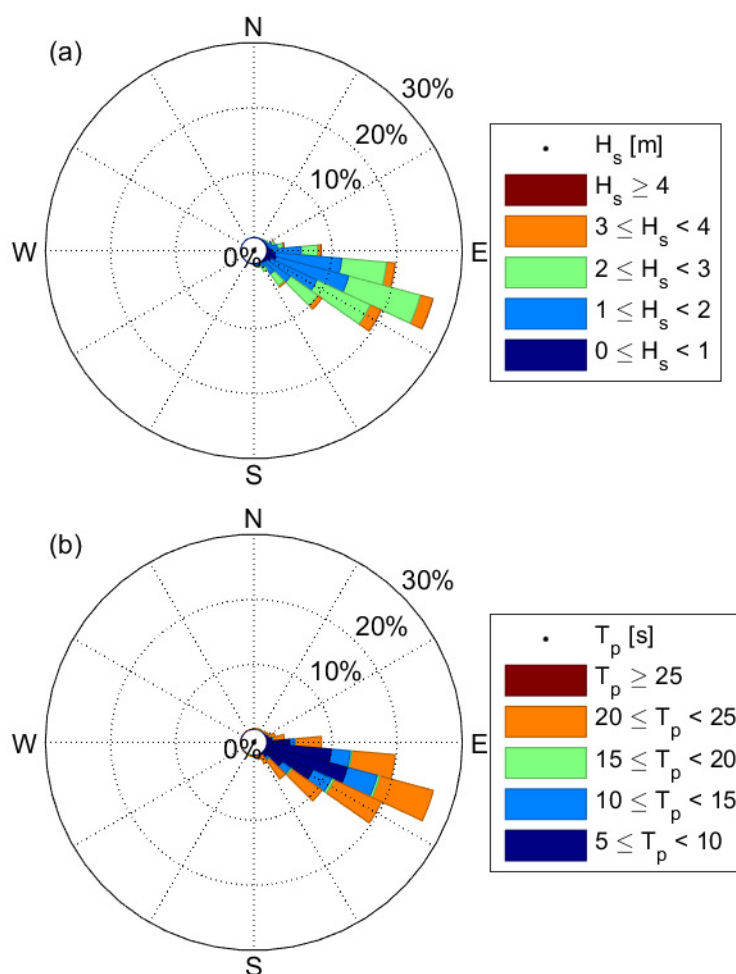


Figure A-1 Wave roses of the incident waves measured at the North-East buoy during the period 09/02/2012 – 14/01/2015. (a) The significant wave height ( $H_s$ ) and (b) peak wave period ( $T_p$ ).

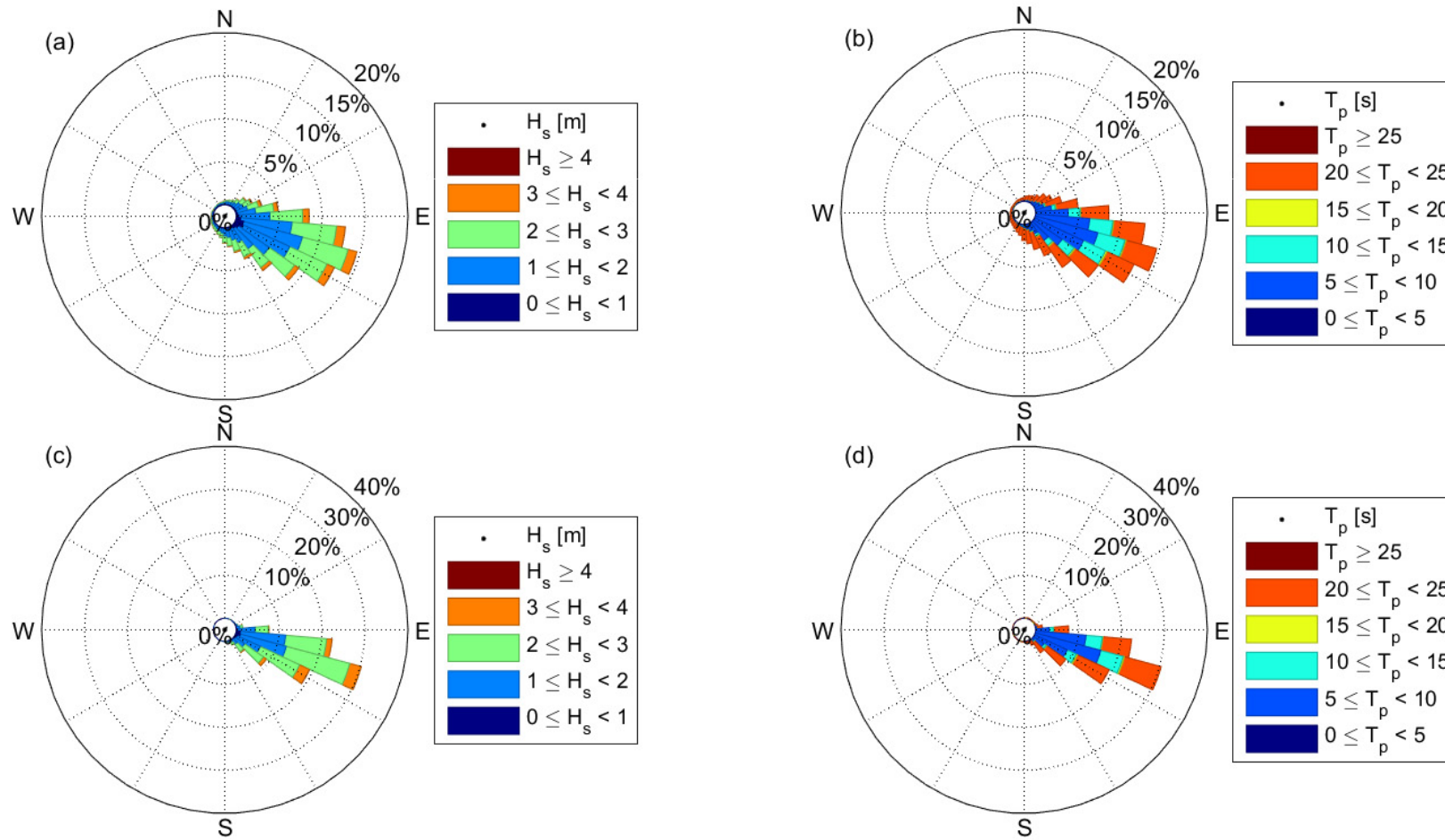


Figure A-2 Wave roses of the incident waves measured at the North-East buoy during the period 09/02/2012 – 14/01/2015. (a) The significant wave height ( $H_s$ ) and (b) peak wave period ( $T_p$ ) during the warm season (November – April,  $N=47577$ ). (c)  $H_s$  and (d)  $T_p$  during

Table A-1 Warm season joint probability occurrence between significant wave height ( $H_s$ ) and peak wave period ( $T_p$ ) (percentage) for measurements at the North-East buoy obtained during the period 09/02/2012 to 14/01/2015 (N=47566). The high proportion of long waves ( $T_p > 17$  s) is questionable. Joint probability occurrence between significant wave height ( $H_s$ ) and the energy weighted mean period ( $T_{m01}$ ) are presented in Appendix B.

		Peak Period ( $T_p$ )																			
		5	6	7	8	9	10	11	12	13	14	15	16	17	18	19	20	21	22	23	>24
Significant wave height ( $H_s$ )	0	0	0	0	0.1	0	0	0	0	0	0	0	0	0	0	0	0.1	0.1	0.2	0.3	1.4
	0.5	0	0.3	1.2	1.7	0.9	0.2	0	0	0	0	0	0	0	0	0	0.1	0	0	0	0.3
	1	0.1	0.5	1.6	3.8	3.8	1.3	0.4	0.1	0	0	0	0.1	0.1	0.2	0.2	0.5	0.5	0.6	0.9	4.4
	1.5	0.1	0.5	1.3	2.9	3.8	2.2	0.5	0.2	0	0	0	0	0.1	0.2	0.3	0.8	1	1.4	2.1	9.2
	2	0	0.2	1.2	2.8	3.5	2.4	0.6	0.3	0.1	0	0	0	0	0.1	0.1	0.5	0.6	1.1	1.8	8.6
	2.5	0	0.1	0.6	2.3	3	2	0.9	0.2	0.1	0	0	0	0	0	0	0.2	0.3	0.5	1	4.7
	3	0	0	0.1	0.7	1.7	1.2	0.4	0	0	0	0	0	0	0	0	0	0	0.1	0.2	1.1
	3.5	0	0	0	0.1	0.4	0.4	0.1	0	0	0	0	0	0	0	0	0	0	0	0	0.1
	4	0	0	0	0	0.1	0	0	0	0	0	0	0	0	0	0	0	0	0	0	0
	4.5	0	0	0	0	0	0	0	0	0	0	0	0	0	0	0	0	0	0	0	0
	>5	0	0	0	0	0	0	0	0	0	0	0	0	0	0	0	0	0	0	0	0

Table A-2 Cool season joint probability occurrence between significant wave height ( $H_s$ ) and peak wave period ( $T_p$ ) (percentage) for measurements at the North-East buoy obtained during the period 09/02/2012 to 14/01/2015 (N=24039). The high proportion of long waves ( $T_p > 17$  s) is questionable. Joint probability occurrence between significant wave height ( $H_s$ ) and the energy weighted mean period ( $T_{m01}$ ) are presented in Appendix B.

		Peak Period ( $T_p$ )																			
		5	6	7	8	9	10	11	12	13	14	15	16	17	18	19	20	21	22	23	>24
Significant wave height ( $H_s$ )	0	0	0	0	0	0	0	0	0	0	0	0	0	0	0	0	0.2	0.2	0.2	0.3	2
	0.5	0	0.1	0.8	1.3	0.5	0.1	0	0	0	0	0	0	0	0	0	0	0	0	0	0.1
	1	0.1	0.3	1.2	2.8	3.1	0.8	0.4	0	0	0	0	0	0	0.1	0.1	0.2	0.2	0.4	0.6	2.5
	1.5	0.1	0.4	1.3	3.5	4.1	2.2	0.3	0.1	0	0	0	0	0.1	0.2	0.3	0.7	0.9	1.2	1.9	7.9
	2	0	0.4	1.6	3.7	4.4	2.6	0.6	0.2	0	0	0	0	0.1	0.1	0.2	0.5	0.6	1.2	1.9	9.2
	2.5	0	0.1	1	3.4	4.5	2.5	0.9	0.1	0	0	0	0	0	0	0	0.2	0.3	0.6	1.1	5.4
	3	0	0	0.1	1	2.3	1.3	0.5	0	0	0	0	0	0	0	0	0	0	0.1	0.2	1.2
	3.5	0	0	0	0.1	0.5	0.5	0	0	0	0	0	0	0	0	0	0	0	0	0	0.1
	4	0	0	0	0	0	0	0	0	0	0	0	0	0	0	0	0	0	0	0	0
	4.5	0	0	0	0	0	0	0	0	0	0	0	0	0	0	0	0	0	0	0	0
	>5	0	0	0	0	0	0	0	0	0	0	0	0	0	0	0	0	0	0	0	0

## Appendix B Additional Buoy Data

### B.1 North-East Buoy

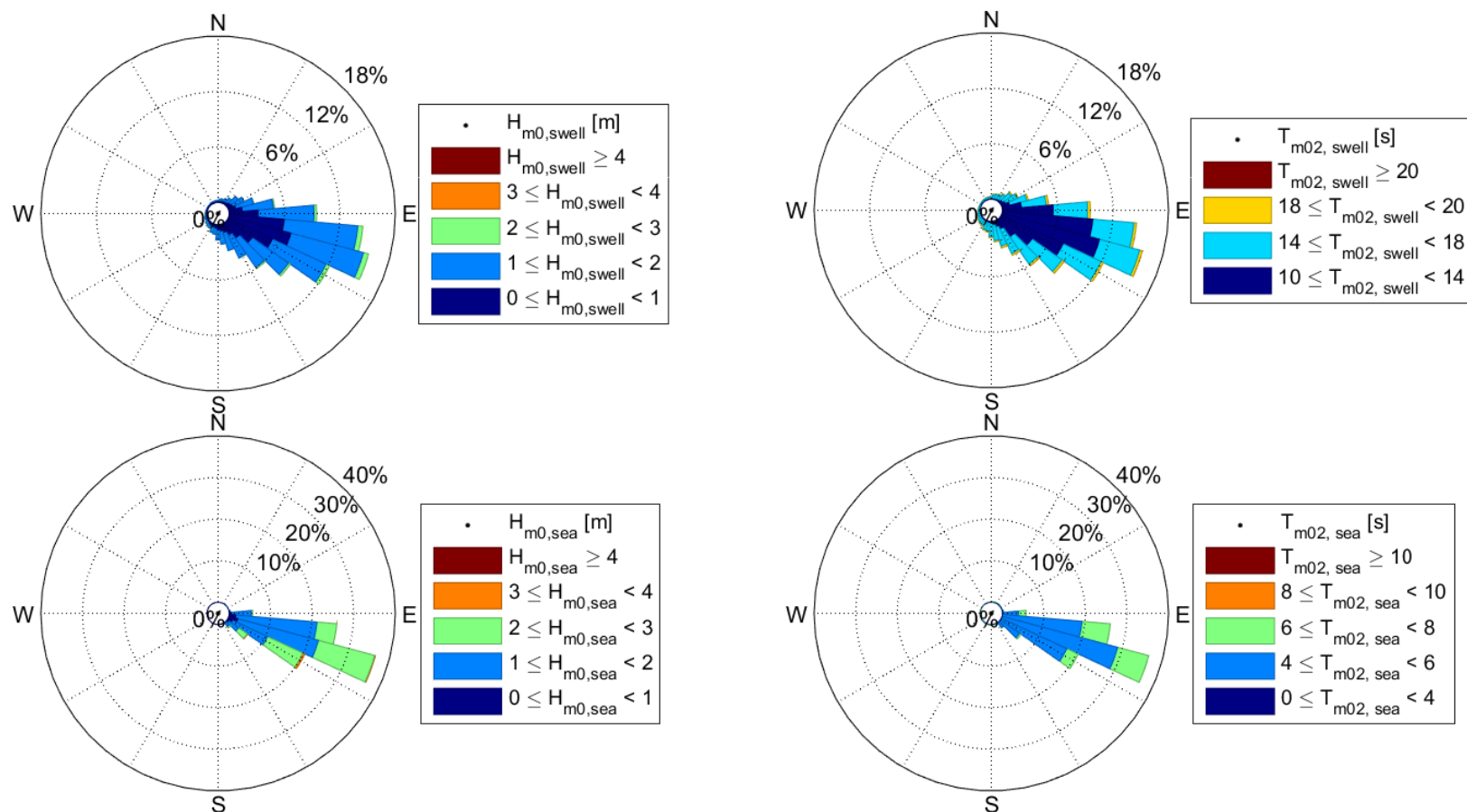


Figure B-1 Wave roses of the incident waves measured ( $N=24039$ ) at the North-East buoy during the cool season (May-October) over the period 09/02/2012 – 14/01/2015. The significant wave height is on the left and the mean wave period is on the right. (top) The swell wave partition and (bottom) the sea wave partition.

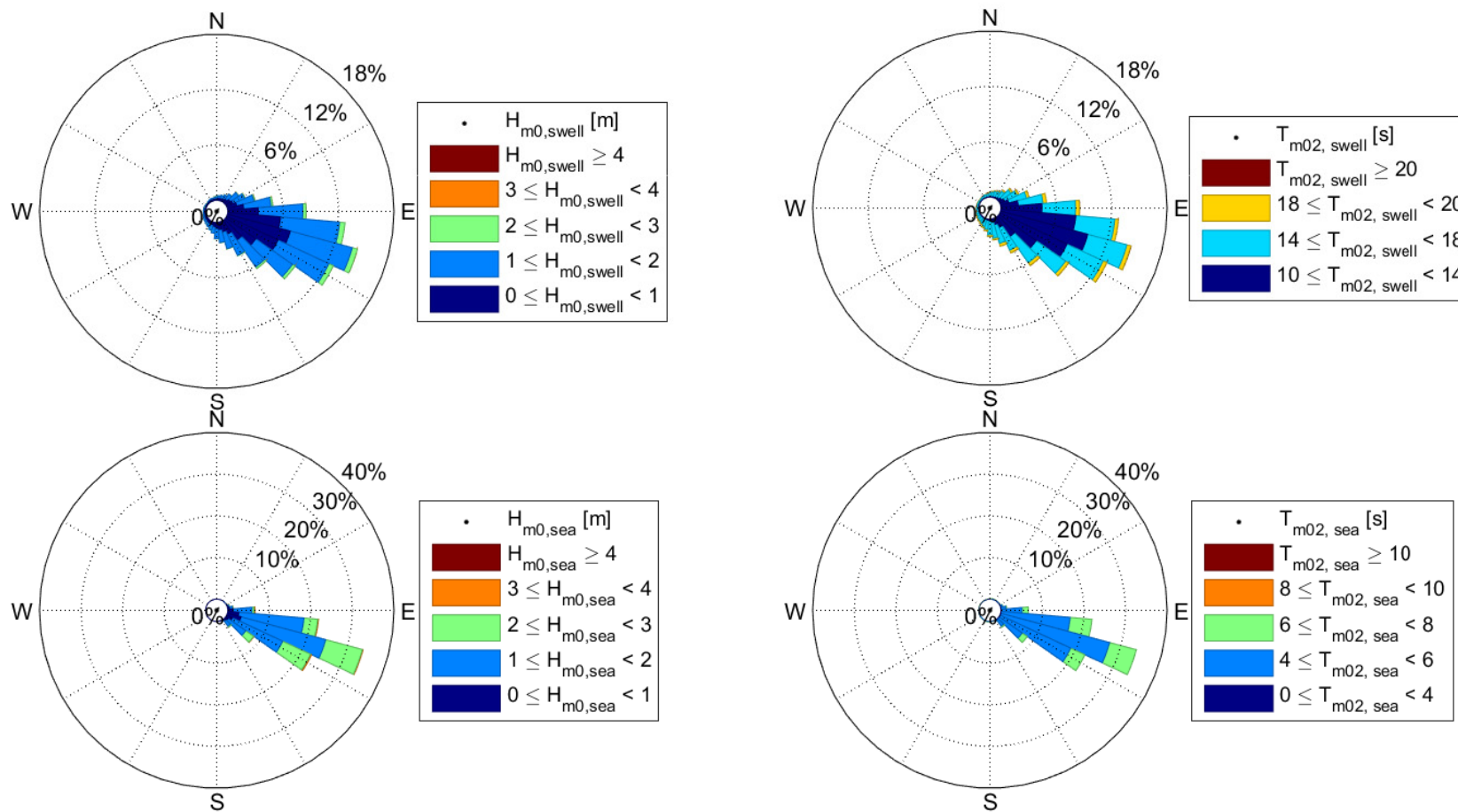


Figure B-2 Wave roses of the incident waves measured ( $N=47577$ ) at the North-East buoy during the warm season (November – April) over the period 09/02/2012 – 14/01/2015. (top) The significant wave height ( $H_{m0}$ ) and (bottom) peak wave period ( $T_p$ ).

Table B-1 Cool season joint probability occurrence between significant wave height ( $H_s$ ) and mean period ( $T_{m01}$ ) (percentage) for measurements ( $N=24039$ ) at the North-East buoy obtained over the period 09/02/2012 to 14/01/2015.

		Mean Period ( $T_{m01}$ )																			
		5	6	7	8	9	10	11	12	13	14	15	16	17	18	19	20	21	22	23	>24
Significant wave height ( $H_s$ )	0	0	0	0	0	0	0	0.1	0.5	0.9	0.9	0.5	0.1	0	0	0	0	0	0	0	0
	0.5	0.4	1.8	0.6	0.1	0	0	0	0	0	0	0	0	0	0	0	0	0	0	0	0
	1	0.6	5.3	5	1.6	0.5	0	0	0	0	0	0	0	0	0	0	0	0	0	0	0
	1.5	0.8	8.6	12.9	2.8	0.3	0	0	0	0	0	0	0	0	0	0	0	0	0	0	0
	2	0.1	8.3	15.3	3.4	0.2	0	0	0	0	0	0	0	0	0	0	0	0	0	0	0
	2.5	0	3.9	12.9	3.2	0.1	0	0	0	0	0	0	0	0	0	0	0	0	0	0	0
	3	0	0.4	4.8	1.6	0	0	0	0	0	0	0	0	0	0	0	0	0	0	0	0
	3.5	0	0	0.8	0.4	0	0	0	0	0	0	0	0	0	0	0	0	0	0	0	0
	4	0	0	0	0.1	0	0	0	0	0	0	0	0	0	0	0	0	0	0	0	0
	4.5	0	0	0	0	0	0	0	0	0	0	0	0	0	0	0	0	0	0	0	0
	>5	0	0	0	0	0	0	0	0	0	0	0	0	0	0	0	0	0	0	0	0

Table B-2 Warm season joint probability occurrence between significant wave height ( $H_s$ ) and mean period ( $T_{m01}$ ) (percentage) for measurements ( $N=47566$ ) at the North-East buoy obtained over period 09/02/2012 to 14/01/2015.

		Mean Period ( $T_{m01}$ )																			
		5	6	7	8	9	10	11	12	13	14	15	16	17	18	19	20	21	22	23	>24
Significant wave height ( $H_s$ )	0	0	0.1	0	0	0	0	0.1	0.3	0.6	0.7	0.4	0.1	0	0	0	0	0	0	0	0
	0.5	0.7	2.3	1.3	0.5	0.2	0.1	0	0	0	0	0	0	0	0	0	0	0	0	0	0
	1	1.4	7.3	6.8	2.7	0.7	0.2	0	0	0	0	0	0	0	0	0	0	0	0	0	0
	1.5	1	8.2	12.1	4.3	0.8	0.2	0	0	0	0	0	0	0	0	0	0	0	0	0	0
	2	0.3	6	12.8	4.3	0.6	0.1	0	0	0	0	0	0	0	0	0	0	0	0	0	0
	2.5	0	2.9	9.2	3.3	0.4	0.1	0	0	0	0	0	0	0	0	0	0	0	0	0	0
	3	0	0.5	3.6	1.5	0.1	0	0	0	0	0	0	0	0	0	0	0	0	0	0	0
	3.5	0	0.1	0.8	0.3	0	0	0	0	0	0	0	0	0	0	0	0	0	0	0	0
	4	0	0	0.1	0.1	0	0	0	0	0	0	0	0	0	0	0	0	0	0	0	0
	4.5	0	0	0	0.1	0	0	0	0	0	0	0	0	0	0	0	0	0	0	0	0
	>5	0	0	0	0	0	0	0	0	0	0	0	0	0	0	0	0	0	0	0	0



## B.2 Souillac Buoy Data

Table B-3 Cool season joint probability occurrence between significant wave height ( $H_s$ ) and mean period ( $T_{m01}$ ) (percentage) for measurements ( $N=2693$ ) at the Souillac buoy obtained over the period 30/06/2016 to 25/01/2017.

		Mean Period ( $T_{m01}$ )																			
		5	6	7	8	9	10	11	12	13	14	15	16	17	18	19	20	21	22	23	>24
Significant wave height ( $H_s$ )	0	0	0	0	0	0	0	0	0	0	0	0	0	0	0	0	0	0	0	0	0
	0.5	0	0.2	0	0	0	0	0	0	0	0	0	0	0	0	0	0	0	0	0	0
	1	2.7	3.8	1.5	0.1	0	0	0	0	0	0	0	0	0	0	0	0	0	0	0	0
	1.5	4.1	7.7	3.8	1.1	0.1	0	0	0	0	0	0	0	0	0	0	0	0	0	0	0
	2	4.4	21.5	7.4	2.3	0.6	0.2	0	0	0	0	0	0	0	0	0	0	0	0	0	0
	2.5	0.2	12.4	3.6	1.7	0.3	0	0	0	0	0	0	0	0	0	0	0	0	0	0	0
	3	0	8.6	6.7	0.9	0.3	0	0	0	0	0	0	0	0	0	0	0	0	0	0	0
	3.5	0	0.2	1.5	0.2	0	0	0	0	0	0	0	0	0	0	0	0	0	0	0	0
	4	0	0	1	0.4	0	0	0	0	0	0	0	0	0	0	0	0	0	0	0	0
	4.5	0	0	0.1	0.3	0	0	0	0	0	0	0	0	0	0	0	0	0	0	0	0
	>5	0	0	0	0.1	0	0	0	0	0	0	0	0	0	0	0	0	0	0	0	0

Table B-4 Warm season joint probability occurrence between significant wave height ( $H_s$ ) and mean period ( $T_{m01}$ ) (percentage) for measurements ( $N=4703$ ) at the Souillac buoy obtained over the period 30/06/2016 to 25/01/2017.

		Mean Period ( $T_{m01}$ )																			
		5	6	7	8	9	10	11	12	13	14	15	16	17	18	19	20	21	22	23	>24
Significant wave height ( $H_s$ )	0	0	0	0	0	0	0	0	0	0	0	0	0	0	0	0	0	0	0	0	0
	0.5	0.7	0.5	0	0	0	0	0	0	0	0	0	0	0	0	0	0	0	0	0	0
	1	13.1	7.6	2.6	0.4	0	0	0	0	0	0	0	0	0	0	0	0	0	0	0	0
	1.5	7.3	10	3.2	0.9	0.1	0	0	0	0	0	0	0	0	0	0	0	0	0	0	0
	2	2.9	14.9	6.4	2.4	0.7	0.2	0	0	0	0	0	0	0	0	0	0	0	0	0	0
	2.5	0.1	7.5	2.4	1.4	0.9	0.3	0	0	0	0	0	0	0	0	0	0	0	0	0	0
	3	0	5	4.4	0.6	0.3	0.2	0.1	0.1	0	0	0	0	0	0	0	0	0	0	0	0
	3.5	0	0.1	1.1	0.1	0	0	0	0	0	0	0	0	0	0	0	0	0	0	0	0
	4	0	0	0.6	0.2	0	0	0	0	0	0	0	0	0	0	0	0	0	0	0	0
	4.5	0	0	0	0.2	0	0	0	0	0	0	0	0	0	0	0	0	0	0	0	0
	>5	0	0	0	0	0	0	0	0	0	0	0	0	0	0	0	0	0	0	0	0

## Appendix C Performance Results

### C.1 Mauritius Domain: North-East Buoy

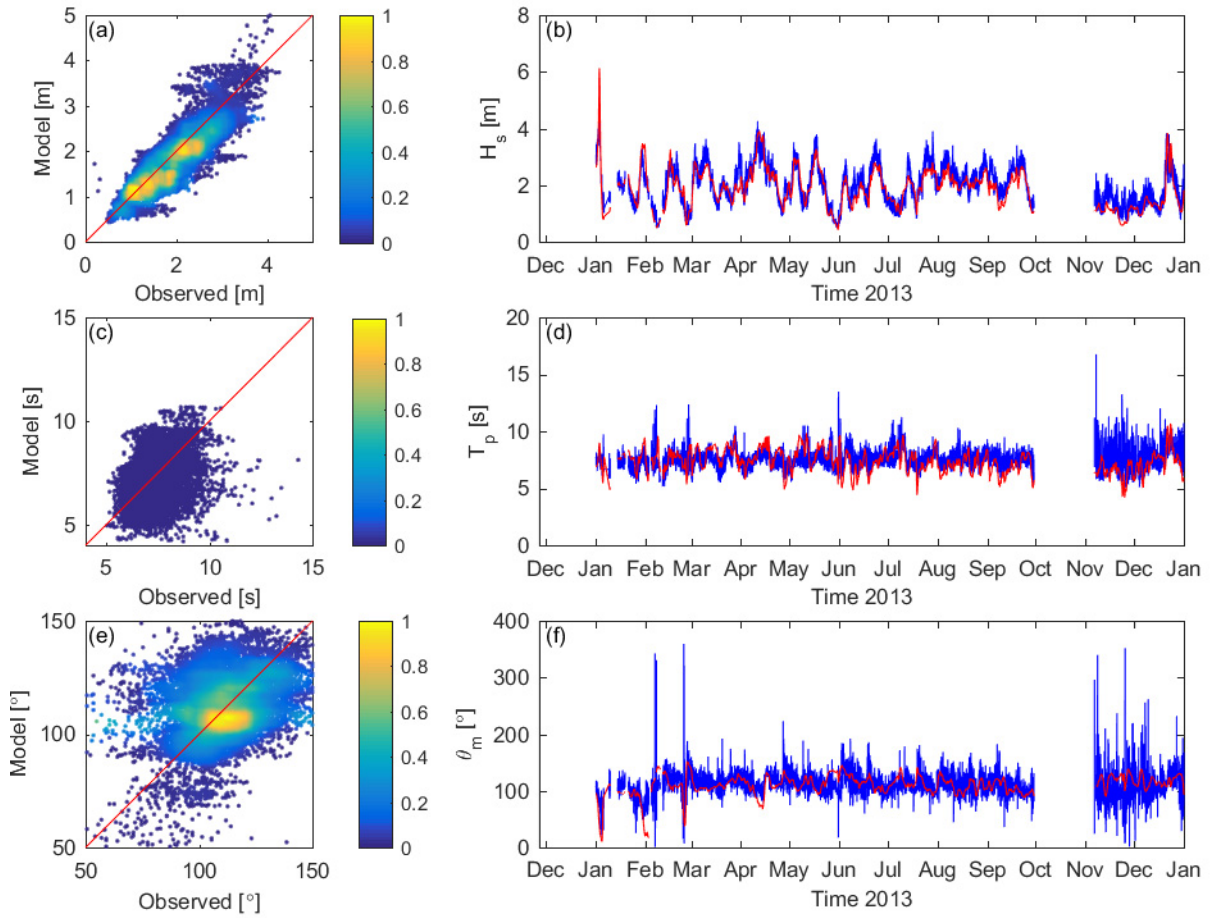


Figure C-1 Validation of the Mauritius domain with buoy data from the North-East measurement location for 2013. Normalized scatter density plot red line indicating 1:1 agreement of (a) significant wave height ( $H_s$ ), Peak Wave Period ( $T_p$ ) and (c) Mean Wave Direction ( $\theta_m$ ). (d) Timeseries from the buoy (blue) and the model (red) of (a)  $H_s$ , (b)  $T_p$  and (c)  $\theta_m$ . The colorbar indicates the normalized density of measurements.

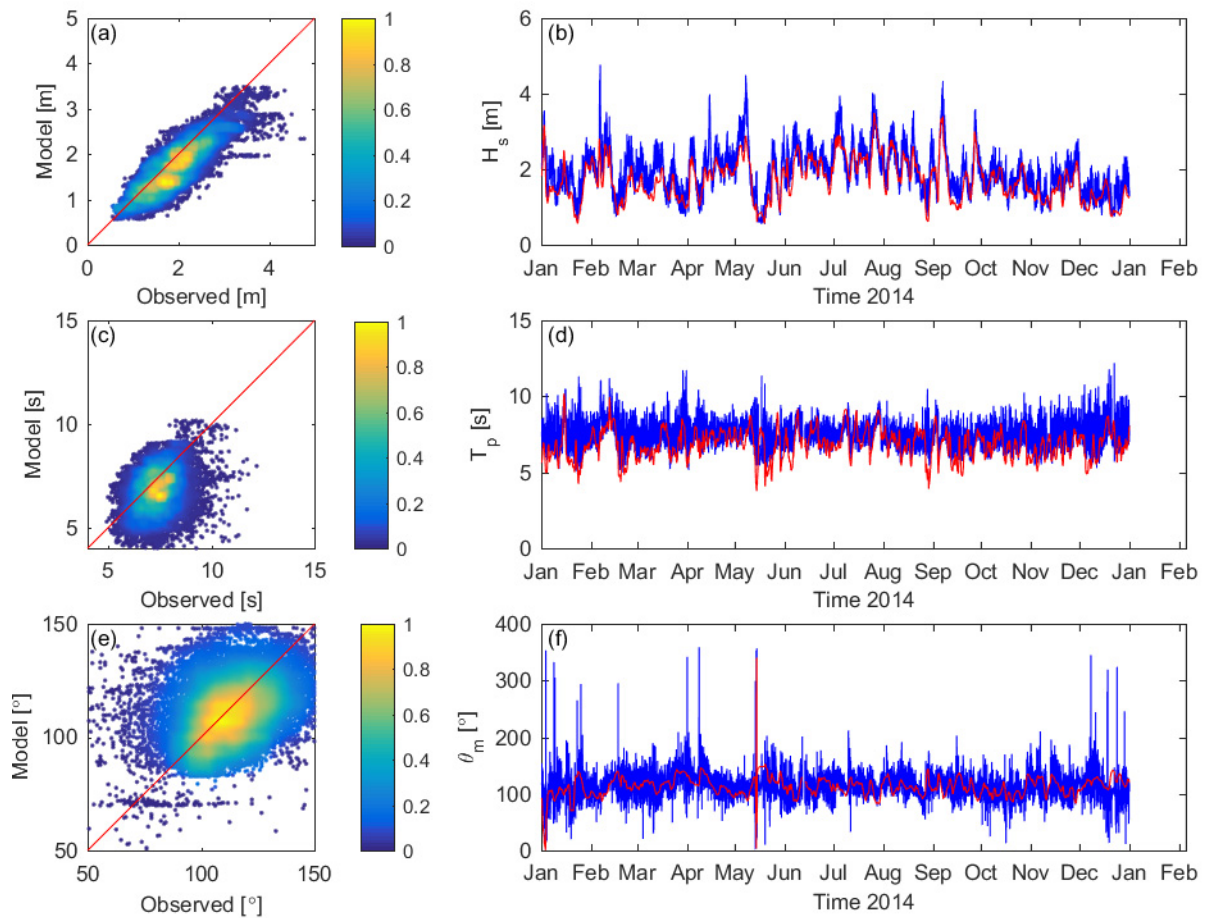


Figure C-2 Validation of the Mauritius domain with buoy data from the North-East measurement location for 2014. Normalized scatter density plot red line indicating 1:1 agreement of (a) significant wave height ( $H_s$ ), Peak Wave Period ( $T_p$ ) and (c) Mean Wave Direction ( $\theta_m$ ). (d) Timeseries from the buoy (blue) and the model (red) of (a)  $H_s$ , (b)  $T_p$  and (c)  $\theta_m$ . The colorbar indicates the normalized density of measurements.

*Table C-1 Statistical measures of the model performance in comparison to the Souillac buoy data for 2016 for the significant wave height ( $H_s$ ), Peak Wave Period ( $T_p$ ) and Mean Wave Direction ( $\theta_m$ ). The statistical measures used here were the Root-Mean-Squared Error (RMSE), Bias and the Scatter Index (SI).*

<b>Year</b>	<b>Parameter</b>	<b>RMSE</b>	<b>Bias</b>	<b>SI</b>
2012	$H_s$	0.39	0.00	0.18
	$T_p$	1.1	0.3	0.15
	$\theta_m$	19.3	-4.24	0.17
2013	$H_s$	0.35	-0.10	0.18
	$T_p$	1.1	-0.1	0.14
	$\theta_m$	20.0	-0.74	0.18
2014	$H_s$	0.39	-0.22	0.20
	$T_{m01}$	1.2	-0.6	0.16
	$\theta_m$	21.6	-1.16	0.19

## C.2 South-East Domain: Blue Bay Buoy

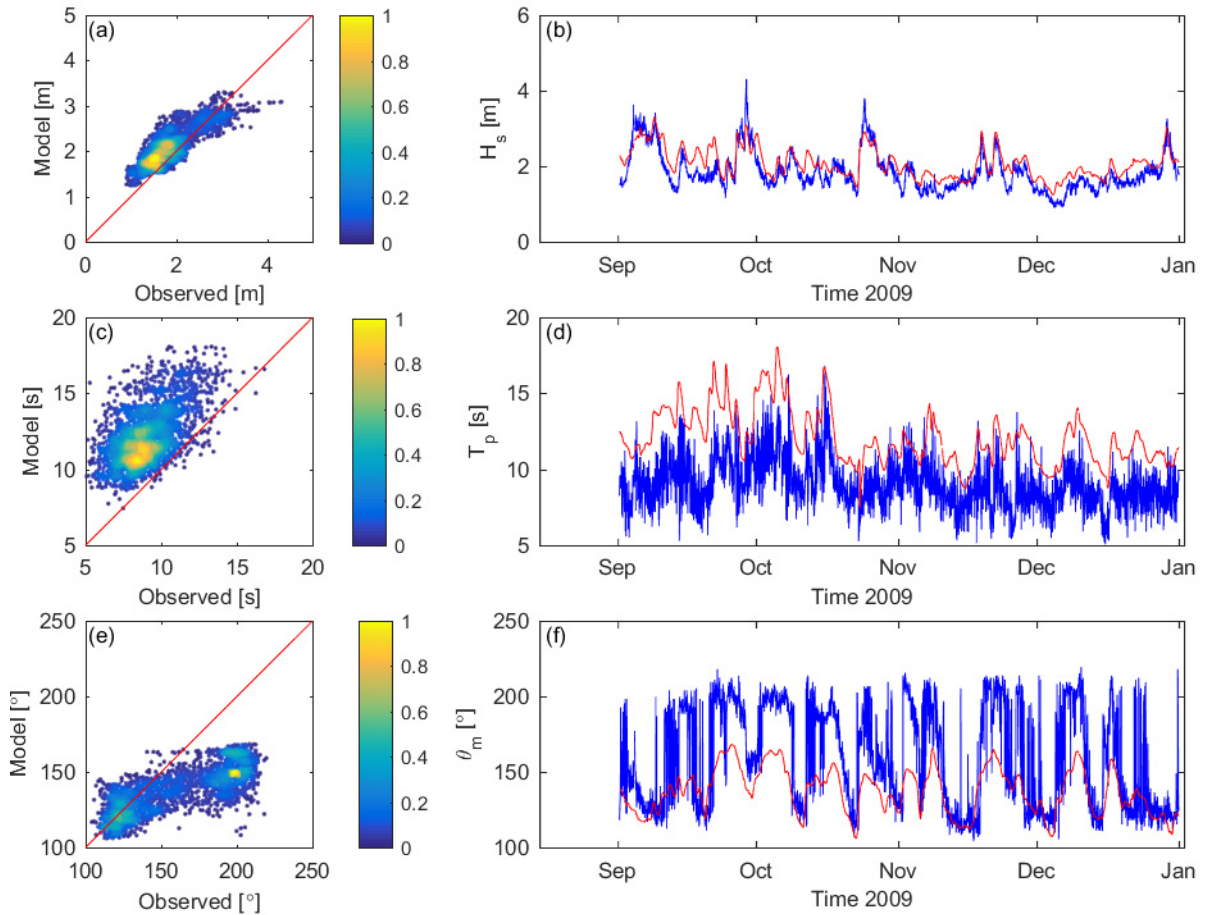
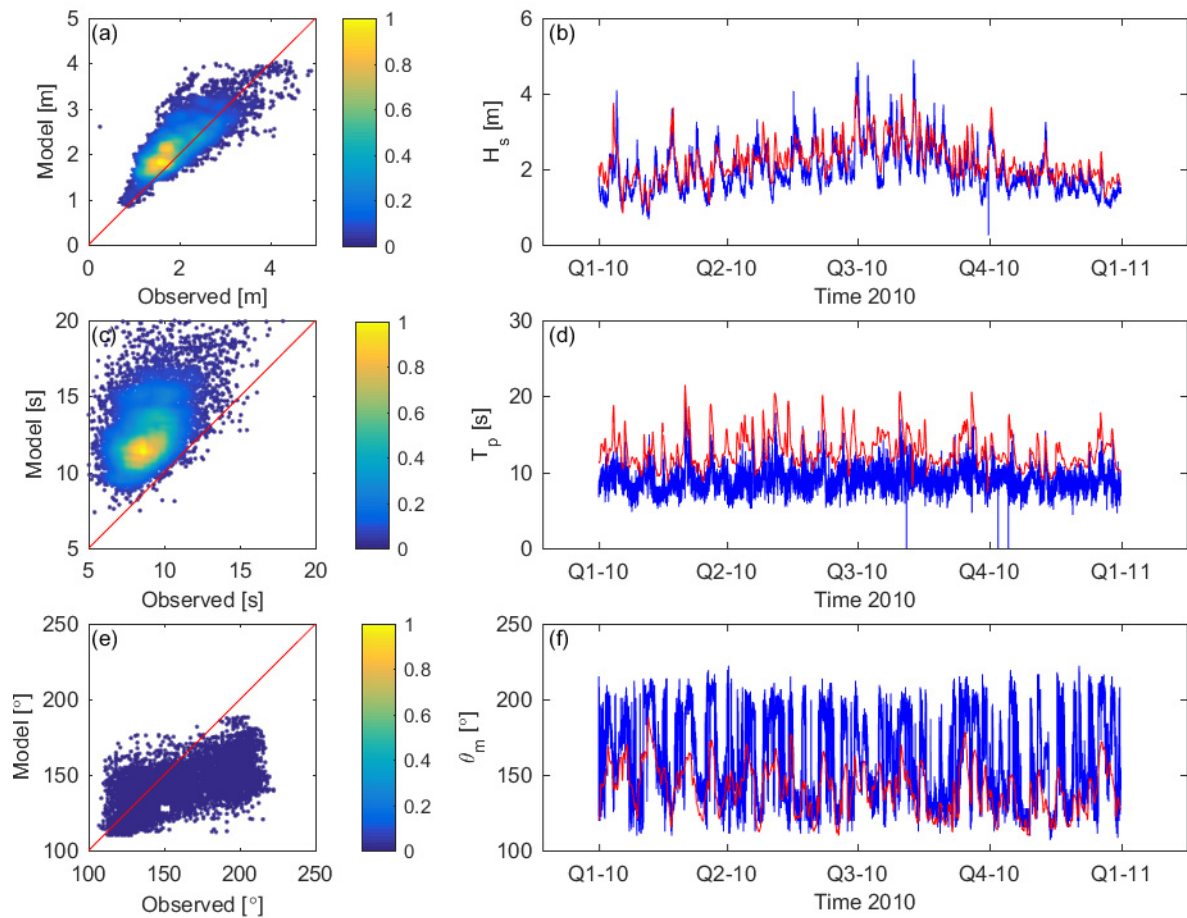
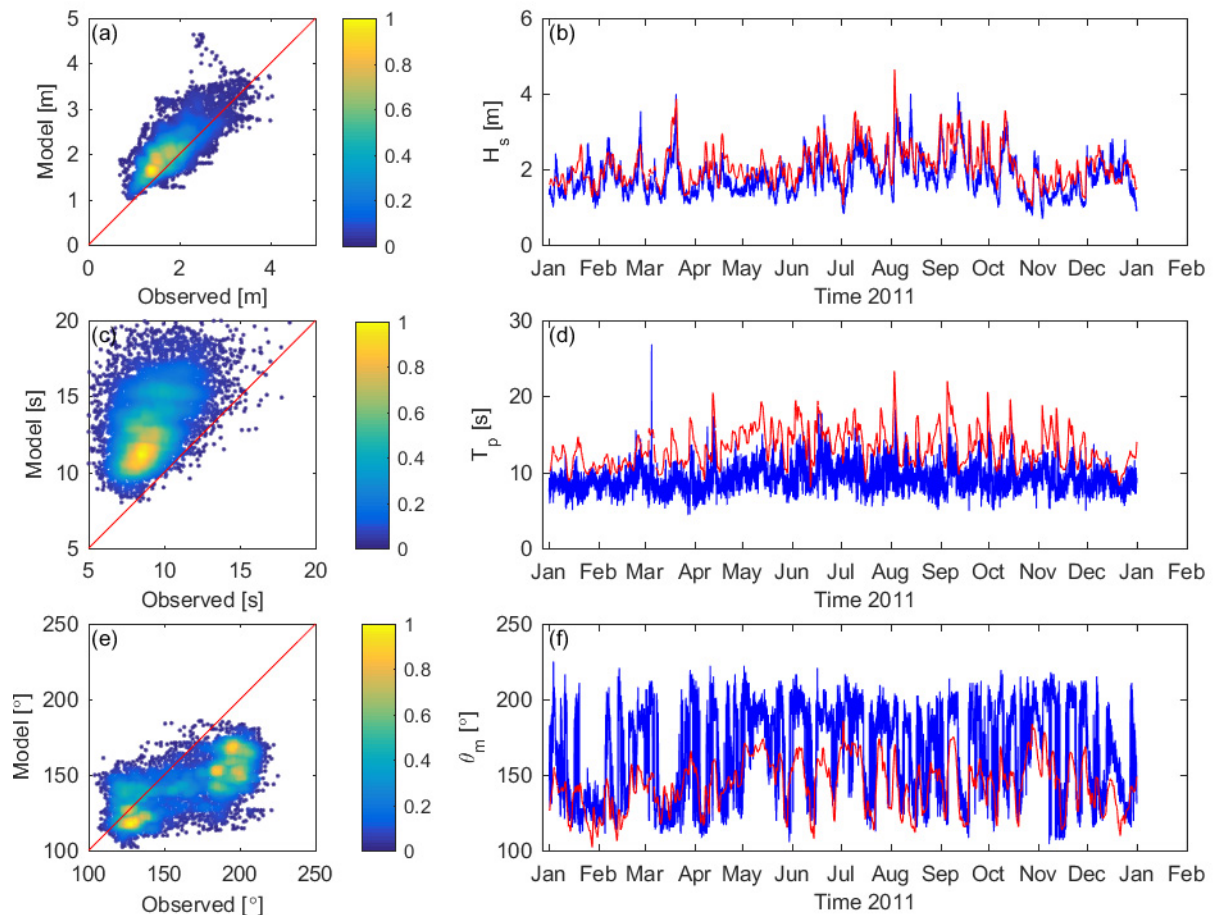


Figure C-3 Validation of the South-East coast domain with buoy data from the Blue Bay measurement location for 2009. Normalized scatter density plot red line indicating 1:1 agreement of (a) significant wave height ( $H_s$ ), Peak Wave Period ( $T_p$ ) and (c) Mean Wave Direction ( $\theta_m$ ). (d) Timeseries from the buoy (blue) and the model (red) of (a)  $H_s$ , (b)  $T_p$  and (c)  $\theta_m$ . The colorbar indicates the normalized density of measurements.



**Figure C-4 Validation of the South-East coast domain with buoy data from the Blue Bay measurement location for 2010. Normalized scatter density plot red line indicating 1:1 agreement of (a) significant wave height ( $H_s$ ), Peak Wave Period ( $T_p$ ) and (c) Mean Wave Direction ( $\theta_m$ ). (d) Timeseries from the buoy (blue) and the model (red) of (a)  $H_s$ , (b)  $T_p$  and (c)  $\theta_m$ . The colorbar indicates the normalized density of measurements.**





**Figure C-5 Validation of the South-East coast domain with buoy data from the Blue Bay measurement location for 2011. Normalized scatter density plot red line indicating 1:1 agreement of (a) significant wave height ( $H_s$ ), Peak Wave Period ( $T_p$ ) and (c) Mean Wave Direction ( $\theta_m$ ). (d) Timeseries from the buoy (blue) and the model (red) of (a)  $H_s$ , (b)  $T_p$  and (c)  $\theta_m$ . The colorbar indicates the normalized density of measurements.**



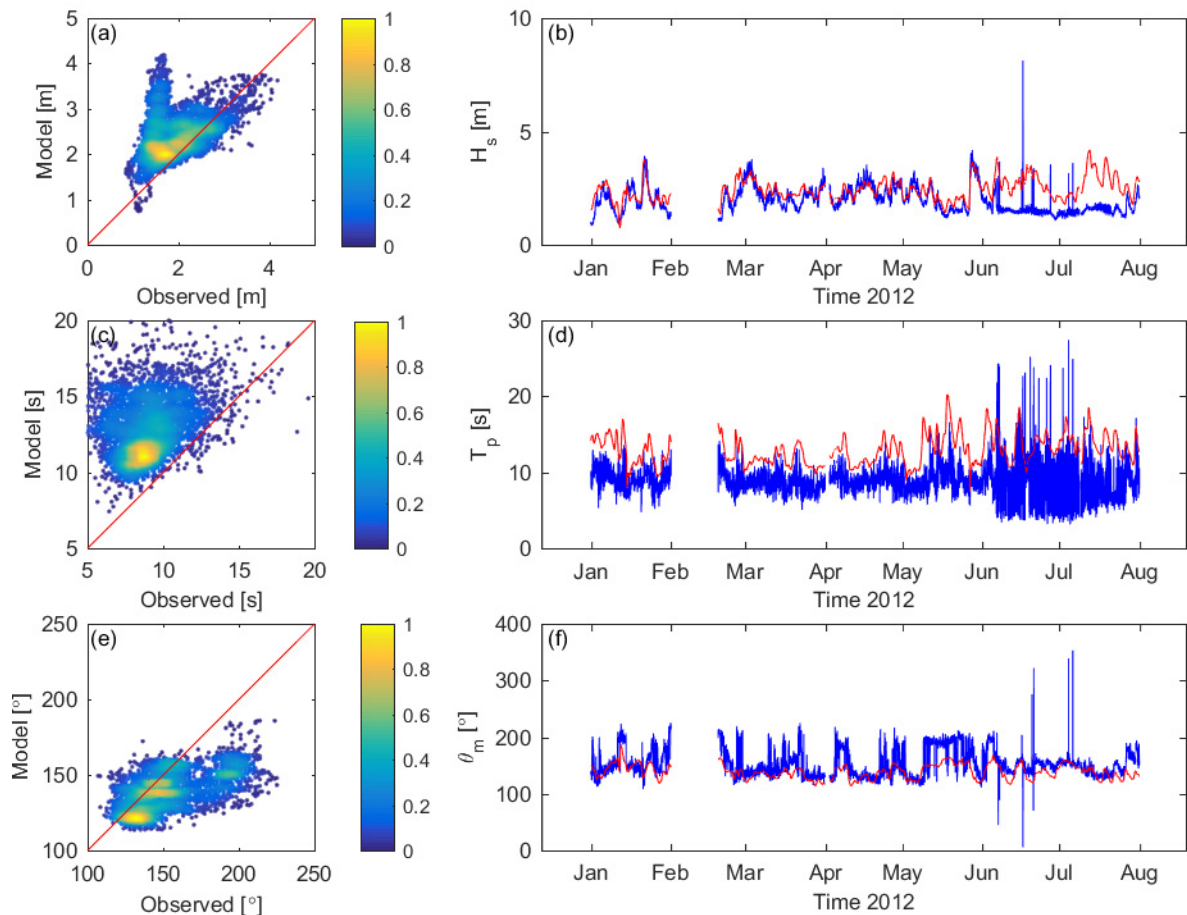


**Figure C-6 Validation of the South-East coast domain with buoy data from the Blue Bay measurement location for 2012. Normalized scatter density plot red line indicating 1:1 agreement of (a) significant wave height ( $H_s$ ), Peak Wave Period ( $T_p$ ) and (c) Mean Wave Direction ( $\theta_m$ ). (d) Timeseries from the buoy (blue) and the model (red) of (a)  $H_s$ , (b)  $T_p$  and (c)  $\theta_m$ . The colorbar indicates the normalized density of measurements.**

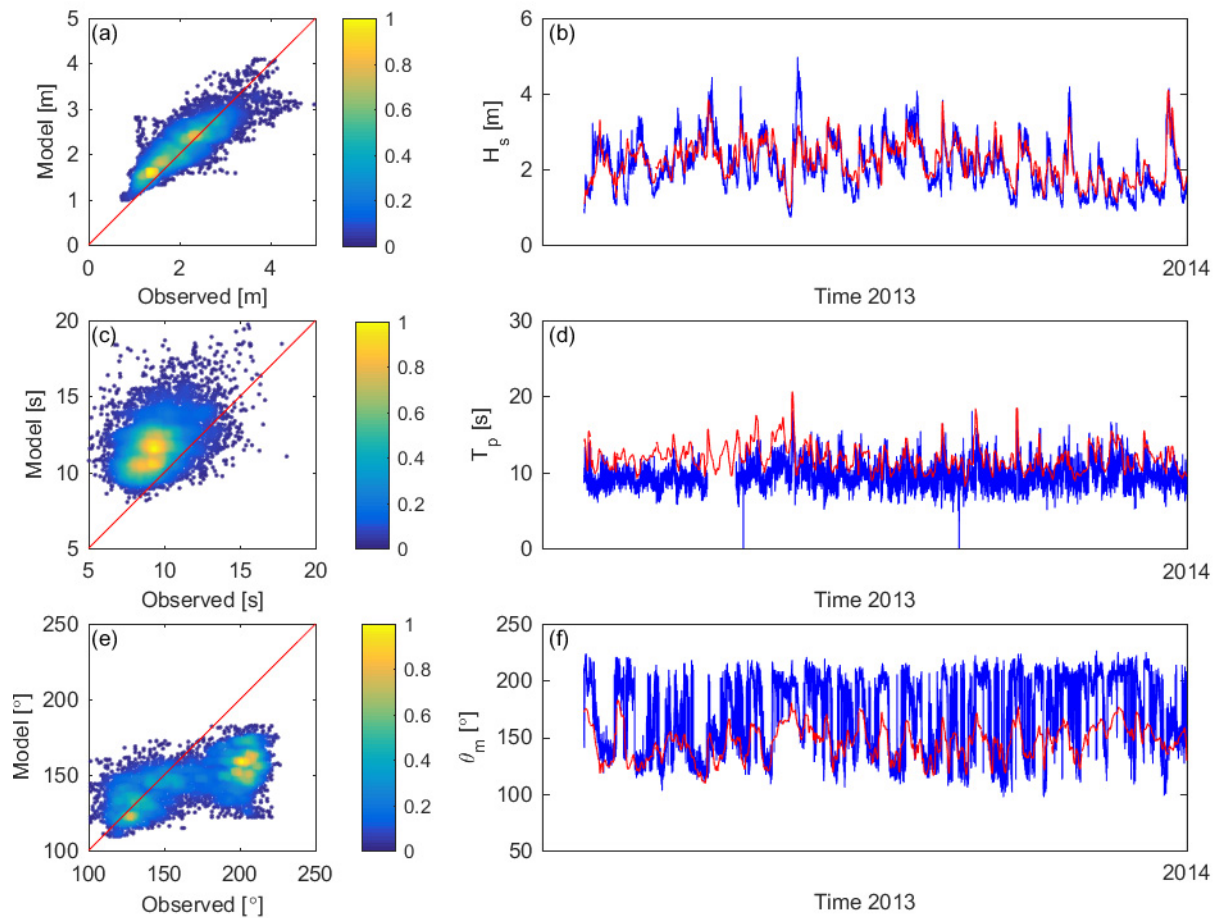


**Figure C-7 Validation of the South-East coast domain with buoy data from the Blue Bay measurement location for 2013. Normalized scatter density plot red line indicating 1:1 agreement of (a) significant wave height ( $H_s$ ), Peak Wave Period ( $T_p$ ) and (c) Mean Wave Direction ( $\theta_m$ ). (d) Timeseries from the buoy (blue) and the model (red) of (a)  $H_s$ , (b)  $T_p$  and (c)  $\theta_m$ . The colorbar indicates the normalized density of measurements.**

*Table C-2 Statistical measures of the model performance in comparison to the Souillac buoy data for 2016 for the significant wave height ( $H_s$ ), Peak Wave Period ( $T_p$ ) and Mean Wave Direction ( $\theta_m$ ). The statistical measures used here were the Root-Mean-Squared Error (RMSE), Bias and the Scatter Index (SI).*

<b>Year</b>	<b>Parameter</b>	<b>RMSE</b>	<b>Bias</b>	<b>SI</b>
2009	$H_s$	0.36	0.22	0.20
	$T_p$	3.5	3.1	0.39
	$\theta_m$	32.5	-22.0	0.20
2010	$H_s$	0.43	0.23	0.22
	$T_p$	4.3	3.7	0.47
	$\theta_m$	28.8	-17.9	0.18
2011	$H_s$	0.44	0.27	0.24
	$T_p$	4.6	4.0	0.50
	$\theta_m$	31.4	-21.5	0.19
2012	$H_s$	0.73	0.44	0.38
	$T_p$	4.6	3.6	0.52
	$\theta_m$	23.7	-13.0	0.15
2013	$H_s$	0.38	0.09	0.18
	$T_p$	2.9	2.2	0.30
	$\theta_m$	35.3	-22.8	0.21
2014	$H_s$	0.38	0.00	0.18
	$T_{m01}$	2.2	1.4	0.23
	$\theta_m$	35.2	-23.7	0.21



## Appendix D South-East coast seasonal wave climate

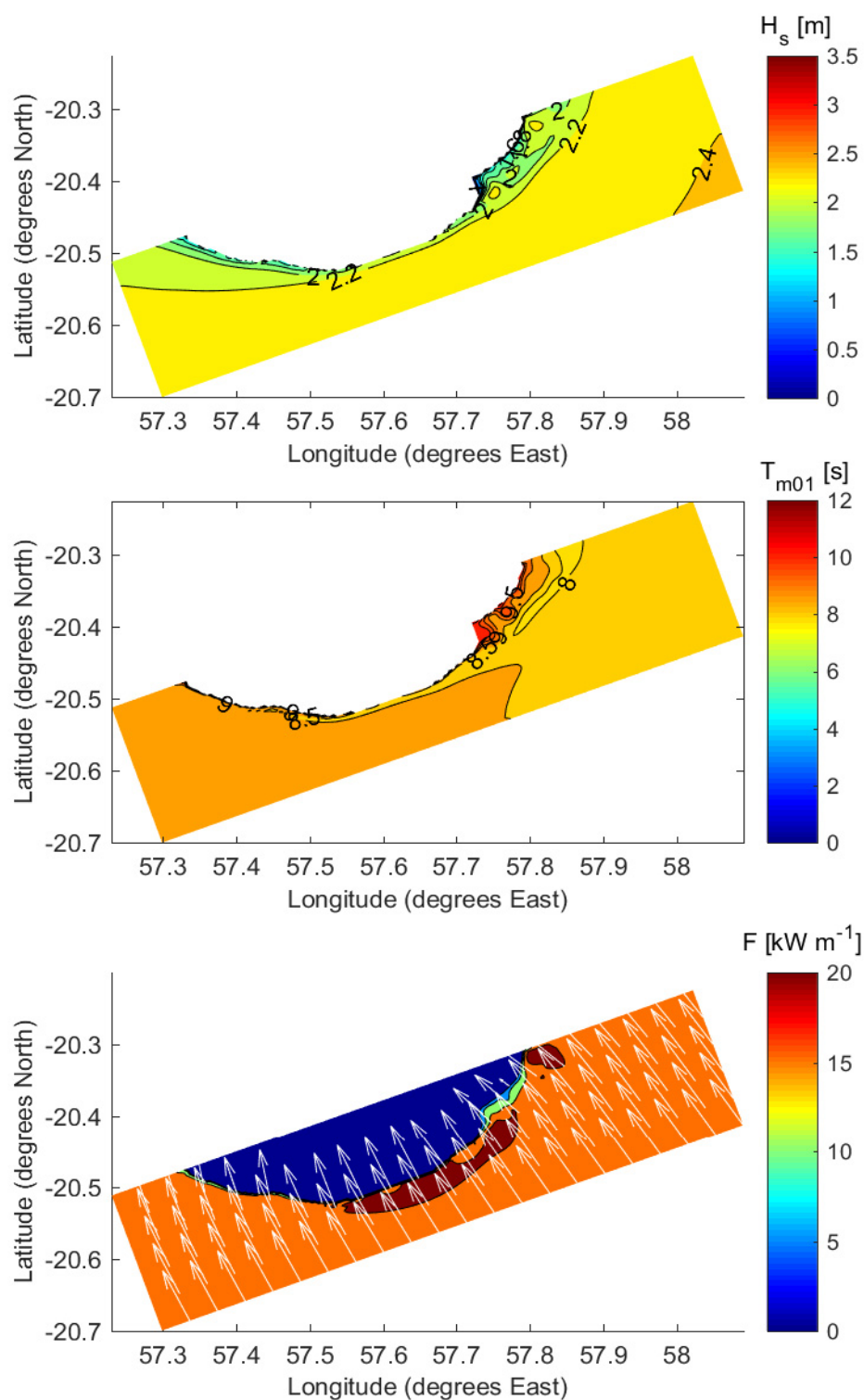
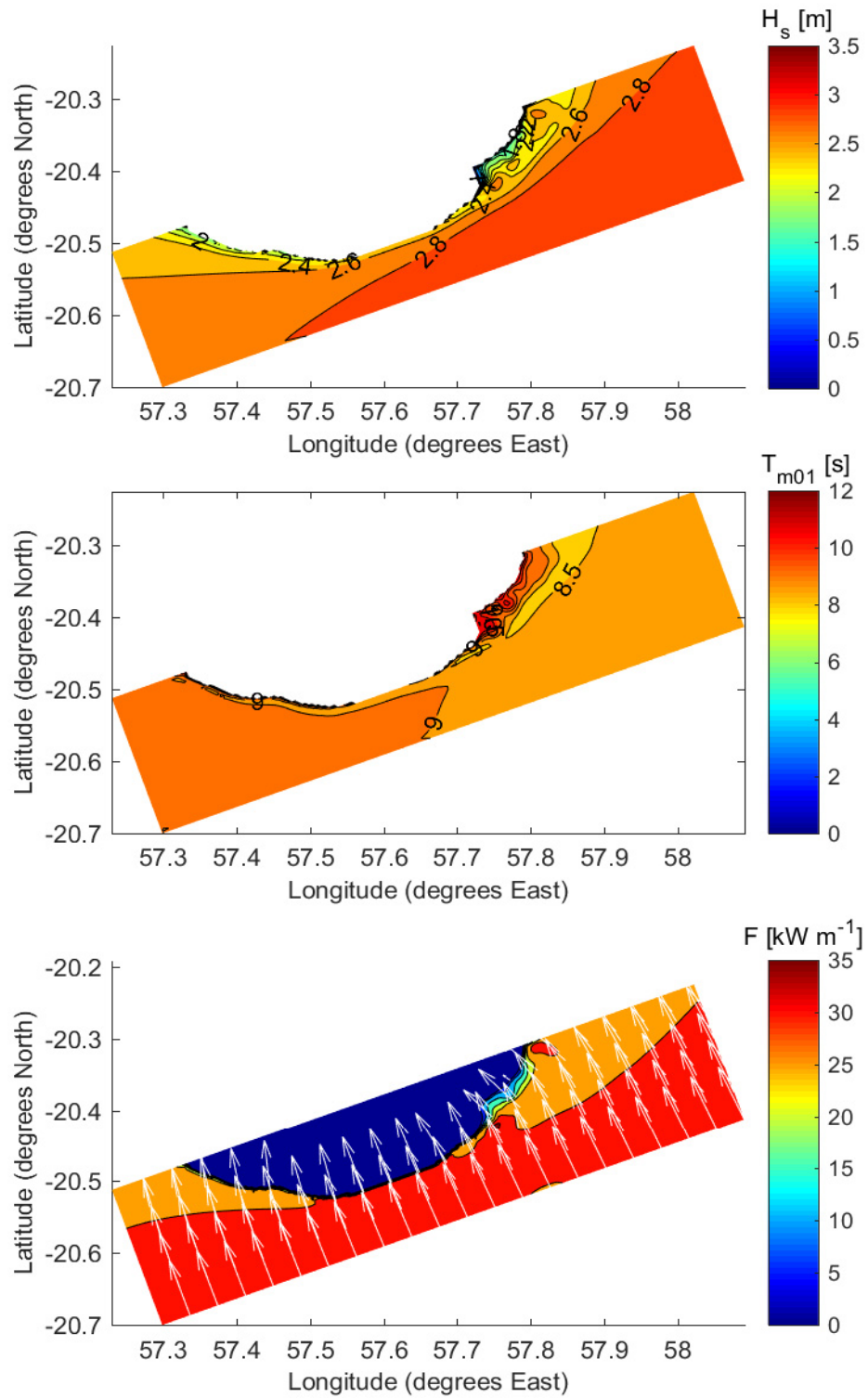


Figure D-1 Spatial distribution of the significant wave height ( $H_s$ ), period ( $T_{m01}$ ) and wave energy flux ( $F$ ) for the hindcast period 2006-2015 for the warm season (November – April) along the South-East coastline from Souillac to Blue Bay. The colourbar indicates the wave height in meters, period in seconds and wave energy flux in  $\text{kW m}^{-1}$ .



*Figure D-2 Spatial distribution of the significant wave height ( $H_s$ ), period ( $T_{m01}$ ) and wave energy flux ( $F$ ) for the hindcast period 2006-2015 for the cool season (May – October) along the South-East coastline from Souillac to Blue Bay. The colourbar indicates the wave height in meters, period in seconds and wave energy flux in  $\text{kW m}^{-1}$ .*

## Appendix E Monthly joint occurrence tables

Table E-1 January joint probability occurrence between significant wave height ( $H_s$ ) and mean period ( $T_{m01}$ ) (percentage) for the representative location at 50 m depth.

		Mean Period ( $T_{m01}$ )																			
		5	6	7	8	9	10	11	12	13	14	15	16	17	18	19	20	21	22	23	>24
Significant wave height ( $H_s$ )	0	0	0	0	0	0	0	0	0	0	0	0	0	0	0	0	0	0	0	0	0
	0.5	0.1	0.1	0.1	0.1	0	0	0	0	0	0	0	0	0	0	0	0	0	0	0	0
	1	1	4.7	3.7	1.7	0.6	0	0	0	0	0	0	0	0	0	0	0	0	0	0	0
	1.5	2.1	10.9	15.5	13.9	4.4	2.2	0.4	0	0	0	0	0	0	0	0	0	0	0	0	0
	2	0.2	1.7	7.6	9.6	5.9	3.1	0.3	0	0	0	0	0	0	0	0	0	0	0	0	0
	2.5	0	0.6	0.4	1.8	3.1	1	0	0	0	0	0	0	0	0	0	0	0	0	0	0
	3	0	0.1	0	0.1	0.4	0.4	0.1	0	0	0	0	0	0	0	0	0	0	0	0	0
	3.5	0	0.4	0	0.2	0.2	0.6	0	0.2	0	0	0	0	0	0	0	0	0	0	0	0
	4	0	0	0.2	0.1	0	0	0	0	0	0	0	0	0	0	0	0	0	0	0	0
	4.5	0	0	0	0	0	0	0	0	0	0	0	0	0	0	0	0	0	0	0	0
	>5	0	0	0	0	0	0	0	0	0	0	0	0	0	0	0	0	0	0	0	0

Table E-2 February joint probability occurrence between significant wave height ( $H_s$ ) and mean period ( $T_{m01}$ ) (percentage) for the representative location at 50 m depth.

		Mean Period ( $T_{m01}$ )																			
		5	6	7	8	9	10	11	12	13	14	15	16	17	18	19	20	21	22	23	>24
Significant wave height ( $H_s$ )	0	0	0	0	0	0	0	0	0	0	0	0	0	0	0	0	0	0	0	0	0
	0.5	0.1	0.1	0.3	0	0	0	0	0	0	0	0	0	0	0	0	0	0	0	0	0
	1	1.1	3.2	2.1	2.1	0.8	0.7	0	0	0	0	0	0	0	0	0	0	0	0	0	0
	1.5	3	6.4	12.4	11.1	3.4	1.1	0.1	0	0	0	0	0	0	0	0	0	0	0	0	0
	2	0.4	2.7	11.2	11.3	6.5	0.1	0.1	0	0	0	0	0	0	0	0	0	0	0	0	0
	2.5	0	0.7	2.6	3.9	4	1.9	0.1	0	0	0	0	0	0	0	0	0	0	0	0	0
	3	0	0.7	0.8	0.9	1.5	0.8	0.3	0	0	0	0	0	0	0	0	0	0	0	0	0
	3.5	0	0.2	0.3	0.1	0.2	0	0	0	0	0	0	0	0	0	0	0	0	0	0	0
	4	0	0	0.2	0	0	0	0	0	0	0	0	0	0	0	0	0	0	0	0	0
	4.5	0	0	0.1	0	0	0	0	0	0	0	0	0	0	0	0	0	0	0	0	0
	>5	0	0	0.1	0	0	0	0	0	0	0	0	0	0	0	0	0	0	0	0	0



Table E-3 March joint probability occurrence between significant wave height ( $H_s$ ) and mean period ( $T_{m01}$ ) (percentage) for the representative location at 50 m depth.

		Mean Period ( $T_{m01}$ )																			
		5	6	7	8	9	10	11	12	13	14	15	16	17	18	19	20	21	22	23	>24
Significant wave height ( $H_s$ )	0	0	0	0	0	0	0	0	0	0	0	0	0	0	0	0	0	0	0	0	0
	0.5	0	0	0	0	0	0	0	0	0	0	0	0	0	0	0	0	0	0	0	0
	1	0.2	1.5	1.9	0.4	0	0	0	0	0	0	0	0	0	0	0	0	0	0	0	0
	1.5	0.2	4.6	9	10.8	2.8	0.6	0	0	0	0	0	0	0	0	0	0	0	0	0	0
	2	0	4.7	15.3	16.4	7.7	1.8	0.4	0.2	0.1	0	0	0	0	0	0	0	0	0	0	0
	2.5	0	0.8	5.3	6.8	3	0.8	0.6	0.1	0.2	0	0	0	0	0	0	0	0	0	0	0
	3	0	0.1	1.2	0.8	0.6	0.2	0	0	0	0	0	0	0	0	0	0	0	0	0	0
	3.5	0	0	0	0	0.2	0.3	0	0	0	0	0	0	0	0	0	0	0	0	0	0
	4	0	0	0	0	0	0	0	0	0	0	0	0	0	0	0	0	0	0	0	0
	4.5	0	0	0	0	0	0	0	0	0	0	0	0	0	0	0	0	0	0	0	0
	>5	0	0	0	0	0	0	0	0	0	0	0	0	0	0	0	0	0	0	0	0

Table E-4 April joint probability occurrence between significant wave height ( $H_s$ ) and mean period ( $T_{m01}$ ) (percentage) for the representative location at 50 m depth.

		Mean Period ( $T_{m01}$ )																			
		5	6	7	8	9	10	11	12	13	14	15	16	17	18	19	20	21	22	23	>24
Significant wave height ( $H_s$ )	0	0	0	0	0	0	0	0	0	0	0	0	0	0	0	0	0	0	0	0	0
	0.5	0	0	0	0	0	0	0	0	0	0	0	0	0	0	0	0	0	0	0	0
	1	0	0	0.2	0	0	0	0	0	0	0	0	0	0	0	0	0	0	0	0	0
	1.5	0	1.7	10	5.9	3	0.1	0	0	0	0	0	0	0	0	0	0	0	0	0	0
	2	0	2.9	15.7	15.3	9.4	2.9	0.4	0	0	0	0	0	0	0	0	0	0	0	0	0
	2.5	0	0.3	5.6	8.3	6.6	2.9	1	0.3	0.1	0	0	0	0	0	0	0	0	0	0	0
	3	0	0	0.2	1.8	2.9	0.8	0.5	0.1	0	0	0	0	0	0	0	0	0	0	0	0
	3.5	0	0	0	0.1	0.4	0.1	0	0	0	0	0	0	0	0	0	0	0	0	0	0
	4	0	0	0	0	0.1	0.1	0	0	0	0	0	0	0	0	0	0	0	0	0	0
	4.5	0	0	0	0	0	0	0	0	0	0	0	0	0	0	0	0	0	0	0	0
	>5	0	0	0	0	0	0	0	0	0	0	0	0	0	0	0	0	0	0	0	0

Table E-5 May joint probability occurrence between significant wave height ( $H_s$ ) and mean period ( $T_{m01}$ ) (percentage) for the representative location at 50 m depth.

		Mean Period ( $T_{m01}$ )																			
		5	6	7	8	9	10	11	12	13	14	15	16	17	18	19	20	21	22	23	>24
Significant wave height ( $H_s$ )	0	0	0	0	0	0	0	0	0	0	0	0	0	0	0	0	0	0	0	0	0
	0.5	0	0	0	0	0	0	0	0	0	0	0	0	0	0	0	0	0	0	0	0
	1	0.1	0.1	0.4	1.1	0.4	0.3	0	0	0	0	0	0	0	0	0	0	0	0	0	0
	1.5	0	1	5.5	9.5	5.7	2.3	0.4	0	0	0	0	0	0	0	0	0	0	0	0	0
	2	0	2.3	6.7	11.8	10.8	5.7	2.1	0.3	0.1	0	0	0	0	0	0	0	0	0	0	0
	2.5	0	0.8	6.4	5	4.9	3.6	2.1	0.3	0.4	0.1	0	0	0	0	0	0	0	0	0	0
	3	0	0.1	1.1	1.5	1.6	2.1	0.5	0.4	0.2	0.1	0	0	0	0	0	0	0	0	0	0
	3.5	0	0	0.3	0.4	0.2	0.2	0	0.2	0	0	0	0	0	0	0	0	0	0	0	0
	4	0	0	0	0	0.1	0	0	0.1	0.2	0	0	0	0	0	0	0	0	0	0	0
	4.5	0	0	0	0	0	0	0	0	0	0	0	0	0	0	0	0	0	0	0	0
	>5	0	0	0	0	0	0	0	0	0	0	0	0	0	0	0	0	0	0	0	0

Table E-6 June joint probability occurrence between significant wave height ( $H_s$ ) and mean period ( $T_{m01}$ ) (percentage) for the representative location at 50 m depth.

		Mean Period ( $T_{m01}$ )																			
		5	6	7	8	9	10	11	12	13	14	15	16	17	18	19	20	21	22	23	>24
Significant wave height ( $H_s$ )	0	0	0	0	0	0	0	0	0	0	0	0	0	0	0	0	0	0	0	0	0
	0.5	0	0	0	0	0	0	0	0	0	0	0	0	0	0	0	0	0	0	0	0
	1	0	0	0	0	0	0	0	0	0	0	0	0	0	0	0	0	0	0	0	0
	1.5	0	1.1	3.8	3.6	1	0.4	0	0	0	0	0	0	0	0	0	0	0	0	0	0
	2	0	1.6	8.9	10.2	6.6	2.3	0.7	0	0	0	0	0	0	0	0	0	0	0	0	0
	2.5	0	1.5	16.6	9.7	7.6	5.3	1.3	0.3	0.1	0	0	0	0	0	0	0	0	0	0	0
	3	0	0	3.1	4.4	2	1.2	1.3	0.6	0.1	0.1	0	0	0	0	0	0	0	0	0	0
	3.5	0	0	0.1	1.4	1.2	0.1	0	0	0	0	0	0	0	0	0	0	0	0	0	0
	4	0	0	0	0.5	0.4	0.3	0	0	0	0	0	0	0	0	0	0	0	0	0	0
	4.5	0	0	0	0	0	0	0.3	0	0	0	0	0	0	0	0	0	0	0	0	0
	>5	0	0	0	0	0	0	0	0	0	0	0	0	0	0	0	0	0	0	0	0

Table E-7 July joint probability occurrence between significant wave height ( $H_s$ ) and mean period ( $T_{m01}$ ) (percentage) for the representative location at 50 m depth.

		Mean Period ( $T_{m01}$ )																			
		5	6	7	8	9	10	11	12	13	14	15	16	17	18	19	20	21	22	23	>24
Significant wave height ( $H_s$ )	0	0	0	0	0	0	0	0	0	0	0	0	0	0	0	0	0	0	0	0	0
	0.5	0	0	0	0	0	0	0	0	0	0	0	0	0	0	0	0	0	0	0	0
	1	0	0	0	0.1	0	0	0	0	0	0	0	0	0	0	0	0	0	0	0	0
	1.5	0	0.4	2.5	2.8	0.6	0.6	0	0	0	0	0	0	0	0	0	0	0	0	0	0
	2	0	2.9	7.2	8.4	6.2	2.6	0.4	0.1	0	0	0	0	0	0	0	0	0	0	0	0
	2.5	0	3	10.8	11.6	6.9	2.3	1.1	0.3	0	0	0	0	0	0	0	0	0	0	0	0
	3	0	0	3.5	8.6	6.1	2.6	1.3	0.2	0.1	0	0	0	0	0	0	0	0	0	0	0
	3.5	0	0	0.7	1.4	1.8	0.7	0.3	0.4	0	0	0	0	0	0	0	0	0	0	0	0
	4	0	0	0	0.5	0.1	0.5	0.2	0	0	0	0	0	0	0	0	0	0	0	0	0
	4.5	0	0	0	0	0	0	0	0	0	0	0	0	0	0	0	0	0	0	0	0
	>5	0	0	0	0	0	0	0	0	0	0	0	0	0	0	0	0	0	0	0	0

Table E-8 August joint probability occurrence between significant wave height ( $H_s$ ) and mean period ( $T_{m01}$ ) (percentage) for the representative location at 50 m depth.

		Mean Period ( $T_{m01}$ )																			
		5	6	7	8	9	10	11	12	13	14	15	16	17	18	19	20	21	22	23	>24
Significant wave height ( $H_s$ )	0	0	0	0	0	0	0	0	0	0	0	0	0	0	0	0	0	0	0	0	0
	0.5	0	0	0	0	0	0	0	0	0	0	0	0	0	0	0	0	0	0	0	0
	1	0	0	0.2	0.1	0	0	0	0	0	0	0	0	0	0	0	0	0	0	0	0
	1.5	0.5	1.4	4.6	2.7	0.7	0.2	0	0	0	0	0	0	0	0	0	0	0	0	0	0
	2	0.2	4	12.2	10.8	6.9	1.8	0.2	0.1	0	0	0	0	0	0	0	0	0	0	0	0
	2.5	0	1.7	12	10.2	8.9	3.5	1.5	0.1	0	0	0	0	0	0	0	0	0	0	0	0
	3	0	0.1	2.8	4.5	2.2	1.3	0.6	0	0	0	0	0	0	0	0	0	0	0	0	0
	3.5	0	0	0.1	0.9	1.2	0.5	0.4	0	0	0	0	0	0	0	0	0	0	0	0	0
	4	0	0	0	0	0.2	0.3	0	0	0	0	0	0	0	0	0	0	0	0	0	0
	4.5	0	0	0	0	0	0	0	0	0	0.1	0	0	0	0	0	0	0	0	0	0
	>5	0	0	0	0	0	0	0	0	0	0	0.1	0	0	0	0	0	0	0	0	0

Table E-9 September joint probability occurrence between significant wave height ( $H_s$ ) and mean period ( $T_{m01}$ ) (percentage) for the representative location at 50 m depth.

		Mean Period ( $T_{m01}$ )																			
		5	6	7	8	9	10	11	12	13	14	15	16	17	18	19	20	21	22	23	>24
Significant wave height ( $H_s$ )	0	0	0	0	0	0	0	0	0	0	0	0	0	0	0	0	0	0	0	0	0
	0.5	0	0	0	0	0	0	0	0	0	0	0	0	0	0	0	0	0	0	0	0
	1	0	0	0.2	0	0	0	0	0	0	0	0	0	0	0	0	0	0	0	0	0
	1.5	0.7	4.5	5.2	4.8	2.3	0.2	0	0	0	0	0	0	0	0	0	0	0	0	0	0
	2	0.4	4.4	12.7	13.5	6.4	2.9	0.4	0.1	0	0	0	0	0	0	0	0	0	0	0	0
	2.5	0	0.8	5.5	6.7	6.3	4.1	1.7	0.1	0	0	0	0	0	0	0	0	0	0	0	0
	3	0	0.1	1.9	3.4	2	2.1	2	0.7	0.2	0	0	0	0	0	0	0	0	0	0	0
	3.5	0	0	0.3	0.7	0.9	0.4	0.3	0.2	0.5	0	0	0	0	0	0	0	0	0	0	0
	4	0	0	0	0	0.1	0	0	0.1	0	0	0	0	0	0	0	0	0	0	0	0
	4.5	0	0	0	0	0	0	0	0	0	0	0	0	0	0	0	0	0	0	0	0
	>5	0	0	0	0	0	0	0	0	0	0	0	0	0	0	0	0	0	0	0	0

Table E-10 October joint probability occurrence between significant wave height ( $H_s$ ) and mean period ( $T_{m01}$ ) (percentage) for the representative location at 50 m depth.

		Mean Period ( $T_{m01}$ )																			
		5	6	7	8	9	10	11	12	13	14	15	16	17	18	19	20	21	22	23	>24
Significant wave height ( $H_s$ )	0	0	0	0	0	0	0	0	0	0	0	0	0	0	0	0	0	0	0	0	0
	0.5	0	0.1	0	0	0	0	0	0	0	0	0	0	0	0	0	0	0	0	0	0
	1	0.7	1	1.2	1	0.6	0	0	0	0	0	0	0	0	0	0	0	0	0	0	0
	1.5	0	7.7	13.8	7.9	2.8	0.8	0	0	0	0	0	0	0	0	0	0	0	0	0	0
	2	0.1	3.9	12.4	15.1	6.6	3.1	0.8	0.1	0	0	0	0	0	0	0	0	0	0	0	0
	2.5	0	1.1	3.7	5.3	4.2	0.7	0	0	0	0	0	0	0	0	0	0	0	0	0	0
	3	0	0	0.7	1.5	1.2	0.9	0.1	0	0	0	0	0	0	0	0	0	0	0	0	0
	3.5	0	0	0.2	0.2	0.4	0.2	0	0	0	0	0	0	0	0	0	0	0	0	0	0
	4	0	0	0	0	0	0	0	0	0	0	0	0	0	0	0	0	0	0	0	0
	4.5	0	0	0	0	0	0	0	0	0	0	0	0	0	0	0	0	0	0	0	0
	>5	0	0	0	0	0	0	0	0	0	0	0	0	0	0	0	0	0	0	0	0

Table E-11 November joint probability occurrence between significant wave height ( $H_s$ ) and mean period ( $T_{m01}$ ) (percentage) for the representative location at 50 m depth.

		Mean Period ( $T_{m01}$ )																			
		5	6	7	8	9	10	11	12	13	14	15	16	17	18	19	20	21	22	23	>24
Significant wave height ( $H_s$ )	0	0	0	0	0	0	0	0	0	0	0	0	0	0	0	0	0	0	0	0	0
	0.5	0	0	0	0	0	0	0	0	0	0	0	0	0	0	0	0	0	0	0	0
	1	0.2	2.2	3.2	1.7	0.9	0	0	0	0	0	0	0	0	0	0	0	0	0	0	0
	1.5	0.4	6.3	20	17	6.1	2.8	0.2	0	0	0	0	0	0	0	0	0	0	0	0	0
	2	0	1.6	7.9	12	9.3	3.1	0.9	0.1	0	0	0	0	0	0	0	0	0	0	0	0
	2.5	0	0	0.6	0.6	1.4	0.8	0.2	0	0	0	0	0	0	0	0	0	0	0	0	0
	3	0	0	0.1	0.3	0	0	0	0	0	0	0	0	0	0	0	0	0	0	0	0
	3.5	0	0	0	0	0	0	0	0	0	0	0	0	0	0	0	0	0	0	0	0
	4	0	0	0	0	0	0	0	0	0	0	0	0	0	0	0	0	0	0	0	0
	4.5	0	0	0	0	0	0	0	0	0	0	0	0	0	0	0	0	0	0	0	0
	>5	0	0	0	0	0	0	0	0	0	0	0	0	0	0	0	0	0	0	0	0

Table E-12 December joint probability occurrence between significant wave height ( $H_s$ ) and mean period ( $T_{m01}$ ) (percentage) for the representative location at 50 m depth.

		Mean Period ( $T_{m01}$ )																			
		5	6	7	8	9	10	11	12	13	14	15	16	17	18	19	20	21	22	23	>24
Significant wave height ( $H_s$ )	0	0	0	0	0	0	0	0	0	0	0	0	0	0	0	0	0	0	0	0	0
	0.5	0	0	0	0	0	0	0	0	0	0	0	0	0	0	0	0	0	0	0	0
	1	1	1.8	1.5	1.4	0.5	0.2	0.1	0	0	0	0	0	0	0	0	0	0	0	0	0
	1.5	1.2	10.6	19.9	16.9	4.8	1.4	0.6	0	0	0	0	0	0	0	0	0	0	0	0	0
	2	0	2.8	10.4	12.2	5.5	1.4	0.3	0	0	0	0	0	0	0	0	0	0	0	0	0
	2.5	0	0	0.5	2.4	0.5	0.2	0.3	0.2	0	0	0	0	0	0	0	0	0	0	0	0
	3	0	0	0.1	0.2	0.2	0	0	0.1	0	0	0	0	0	0	0	0	0	0	0	0
	3.5	0	0	0	0.2	0.2	0	0	0	0	0	0	0	0	0	0	0	0	0	0	0
	4	0	0	0	0.1	0.2	0	0	0	0	0	0	0	0	0	0	0	0	0	0	0
	4.5	0	0	0	0	0	0	0	0	0	0	0	0	0	0	0	0	0	0	0	0
	>5	0	0	0	0	0	0	0	0	0	0	0	0	0	0	0	0	0	0	0	0

